THE DEVELOPMENT OF A ONE-DIMENSIONAL QUASI-STEADY STATE MODEL FOR THE DESULPHURISATION PROCESS AT SALDANHA STEEL

by

EMILE SCHEEPERS

A thesis submitted in partial fulfillment of the requirements for the degree of

Master of Science in Engineering
(Extractive Metallurgy)

at the Department of Chemical Engineering at the
University of Stellenbosch

Supervisors:
Mr. JJ Eksteen
Prof. C Aldrich

STELLENBOSCH

APRIL 2003

DECLARATION

I, the undersigned, hereby declare that this thesis is my own original work, except where specifically acknowledged in the text. Neither the present thesis, nor any part thereof, has previously been submitted for a degree at any university.

_____

Emile Scheepers

April 2003

SUMMARY

The pneumatic injection of reagent powder into molten iron has become the preferred way to carry out iron and steel desulphurisation. It is therefore essential to not only understand the thermodynamic implications, but also the kinetic principles that govern the desulphurisation process. Key variables that influence the kinetics of the procedure are the condition and composition of the top slag and the melt as well as the injection conditions. Notable injection parameters include reagent flowrate, injection-lance depth and carrier gas flowrate.

Owing to sampling restrictions, the subsequent data from Saldanha Steel$^{®}$, South Africa does not provide adequate insight into the kinetic behaviour of the desulphurisation process and it was therefore the focus of this research to provide an improved quantitive comprehension of the calcium carbide injection procedure at Saldanha Steel.

For this purpose a one-dimensional quasi-steady state model for momentum, heat- and mass transfer in rising gas-liquid-powder plumes has been developed for conditions relevant to the Saldanha Steel refining process. Combined with a model predicting the contribution of the topslag to the process, the overall rate of desulphurisation as a function of time can be determined, thus affording the ability to quantitatively explore and analyse the influence of the afore-mentioned injection parameters, as well as the nature of both the topslag and the melt, on the kinetics of the desulphurisation process.

Sensitivity analyses concluded that individual increases in the calcium carbide flowrate, the depth of injection and the amount of carry-over slag will result in a reduction in the injection time, while a decrease in the

reagent particle diameter and the initial mass of iron in the ladle will have the same effect.

Molten iron temperature losses brought about by prolonged injection needs to be electrically recovered within a steelmaking furnace at a high cost. Owing to the high cost of the desulphurising agent, any reduction in the required injection time, while still maintaining product specifications, will therefore result in diminishing overall production costs.

Although all the results contained in this study is of particular interest to the Saldanha Steel scenario, it also provides invaluable information and insights into the important variables and parameters playing a role in injection desulphurisation processes in general, along with the influence that changing conditions can have on the end result of such a procedure.

OPSOMMING

Die pneumatiese inspuiting van reagentpoeier is die populêrste ontswawelingsmetode in die yster- en staal bedryf. Dit is dus van groot belang dat die gepaardgaande termodinamiese en kinetiese beginsels betrokke by die ontswawelingsreaksies baie goed verstaan word. Die kondisie en samestelling van die bo-slak en die vloeibare yster, asook die inspuitingkondisies is twee van die belangrikste veranderlikes wat die kinetika van die ontswawelingsproses beïnvloed.

Beperkte monsternemingsgeleenthede het veroorsaak dat die relevante data, soos voorsien deur Saldanha Staal®, nie die nodige kinetiese insig in verband met die ontswawelingreaksie weergee nie. Dit is dus die doel van hierdie werkstuk om 'n verbeterde kwantitatiewe begrip van die ontswawelingsproses by Saldanha Staal daar te stel.

Vir hierdie doeleinde is 'n een-dimensionele, kwasi-gestadigde toestand model vir stygende gas-vloeistof pluime ontwikkel. Die model inkorporeer momentum-, hitte- en massaoordragsprinsiepe en is verteenwoordigend van die ontswawelingsproses by Saldanha Staal. 'n Tweede model simuleer die bydrae wat die bo-slak tot die algehele ontswawelingsproses maak en saam gee hierdie twee modelle die algehele ontswawelingstempo weer as 'n funksie van tyd. Die modelle word ook gebruik om die invloed van die bogenoemde inspuitingsveranderlikes op die proses te ondersoek.

Deeglike sensitiwiteitsanalise het gewys dat 'n verhoging in die kalsium karbied vloeitempo, asook die inspuitingsdiepte van die lans en die hoeveelheid slak wat vanaf die boogoond na die ontswawelingseenheid oorgedra word, 'n vermindering in die vereisde inspuitingstyd te weeg bring. Verkleining in die kalsium kardied partikels se gemiddelde

diameter en vermindering van die hoeveelheid yster in die torpedokarre aan die begin van die proses, het dieselfde uitwerking op die vereisde inspuitingstyd.

Geweldig baie geld moet aan elektrisiteit spandeer word om die temperatuur wat verlore gaan as gevolg van onnodige lang inspuitingstye, in die staalmaakoonde te herwin. Gekombineerd met die feit dat die kalsium karbied reagent baie duur is, beteken dit dat reduksies in die vereisde ontswaweling inspuitingstyd groot besparings te weeg kan bring.

Alhoewel die saamgevatte resultate van spesifieke belang is vir die Saldanha Staal proses, verskaf hierdie studie waardevolle informasie oor die belangrikheid van verskeie veranderlikes, asook die rol wat veranderende toestande op die eindresultate van die ontswawelingproses kan hê.

ACKNOWLEDGEMENTS

The work presented in this thesis was carried out in the Department of Chemical Engineering at the University of Stellenbosch, South Africa.

I wish to express my most sincere appreciation to:

DEDICATION

Hierdie graad word opgedra aan my familie – Baie dankie vir al julle ondersteuning

LIST OF FIGURES

LIST OF TABLES

LIST OF SYMBOLS

[]	denotes the concentration of a specie in the metal
()	denotes the concentration of a specie in the slag
A	area [m]
abs	absolute value
$a_{S^{2-}}$	activity of sulphur $[(\text{wt}\%S) \cdot f_{S^{2-}}]$
b	regression coefficients
$C_{Ca}^{r_i}$	calcium concentration on the surface of unreduced core of the calcium carbide particle [mol/m³]
$C_{Ca/S}^{ip}$	calcium / sulphur concentration on the surface of calcium carbide particles [mol/m³]
$C_{Ca/S}^{ib}$	calcium / sulphur concentration on the surface of carrier gas bubble [mol/m]
C_D	drag coefficient
Cov	covariance
C_P	molar density of particles [mol/m³]
Cp	specific heat capacity at constant pressure [J/kg/K]
$C_{S/Ca}$	sulphur / calcium concentration [mol/m³]
$C_{S/Ca,i}$	initial sulphur / calcium concentration in the metal [mol/m³]
C_S^{pl}	sulphur concentration in the plume [mol/m³]
C_S^{Slag}	sulphur concentration in the slag [mol/m³]
C_S^{b}	sulphur concentration in the bulk metal [mol/m³]
$D_{Ca,eff}$	effective diffusivity of calcium in liquid iron [m²/s]
D_O	outside diameter of lance orifice [m]
$D_{S/Ca}$	diffusivity of sulphur / calcium in liquid iron [m²/s]
d	diameter [m]
F	force [Newton]
F	f-statistic
F_{gp}^{B}	buoyancy force on the gas-powder in the liquid [N/m]

F^B_p	buoyancy force on the powder in the liquid [N/m]
F^D_{gp-l}	drag force on the gas-powder (in gas) mixture [N/m]
F^D_{p-l}	drag force on the powder in the liquid [N/m]
f	fraction of powder inside gas bubbles
$f_{O/S}$	activity coefficient of oxygen / sulphur
$f_{O^{2-}}$	oxide activity coefficient
$f_{S^{2-}}$	sulphide activity coefficient
g	gravitational acceleration [m/s^2]
G_1	heat transfer function for radiation [W/m^3/K^4]
$G_{2, 3, 4}$	heat transfer functions for convection [W/m^3/K]
h	heat transfer coefficient [W/m^2/K]
H	depth of the plume [m]
J	mass transfer function [1/s]
K_{eq}	equilibrium constant of reaction
k	mass transfer coefficient [m/s]
k	amount of independent variables in the regression function
kc	thermal conductivity [W/m/K]
L_S	sulphur partition ration
M	mass [kg]
M	represents Ca, Mg, Mn, Fe, Si
Mr	molecular weight [mol/g]
METWT	mass of iron [kg]
MFRP	mass flow rate of desulphurisation reagent [kg/s]
MFRG	mass flow rate of the carrier gas [kg/s]
MSE	mean square due to error
MSR	mean square due to regression
N_{specie}	molar flux of specie [mol/m^2·s] - (Na, Ca, S)
n	number of data rows represented in the sampling group
P	pressure [Pa]
Pr	prantl number
p_{O_2}	partial pressure of oxygen [Pascal]
p_{S_2}	partial pressure of sulphur [Pascal]
Q_{gm}	mean gas flow rate [m^3/s]
QR	volumetric flow rate of the carrier gas [m^3/s]

q	heat transfer rate [W] [
R	universal gas constant [J/kg/K]
R_{Ca}	Rate of mass transfer of calcium vapour through product layer [mol/s]
Re	reynolds number
R_{eng}	engineering gas constant [J/kg/K]
$R_{s, bl}$	rate of mass transfer of sulphur through hot metal boundary layer around the calcium carbide particle [mol/s]
$R_{S,total}$	total rate of mass transfer of sulphur across particle / metal Interface [mol/s]
R_{specie}	rate of reaction of specie [mol/m^3·s]
r	coefficient of correlation
r^2	coefficient of determination
r_o	distance from center of particle to outer shell [m]
r_i	distance from center to surface of unreduced core [m]
Sc	Schmidt number
Sh	Sherwood number
SSE	sum of squares of error
SSR	sum of squares of regression
SST	sum of squares of the total
S_{XX}	sum of squares of the independent variable(s)
S_{XY}	sum of cross-products of the dependent and independent variable(s)
S_{YY}	sum of squares of the dependent variable(s)
t	time [s]
T	temperature [K]
Temp	temperature of the iron [K]
U	velocity [m/s]
U_{l-ini}	initial liquid velocity at the bottom of the plume [m/s]
U_{p-ini}	initial particle velocity at the bottom of the plume [m/s]
V	volume [m^3]
X	independent variable
Y	variable

$\hat{Y}$ dependent variable

Z   vertical distance from bottom of the plume [m]

Greek characters

ρ density of the bubble-powder mixture [kg/m^3]

θ phase volume fraction

σ Stefan-Boltzman constant [W/m^2/K^4]

ε emissivity / a constant value in Equation 2.35 / error approximation

α molar fraction of particle phase reacted (utilisation)

ν kinematic viscosity [m^2/s]

μ effective viscosity [kg/m/s]

Subscripts

atm   atmosphere

b   bubble

g   gas

l   liquid

L   ladle

m   mixture of particles and gas

p   particle

pg   particles trapped inside the gas

S   sulphur

p   particle

Res   residence time

ts   topslag

Term   terminal

Superscripts

b   bulk or buoyancy

ib   bubble-particle interface

ip   particle-liquid interface

pl   plume or particle associated with liquid

ts   topslag

CONTENTS

1. INTRODUCTION

BACKGROUND

Sulphur is a very problematic impurity in the steelmaking industry, contributing to unwanted metallic characteristics like brittleness. Brittleness in the region of the solidus temperature is believed to be due to continuous intergranular liquid films between the cracks of the solidified steel. One of the reasons for the formation of these liquid films is the presence of impurities like sulphur in the steel. Sulphur will be rejected to the grain boundaries of primary austenite grains, promoting intergranular weakness and solidification cracking. Sulphur, apart from segregating to the grain boundaries, may also separate out to crack tips of the interdendritic regions in the steel where it will lower the melting point and reduce intergranular cohesion and strength of the steel (Lancaster, 1993).

Inside a blast furnace, sulphur is introduced into the iron through the organic sulphur found in the coke and coal, the pyritic materials within the iron ore, the sulphides associated within the ore and recycled material and scrap used during steelmaking. Upon tapping of the blast furnace melt, all possible iron oxide would have been reduced to elemental iron and the melt itself would be highly reduced and saturated with carbon. It is under these extremely reducing conditions that the removal of sulphur from the melt is at an optimum and the reason why most of the metal produced in the iron blast furnace is desulphurised before steelmaking.

At the majority of steel plants, desulphurisation of the blast furnace iron takes place inside a ladle via the injection of a desulphurising agent through a ceramic lance immersed in the metal. Processes using injection of gas-solid mixtures as a means of desulphurising the iron had been suggested as early as 1956 and is now being used on a large scale. Currently the use of powder injection technology to treat hot metal or steel is a key step for mass production of higher quality steel with low sulphur impurity levels.

SALDANHA STEEL: PROBLEM STATEMENT

Saldanha Steel is a state-of-the-art steel mill located on South Africa's west coast. The export-focussed plant is in close proximity to the deep-sea port of Saldanha and employs 800 staff. The plant commissioned its first hot rolled coil (HRC) in late 1998 and is currently ramping up production to its nameplate capacity of 1.25 million tons per annum. The ISO 9002 and ISO 14001 accredited plant is the only steel mill in the world to have successfully combined the Corex/Midrex process into a continuous casting chain. This process replaces the need for coke ovens and blast furnaces, making the plant a world leader in emission control and environmental management. Based on the mini-mill concept, the facility is smaller and more efficient than traditional 'integrated' steel mills, which generally have capacities of over 4 million tons per annum. The continuous production chain is exceptionally short, taking only 16 hours from the time iron ore enters either the Corex or Midrex units to the end product. All the individual processes are linked very closely with virtually no intermediate or process stock between the units.

At Saldanha Steel the desulphurising agent used for desulphurisation is calcium carbide with reaction taking place in accordance to the following equation (Irons, 1999).

$$CaC_2 + S_{(\% \, in \, Fe)} \iff CaS + 2C \qquad (1.1)$$

❑ Current utilisation of the CaC_2 particles at the Liquid Iron Desulphurisation (LID) section at the Saldanha Steel plant is between 30 and 35% of that expected from the above-mentioned stoichiometric reaction (See Appendix C.4). This type of problem is indicative of kinetic limitations.

❑ Owing to unassailable process constraints at the LID unit, a representative sample of the iron can only be taken before and after the calcium carbide injection cycle has been performed, with subsequent laboratory analyses providing little or no insight into the kinetic path of the process itself.

This current lack of kinetic knowledge, combined with a limited fundamental understanding of the desulphurisation process can lead to erroneous and uninformed decisions concerning the important control variables influencing the eventual overall calcium carbide utilisation.

OBJECTIVES

Since injection is the predominant desulphurisation process, the iron and steel industries' quest to improve energy utilisation, reduce capital costs and boost operating flexibility has put focus on the optimal design of the procedure. It is therefore imperative to gain a better understanding of the fundamental kinetic principles that govern the desulphurisation

process, thereby providing an improved quantitative comprehension of the calcium carbide injection procedure at Saldanha Steel.

More specifically, the main objectives of this work are as follows

❑ To conduct a review of literature and highlight the thermodynamic, kinetic and technological aspects of the desulphurisation process and investigate the occurrence and behaviour of sulphur in slag and iron during smelting and refining

❑ To explore actual desulphurisation data provided by Saldanha Steel to see if employing linear and non-linear modelling techniques can capture underlying patterns.

❑ To develop a one-dimensional quasi-steady state model for the momentum; heat and mass transfer in an ascending gas-liquid-powder plume for the conditions relevant to the Saldanha Steel desulphurisation injection process, along with a model accounting for the contribution of topslag (carry over as well as reagent flux) to the overall desulphurisation rate.

❑ Verification of the general applicability of the model against actual data obtained from Saldanha Steel

❑ To investigate the influence of process variables on the final outcome of the desulphurisation process

❑ To perform a preliminary cost estimation of suggested changes to the process

2.   LITERATURE STUDY

THE DETRIMENTAL EFFECT OF SULPHUR ON IRON

Sulphur is a very undesirable element in steel and if possible, the steel industry would remove all traces of sulphur from the final product (Hayes, 1993).   There are numerous areas in manufacturing, engineering, production and business where the deleterious effects of sulphur regrettably play an important role. Welding is of extreme importance to all these sectors and a subject where an extensive knowledge of sulphur inclusions and their effects are imperative. The problems experienced in the welding industry will be used as an example of the potentially detrimental effects of sulphur inclusions.

Welding

Welding relies on the bulk melting of the parts to be joined and joints are made by fusing and running together adjacent edges or surfaces.

In fusion welding, the heat-affected zone is the base metal that acts as the parent of the welded joint. The solidified weld metal part (weld deposit zone) is the metal generated by a fusible electrode in for example arc welding, the most important of the fusion processes.

In general the heat-affected zone may be divided into two regions:

- The high-temperature region, in which major structural changes such as grain growth take place
- The lower temperature region, in which secondary effects such as precipitation may occur.

Sulphur inclusions in the metal not only negatively affects the welding process itself but also contributes to other sometimes-unwanted metallic characteristics like brittleness inside the weld deposit zone. The restrained contraction of a weld deposit and the heat-affected zone during cooling sets up tensile stresses in the joint and sulphur plays a very detrimental part in one of the most serious of weld defects known as solidification cracking (Callister, 1994).

Solidification Cracking

The mechanical properties of the metal in the region of the solidus are important in relation to solidification cracking. On cooling a liquid alloy after welding below its liquidus temperature, solid crystals are nucleated and start growing until, at a certain temperature, they join together and form a coherent, although not completely solidified, mass. At this temperature (the coherence temperature) the alloy first acquires mechanical strength. At first it is a little brittle, but on further cooling to the nil-ductility temperature, ductility appears and rises sharply as the temperature is reduced still further. The interval between the coherence and nil-ductility temperatures is known as the brittle temperature range. Alloys that have a long brittle range are usually very receptive to weld cracking, whereas those having a short brittle range are not. Brittleness in the region of the solidus temperature is believed to be due to continuous intergranular liquid films between the cracks. One of the reasons for the formation of these liquid films is the presence of impurities like sulphur in the steel. A film will only form if the liquid's surface energy is lower relative to the surface of the grain boundary, in other words, if the liquid is capable of wetting the grain boundaries (Lancaster, 1993).
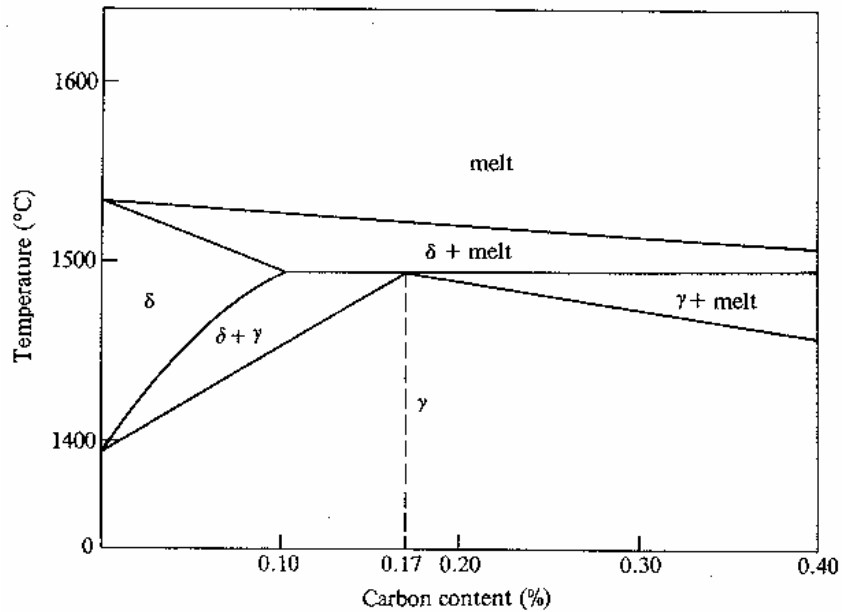
Figure 2.1 A section of iron-carbon equilibrium diagram showing the peritectic reaction (Lancaster, 1993)

Figure 2.1 shows the peritectic section of the iron-carbon equilibrium diagram. When the carbon content is below 0.10 %, the metal solidifies as δ-ferrite. At higher carbon contents, the primary crystals are γ-austenite but just below 1500°C, a peritectic reaction takes place and the remainder of the weld solidifies as austenite.

The solubility of sulphur in ferrite as shown in Figure 2.2, is relatively high, but in austenite it is relatively low. Consequently, there is a risk with C > 0.1 % that sulphur will be rejected to the grain boundaries of primary austenite grains, promoting the above-mentioned intergranular weakness and solidification cracking.
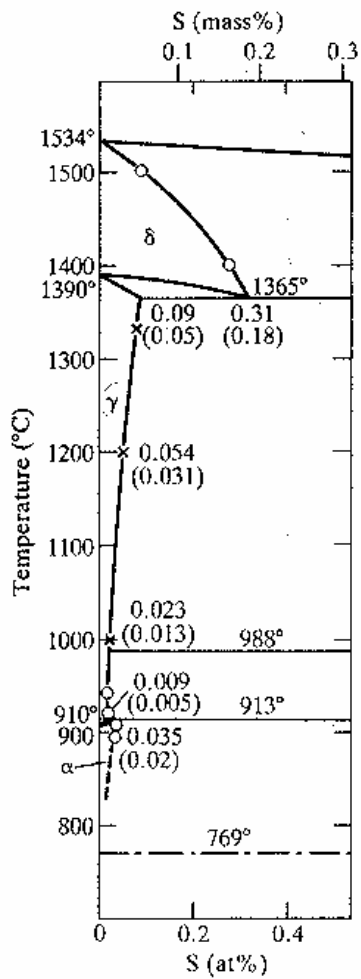
Figure 2.2 Part of the Fe-S binary equilibrium diagram (Lancaster, 1993).

Sulphur, apart from segregating to the grain boundaries, may also separate out to crack tips of the interdendritic regions (Figure 2.3) where it will lower the melting point and reduce intergranular cohesion.
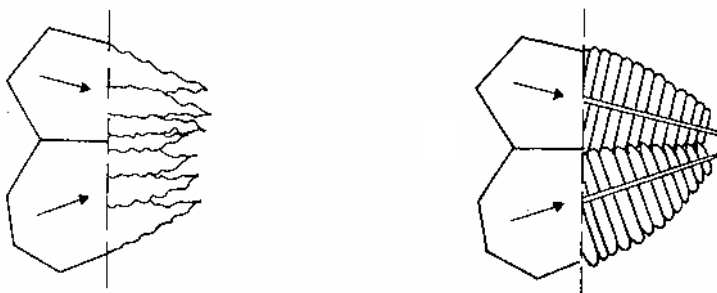
Figure 2.3 Solidification modes: Cellular dendritic and columnar dendritic growth (Lancaster, 1993).

When manganese and sulphur are both present though, the manganese does tend to globularise the sulphides. This phenomenon will therefore inhibit the development of intergranular sulphide liquid films in the weld deposit and heat-affected zone and will hinder further crack formation. The higher the carbon content though, the higher the manganese sulphur ratio has to be to avoid cracking as can be seen from Figure 2.4.
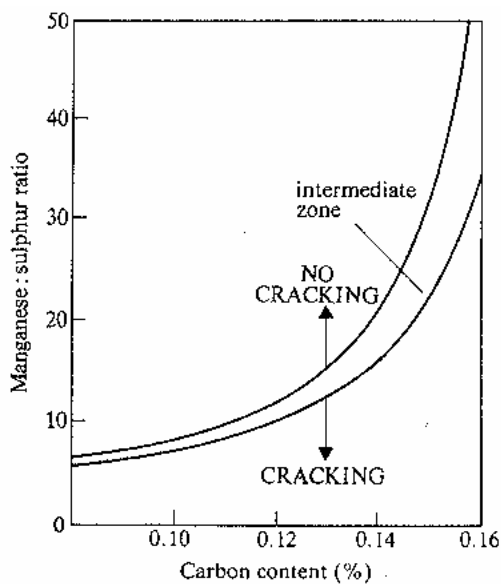
Figure 2.4 The effect of manganese/sulphur ratio and of carbon content on the susceptibility of carbon-steel weld metal to hot cracking (Lancaster, 1993)

Overheating

Upon heating carbon or ferritic alloy steels (in the heat-affected zone) through the temperature range between the upper critical temperature and close to 1200 °C, the austenite grains form and grow relatively slowly but above a specific point called the grain coarsening temperature, the rate of growth increases sharply. In this coarse-grained region of the heat-affected zone, the steel has been raised to temperatures that are in the overheating ranges. Overheating is a common phenomenon in forging technology. Upon slowly cooling steel that has been held at or

above the grain coarsening temperature, the material is embrittled. The embrittlement is due in most instances to the solution of sulphides at high temperature, followed by their reprecipitation at grain boundaries on cooling through the austenite range (Lancaster, 1993).

Hardenability

Sulphide inclusions have an effect on the hardenability of the heat-affected zone. They nucleate ferrite within the transforming austenite grains and this produces a lower hardness than what is attainable in "cleaner" steel.

Lamellar tearing

By the same mechanism of segregation of sulphur to the grain boundaries, another type of defect is also promoted. Lamellar tearing is a form of cracking that occurs in the base metal of a weldment due to the combination of high-localised stress and low ductility of the steel in the "width" direction and is encouraged by sulphide inclusions.

The preceding defects serve as examples of the deleterious effects of sulphur inclusions in iron and steel and serve as enough rationale as to why sulphur removal should remain a top priority.

However, before attempting to understand the dynamics of sulphur in iron it is important to first comprehend how and especially where this detrimental inclusion enters the melt.

BLAST FURNACE

The traditional blast furnace still remains the most popular crude iron extraction process from iron ore. Within a blast furnace two critical functions have to be performed. Firstly, the oxygen combined with the iron in the ore (O in FeO, Fe_2O_3 and Fe_3O_4) must be removed. This is accomplished by chemical reaction between the iron oxides and carbon in the form of coke to produce carbon monoxide, carbon dioxide and metallic iron. Secondly, the process must separate the produced metal from the remaining non-metallic or gangue content of the ore, as well as from the ash residue of the coke. This is achieved by melting the charge and allowing differences in density to cause a separation into a layer of slag containing most of the unwanted non-metallic components that floats on top of the liquid metal.
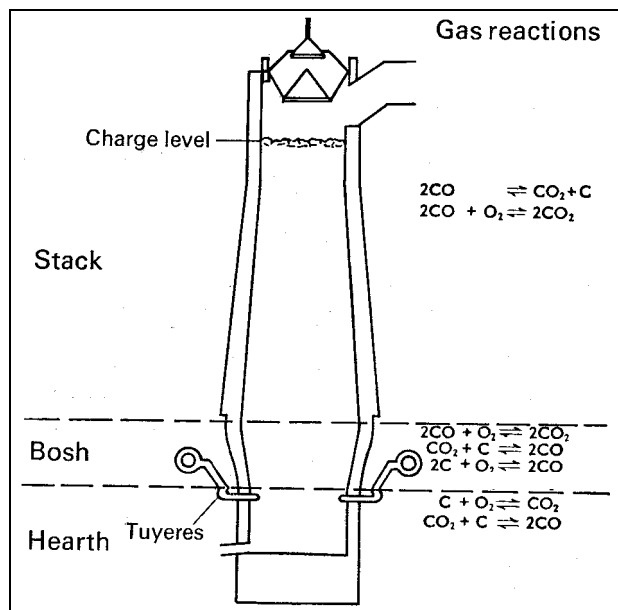
Figure 2.5 The traditional blast furnace (Bodsworth, Bell, 1972).

Immediately preceding the tapping operation the pool of molten metal and slag extends upwards from the bottom of the hearth almost to the tuyere zone. At intermediate times the liquid level varies between these

limits. All the ore is molten by the time it descends to the hearth, but a column of coke, also known as the "dead man" extends to below the upper surface of the slag and possibly to the bottom of the furnace. The inverted, cone section over the hearth is called the bosh and above that is the stack. The temperature decreases fairly uniformly with increasing height above the tuyeres to about 1100°C at the top of the bosh and to about 800°C mid-way up the stack. At this height the temperature decreases rather rapidly to between 550 and 600°C and then continues to decrease at a slower rate, reaching 200 to 250 at the top of the furnace.

At Saldanha Steel the traditional blast furnace has made way for a melter-gasifier called a Corex.   The Corex operates a reduction shaft furnace with CO-H_2 reducing gases, to manufacture direct-reduced iron (DRI). The Corex fulfils several functions:

❑ The burden that leaves the reduction shaft is perhaps 85% metallised and the melter-gasifier completes the reduction
❑ It melts the iron, gangue and fluxes to from hot metal and slag
❑ The reduction gasses utilised by the reduction shaft is produced inside the Corex by burning coal and oxygen

To some extent, the lower part of the Corex performs a similar function to the lower part of a conventional blast furnace (Geldenhuis, 2000): metal and slag pass through a packed bed of reductant (char, often with added coke) on their way to the tapping holes. The final compositions are established during this transport process through the "dead man". This similarity means that the Corex hot metal composition is similar to that of blast furnace hot metal and implies that understanding gained in the blast furnace on how to control – for example – the sulphur levels

should be helpful in devising appropriate process stabilisation and control strategies for the Corex.

For a detailed process description covering the path between the Corex up to the tapping of the Conarc, refer to Appendix F.

ENTRY OF SULPHUR INTO THE IRON THROUGH THE BLAST FURNACE

Upon tapping of blast furnace (or Corex in the case of Saldanha Steel) melt, all possible iron oxides have been reduced to elemental iron and the melt itself would be highly reduced and saturated with carbon. With the iron in such a highly reduced state, it could quite easily pick up sulphur (Rosenqvist, 1974). Although some of the sulphur will be removed from the metal in the hearth of the blast furnace as the iron droplets pass through the slag layer, unacceptable sulphur levels are still found dissolved in the hot metal.

Sulphur can be introduced into the iron through:
❑ organic sulphur found in the coke and coal,
❑ pyritic materials within the iron ore,
❑ sulphides associated with lime,
❑ recycled material and ore that is used in the blast furnace and
❑ scrap used during steelmaking.

It is under these extremely reducing conditions right after tapping of the blast furnace, that 90% of the metal produced in the iron blast furnace is desulphurised and some of the reasons are as follows:

- The activity coefficient of sulphur in the hot metal before steelmaking is much higher than that of sulphur in steel, which means desulphurisation can be accomplished more easily in hot metal

- The higher the carbon activity of the iron the higher the sulphur slag-metal partition (Ls – refer ot Section 2.6.1.3). This is related to the oxygen potential of the slag-iron system and illustrates the fact that conditions in the hot metal before steelmaking are favourable due to the low oxygen potential.

Desulphurisation is therefore the removal of sulphur from the liquid metal by reducing the elemental sulphur in the melt (Richardson, 1974), then allowing it to bond to a suitable cation and forcing the formed compound to be transferred from the melt to the molten slag phase suspended on top of the metal phase.

INJECTION TECHNOLOGY

The early processes (Bodsworth, 1972) of ladle desulphurisation involved the addition of soda ash to the ladle before tapping the blast furnace iron, mixing in this case depending on the energy of the metal stream entering the ladle. Processes using injection of gas-solid mixtures had been suggested as early as 1956 and are now being used on a large scale. Currently the use of powder injection technology to treat hot metal or steel is a key step for mass production of higher quality steel with low costs. The main purpose of this submerged lance technology for steelmaking processes can be outlined in the following advantages:

- The reagent is in powder form and that establishes a large contact area between the reactants. Favourable kinetic conditions for refining reactions are obtained in this way (see Section 6.3.2).

❑ The metal agitation promoted by the gas injection improves the sulphur transfer as the metal-slag interface gets renewed continuously.

❑ Refining reactions can be carried out in simple vessels allowing the refining processes to be divided into separate stages so as to eliminate thermodynamic conflicts between e.g. desulphurisation and dephosphorisation.

The desulphurising agents used are soda ash, calcium oxide, calcium carbide and calcium cyanamide or mixtures of these. Nitrogen or argon is normally used as the carrier gas and the materials injected through a lance immersed in the ladle of molten iron. The desulphurising agent in these compounds is calcium and sulphur is removed as calcium sulphide. At the temperatures involved CaS is solid and if calcium oxide is used the minimum sulphur content can be calculated to be in equilibrium with CaO and CaS at unit activity, i.e.

$$C + CaO + S_{(\% \, in \, Fe)} \quad \Leftrightarrow \quad CaS + CO \left(\log K_{eq} = -\frac{5767}{T} + 5.824 \right) \quad (2.1)$$
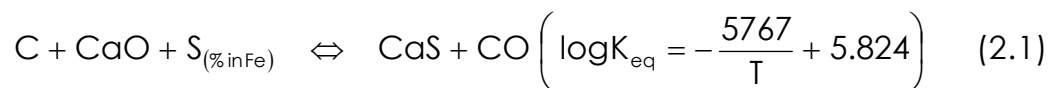
At 1400°C for a typical basic iron the equilibrium sulphur content for a carbon monoxide pressure of one atmosphere would be 0.001 weight %. In practice the reaction is a solid-liquid one and the kinetic consideration limit the degree of desulphurisation. Sulphur levels as low as 0.015 weight % have been reported for lime injection (Bodsworth, 1972).

Using calcium carbide extremely low sulphur contents are theoretically possible, i.e. for the reaction:

$$CaC_2 + S_{(\% \, in \, Fe)} \quad \Leftrightarrow \quad CaS + 2C \left(\log K_{eq} = \frac{9050}{T} - 5.8 \right) \quad (2.2)$$

the sulphur content in equilibrium with unit activities of carbon, calcium sulphide and calcium carbide is 10^{-6} weight % at 1400°C. Sulphur contents of 0.008 weight % have been achieved in practice.

FUNDAMENTALS OF DESULPHURISATION

When the injection process is used, desulphurisation of hot metal occurs in the ascending plume of the injected calcium carbide, as well as the top slag-metal interface consisting of both the injected flux and some carry-over slag from the blast furnace. The following section takes a more in-depth look at the two individual reaction zones.

Topslag

Sulphide and sulphate equilibria

In view of the deleterious effect of sulphur in steel, the behaviour of sulphur in slags has been the object of numerous investigations since the groundbreaking work done by Richardson and Fincham in the 1950's (Richardson, 1952). The slag mixtures studied up until then had usually been complex and the method used had mostly been the measurement of sulphur distribution (Ls) between a molten slag and molten iron after equilibrium has been achieved. With such a method it is not possible to distinguish satisfactorily the separate effects of slag composition and oxygen potential on the sulphur distribution (Ls).

In order to effectively investigate these parameters separately, studies were carried out on the partition of sulphur between flowing gases of controlled oxygen and sulphur potentials and various silicate and aluminate slags at temperatures between 1450°C and 1650°C.

The general gas-slag equilibria method would then require samples of slags to be brought under equilibrium with gas mixtures consisting of combinations of any of the following gases: H_2, H_2S, CO_2, SO_2, CO, Ar, S_2 and N_2. The mixture is then controlled in such a way as to produce the desired partial pressures of oxygen and sulphur at the given temperatures (Nzotta, 1997).

It was shown (Richardson, 1954) that in the reaction of sulphur bearing gases with polymeric melts, the sulphur dissolves in the melt as sulphide ions (S^{2-}) at partial pressures of oxygen below about 10^{-5} atm.

$$SO_2 + \left(O^{2-}\right) \; = \; \left(S^{2-}\right) + \tfrac{2}{3}O_2 \qquad\qquad (2.3)$$

At an oxygen partial pressure of above 10^{-3} atm the sulphur will enter the melt as sulphate ions (SO_4^{2-}).

$$SO_2 + \tfrac{1}{2}O_2 + \left(O^{2-}\right) \; = \; \left(SO_4^{2-}\right) \qquad\qquad (2.4)$$

The result of these two opposing effects is that the sulphur content of a slag in equilibrium with a gas of constant sulphur content has a minimum at an oxygen partial pressure of about 10^{-4} – 10^{-5} atm., depending on the temperature (Analects, Lee, 1993).

In gases consisting of sulphur, oxygen, hydrogen and carbon (irrespective of the argon and the nitrogen), the sulphur exists in several gaseous forms, e.g. S, S_2, SO, SO_2, SO_3, HS, H_2S, COS and CS. These species will have definite partial pressures in equilibrium with one another at the reaction temperature and that is why it can be motivated that any one of the desired forms may be used in representing the gas-slag reaction. For that reason the sulphide mass transfer reaction between the gas and the slag may be represented by:

$$\tfrac{1}{2}S_2 + \left(MO^{2-}\right) \quad = \quad \tfrac{1}{2}O_2 + \left(MS^{2-}\right) \qquad (2.5)$$

for which the equilibrium constant for a given temperature is represented by:

$$K_{(2.5)} \quad = \quad \left(\frac{(\%wtS)\cdot f_{S^{2-}}}{a_{O^{2-}}}\right)\cdot\left(\frac{p_{O_2}}{p_{S_2}}\right)^{\!\!\tfrac{1}{2}} \qquad (2.6)$$

Determination of $K_{(2.5)}$ requires the successful measurement of two thermodynamic properties namely the activity of oxide ions and the activity coefficient of sulphur in the melt. Being such difficult properties to quantify, another equilibrium relation called the sulphide capacity was defined.

Sulphur Capacities of Slags

By applying two functions termed the sulphide and sulphate capacities, the results obtained for melts of various compositions, oxygen and sulphur partial pressures at constant temperatures (and vice versa) can be compared with one another.

The sulphide equilibria in melts can therefore be represented by Equation 2.5, provided that no significant proportion of the sulphur held in the slag is linked to silicon or aluminium, as for example in SiS_2 or Al_2S_3 (Richardson, 1954).

In turn, the sulphide capacity (Cs) can be represented by:

$$Cs \quad = \quad K_{(2.5)}\cdot\left(\frac{a_{O^{2-}}}{f_{S^{2-}}}\right) \quad = \quad (\%wtS)\cdot\left(\frac{p_{O_2}}{p_{S_2}}\right)^{\!\!\tfrac{1}{2}} \qquad (2.7)$$

where $\quad p_{O_2} \quad < \quad 10^{-5}\,atm$

measured under conditions where the sulphur is present only as sulphide ($p_{O_2} < 10^{-5}$ atm), as indicated by the partial pressure requirement.

The sulphide capacity (Cs), as the terminology implies, is a measure of the extent to which a slag can hold sulphur in solution.

It shows the reactivity of the slag to sulphur in the atmosphere above the slag. It must also be mentioned that at a given temperature and slag composition the equilibrium concentration of sulphur in the melt is therefore determined by the <u>ratio</u> $\left(\dfrac{p_{O_2}}{p_{S_2}} \right)^{\frac{1}{2}}$ in the gas phase and not by the individual partial pressures of oxygen and sulphur.

In turn, the equilibrium constant, $K_{(2.5)}$, is a function of temperature and the standard Gibbs energy.

$$K_{(2.5)} \quad = \quad e^{\left(\frac{-\Delta G}{RT} \right)} \qquad\qquad (2.8)$$

This all means that sulphide capacity is directly measurable and can be used to compare widely differing mixtures of oxide slags commonly utilised in iron and steelmaking processes all over the world. The sulphide capacity (Cs) does however not take into account the effect of the various inclusions in the slag on the activities of the sulphur and oxygen ions in a metal-slag system and it is only through defining another thermodynamic property called the sulphur distribution ratio that we can fully explore these effects.

Sulphur Distribution Ratio

At iron- and steelmaking temperatures, elemental sulphur is only stable as a gas but it can be dissolved to form a liquid solution in the slag and

the metal. The control of the sulphur content in the metal must therefore be considered in terms of two different partitionings:

❑ The partitioning between the gaseous compounds containing sulphur and the sulphur in solution at the gas-liquid interface

❑ The partitioning of sulphur between the slag and the metal at the slag-metal interface.

As seen in the previous section, the sulphide capacity expression is the result of studies conducted between slags and gasses of known concentrations and temperature, not taking into account the effect of the various components of the slag on the activities of the sulphur and oxygen ions in a metal-slag system. In order to study the effects of these and various other variables on the desulphurisation process, the partitioning of sulphur between the slag and the metal needs to be taken into account. This partition is called the sulphur distribution (L_S) and is a measure of the thermodynamic ability of a slag to contain sulphur.

Equilibrium considerations

The partitioning of sulphur between the slag and the metal is sometimes considered in terms of three simultaneous reactions that can be expressed as the following:

$$MS_{(Fe)} \iff MS_{(slag)} \qquad\qquad\qquad (2.9)$$

$$MO_{(slag)} + X_{(Fe)} \iff M_{(Fe)} + XO_{(slag\ or\ gas)} \qquad\qquad (2.10)$$

$$MS_{(slag)} + CaO_{(slag)} \iff CaS_{(slag)} + MO_{(slag)} \qquad\qquad (2.11)$$
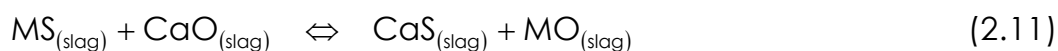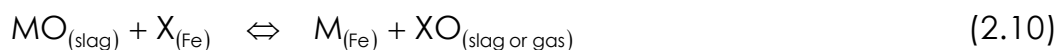
❑ M represents Fe, Mn and Si.

❑ X represents an element such as Al, C, MnO, Mg and Si which combines with the oxygen dissolved in the iron.

The disadvantage of treating the partition in such a way is that only CaO is considered to take part in stabilising the sulphur in the slag. An even better way of representing the partition of sulphur between metal and slag is by expressing them in ionic form.

The transfer of elemental sulphur from the metal into the slag can be written as:

$$S_{(Fe)} + 2e^- \quad \Leftrightarrow \quad S^{2-}_{(slag)} \qquad (2.12)$$

where the $2e^-$ represents the acquisition of two negative electron charges by each atom of sulphur that is transferred across the slag-metal interface. For there to be electro-neutrality, a simultaneous but opposite exchange of electrons across the interface is required – one that releases electron charges as it enters the slag. The transfer of iron as it crosses the interface is used as an example:

$$Fe_{(metal)} \quad \Leftrightarrow \quad Fe^{2-}_{(slag)} + 2e^- \qquad (2.13)$$

In the same way the transfer of one Si atom will release four electrons into the slag and the transfer of one Al atom across the interface will release three electron charges into the slag.

Regard the two electrons absorbed by the sulphur as being transferred from an oxygen ion, which crosses the interface in the reverse direction and enters the metal to take part in the normal oxidising reactions represented by Equation 2.11. The sulphur transfer reaction in terms of the ionic species in the slag can then be written as:

$$S_{(Fe)} + O^{2-}_{(slag)} \quad \Leftrightarrow \quad O_{(Fe)} + S^{2-}_{(slag)} \qquad (2.14)$$

$$\text{with } K_{(2.14)} \quad = \quad \log\frac{(a_{S^{2-}})[a_O]}{(a_{O^{2-}})[a_S]} \quad = \quad -\frac{3750}{T}+1.996 \tag{2.15}$$

The sulphur distribution ratio (Ls) is probably expressed best in terms of the ratio of the weight % concentrations of sulphur in the slag and in the metal i.e.

$$Ls \quad = \quad \frac{(\% \, S)_{slag}}{[\% \, S]_{Fe}} \tag{2.16}$$

and is a quantitive indication of the sulphur bearing potential of the slag.

A simple evaluation of the two above-mentioned equations suggest that, at a given temperature, the sulphur distribution ratio (Ls) between the slag and the metal is raised by increasing either the activity of oxygen ions in the slag, increasing the activity of sulphur in the metal or by decreasing the oxygen activity in the metal (Nzotta, Sichen, 1996).

The sulphur distribution ratio of any slag-metal system is a function of numerous influential variables, one of which is the concentrations of solutes in the iron on the activity coefficient of the sulphur in the metal.
In the any steelmaking furnace, where the atmosphere is oxidising throughout the refining period, the sulphur distribution ratio varies from approximately 1 under acid slag to about 6 when the slag is saturated with basic oxides.
In typical blast furnace conditions it varies from about 20 (Bodsworth, 1972) for a silica-saturated slag to about 40 for a lime-saturated slag, for equilibrium at a metal temperature of 1500°C.
This big difference can be attributed to the vast amount and concentration of inclusions found in the blast furnace melt. As can be

seen in Figure 2.6, the activity coefficient of sulphur in the metal is raised by inclusions like Al, C, P and Si.
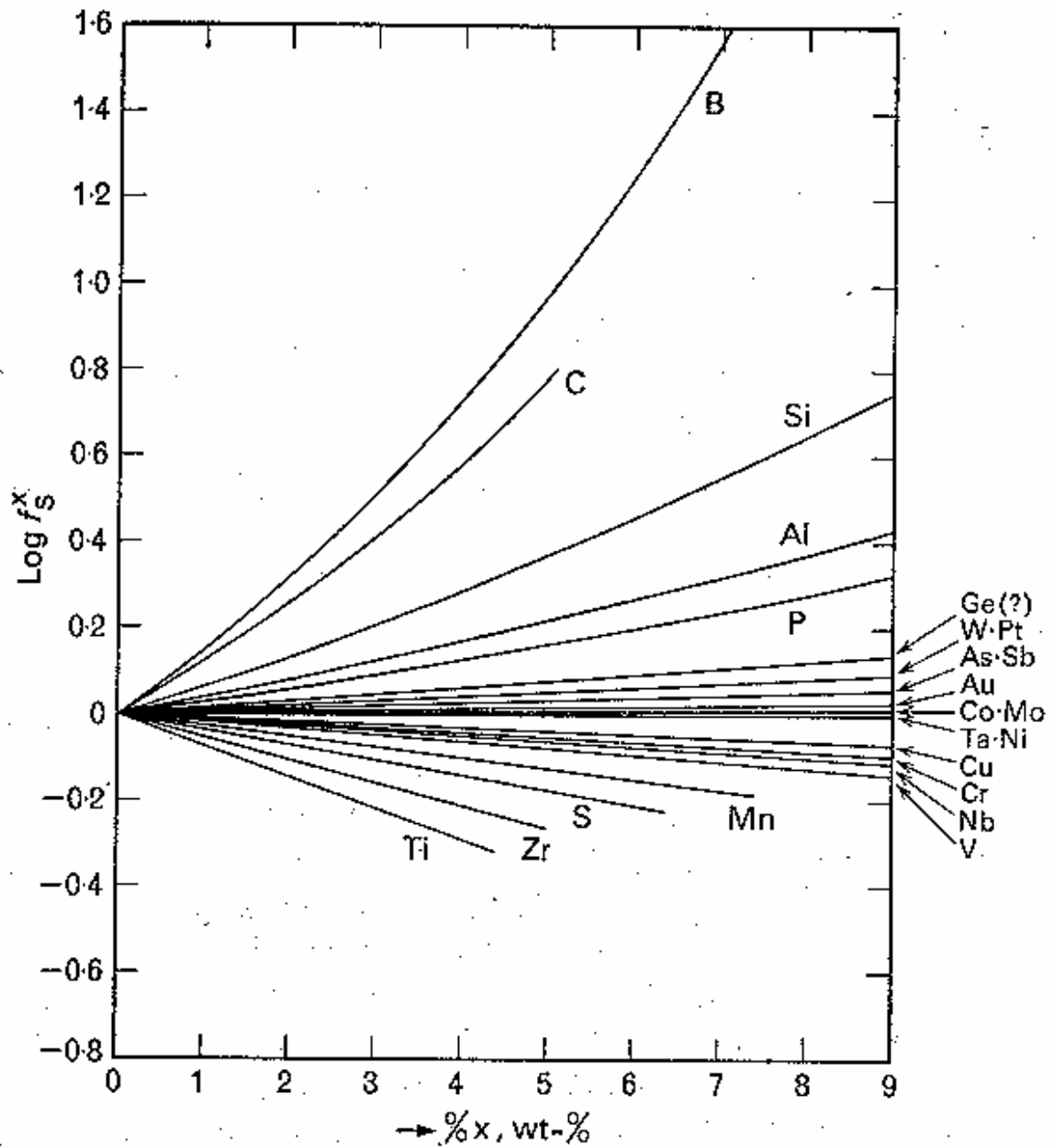
Figure 2.6 The effect of various elements on the activity coefficient of sulphur in liquid iron.

On the other hand, oxygen and nitrogen has no apparent effect on the activity coefficient and inclusion elements like Mn tend to decrease the sulphur activity coefficient.

This implies that the sulphur distribution ratio will be much higher at an early stage of iron production and become less and less substantial as the steel becomes more refined (concentration of solutes in the metal is low towards the end of the refining), therefore reducing the slags' ability to desulphurise the metal and one of the most important reasons why most desulphurisation steps are carried out before steelmaking. If all other conditions remain constant, the changing of the metal composition from that obtained at the blast furnace to normal range (e.g. plain carbon steel) accounts for a substantial decrease in the sulphur distribution ratio.

Kinetics of Topslag Desulphurisation

Three of the key observed experimental facts on the rate of desulphurisation between slag and metal are summarised (Chiang, 1987):

❏ The rate of reaction is enhanced with increasing slag basicity.
❏ The existence of reducible oxide in the slag reduces the rate of desulphurisation
❏ Improvement of bath stirring enhances the desulphurisation rate

The kinetics of sulphur between slag and hot metal has been reported to follow first order reaction kinetics with respect to sulphur. The overall transport process may involve the following three elementary steps

❏ Transfer of sulphur from the metal phase to slag/metal interface
❏ Chemical reaction at the slag/metal interface
❏ Transfer of sulphur from the slag/metal interface to the slag phase

Combining the individual steps the overall rate can be expressed as

$$R_S^{M/S} = \frac{A \cdot \left(C_S^b - \dfrac{C_S^{Slag}}{L_S} \right)}{\left(\dfrac{1}{k_{metal}} + \dfrac{1}{k_{reaction}} + \dfrac{1}{k_{slag}} \right)}$$

(2.17a)

For high temperature metallurgical systems, the chemical reaction is considered fast enough that equilibrium can be assumed. The overall reaction rate is then simplified to

$$R_S^{M/S} = \frac{A \cdot \left(C_S^b - \dfrac{C_S^{Slag}}{L_S} \right)}{\left(\dfrac{1}{k_{metal}} + \dfrac{1}{k_{slag}} \right)}$$

(2.17b)

Plume

During powder injection refining, the reagent powder is injected along with the carrier gas into the melt, creating a three phase ascending plume. When particles are injected into the melt, each particle either penetrates into the melt or is entrapped inside the bubble, depending on the surface properties, hydrodynamic situation and solubility of the reagent material (Talballa, 1976).

It is through contact of these particles (and bubbles) with the hot melt that desulphurisation within the plume takes place. To quantify the rate of desulphurisation in the ascending plume requires a good understanding of the various transfer phenomena influencing the bubbles, particles in the liquid, particles in the bubbles and the liquid itself.

A critical review of the detailed derivation of these and other transfer equations are beyond the scope of this report but certain key equations pertinent to the work are mentioned.

Fluid Transfer

The differential equations of fluid flow can be used in many cases as the starting point in the formulation of fluid mechanics problems, particularly when detailed knowledge of the velocity profile is desired. The differential equations are derived through the mathematical expression of the conservation of various fluid properties over an infinitesimal fluid volume.

The Equation of Continuity

Through the mathematical expression of the conservation of matter of a small fluid element, the equation of continuity is derived. At steady state conditions and for an incompressible fluid, the equation of continuity is

$$\frac{\partial u_x}{\partial x} + \frac{\partial u_y}{\partial y} + \frac{\partial u_z}{\partial z} = 0 \qquad (2.18)$$

The Equation of Motion

Through the mathematical expression of the conservation of momentum of a small fluid element, the equation of motion is derived. For steady state conditions, at constant viscosity for an incompressible flow and with viscous effect playing a negligible part the equation of motion in the x-direction is

$$\rho \left(u_x \frac{\partial u_x}{\partial x} + u_y \frac{\partial u_y}{\partial y} + u_z \frac{\partial u_z}{\partial z} \right) = -\frac{\partial P}{\partial x} + \rho g_x \qquad (2.19)$$

The term on the left represents the convective momentum influencing the control volume, with both terms on the right side of the equation corresponding to the sum of forces acting on the element.

Rising velocity of objects

Whether the element under investigation is a particle, a bubble or an infinitesimal fluid volume, for most metallurgical applications, the prime concern is to establish the net forces acting on the particle and hence to determine its relative velocity with respect to the fluid.

Drag force

When an object is in relative motion to a fluid in which it is immersed, a drag force is exerted on the object. Generally this force is expressed as (Szekely, 1971)

$$F_{drag} = C_{drag} A_{object} \left(\frac{\rho u^2_{relative}}{2} \right) \qquad (2.20)$$

The drag coefficient, C_{drag} is a function of the particular shape of the object as well as the object Reynolds number, which is defined as

$$Re_{object} = \frac{d_{object} \cdot u_{relative} \cdot \rho_{liquid}}{\mu_{liquid}} \qquad (2.21)$$

Buoyancy force

Any object completely or partially submerged in a fluid is buoyed up by a force equal to the weight of the fluid displaced by the body. Generally this force is expressed as (Serway, 1992)

$$F_{buoyancy} \quad = \quad \rho_{liquid} \cdot V_{object} \cdot g \qquad (2.22)$$

Even though the same considerations are used for the velocity calculation of both bubbles and particles, a bubble is not rigid and the forces acting on it may deform its shape. The behaviour of bubbles can be classified into four regions (Szekely, 1971):

- Very small bubbles: $Re_{bubble} \leq 2$
- Intermediate-size spherical bubbles: $2 < Re_{bubble} \leq 400$
- Spherical and ellipsoidal bubbles: $400 < Re_{bubble} \leq 5000$
- Spherical-cap bubbles: $Re_{bubble} > 5000$

Due to the high density of hot metal, the formation of sizeable bubbles at the orifice and the high gas-phase velocities achieved in vessels treated through injection, the Reynolds number of bubbles in pyrometallurgical systems often exceeds 5000 and the shape of the bubbles are spherical-cap as can be seen in Figure 2.7.
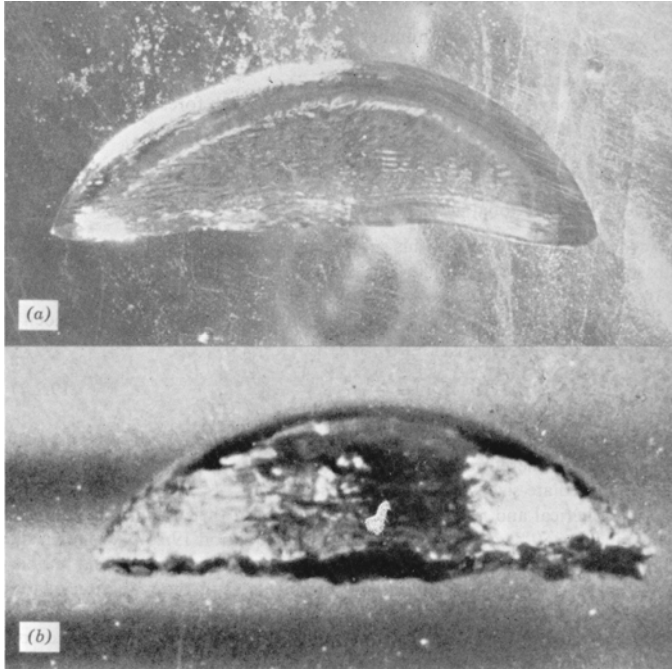
Figure 2.7 Spherical-cap bubbles (Szekely, 1971)

These spherical-cap bubbles rise at a terminal velocity, which is dependent only on the size of the bubble (and independent of the properties of the liquid) and is expressed as (Ilegbusi, Iguchi et al, 2000)

$$U_{terminal} = 1.02 \left(\frac{g\,d_{bubble}}{2} \right)^{\frac{1}{2}} \qquad (2.23)$$

Size of the bubbles

When gas is injected at high flowrate through submerged nozzles into high density metallic liquids, the subsequent volume (and therefore size) of the spherical-cap bubbles was found to be a function of the gas flowrate and the outside diameter of the orifice (Irons, 1978) and can be expressed as

$$V_{bubble} = 0.083 \cdot QR^{0.867} \cdot d_{orifice}^{0.435} \qquad (2.24)$$

Heat Transfer

The differential energy balance equations can be derived by expressing mathematically the conservation of energy over an infinitesimal fluid volume.

Convective Heat Transfer

The mechanism of heat convection is analogous to the convective transfer of momentum discussed in the previous section. Energy is moved from one part of the system to another as a result of the bulk motion of a fluid. The following assumptions can be made.

❑ The net input of kinetic energy by convection and heat energy into the control volume by conduction is negligible

❑ The rate of accumulation of kinetic energy and heat energy = 0

❑ The rate of work done by the fluid element on its surroundings include pressure and viscous forces together with work done against gravity and are considered negligible.

The resulting energy balance equation is (Szekely, 1971)

$$\rho C_P \left(u_x \frac{\partial T}{\partial x} + u_y \frac{\partial T}{\partial y} + u_z \frac{\partial T}{\partial z} \right) = dx\,dy\,dz\,(q) \qquad (2.25)$$

The total amount of heat transferred per unit time (W) may be represented by the following expression

$$q = h \cdot A \left(T_{fluid} - T_{object} \right) \qquad (2.26)$$

where h is called the heat transfer coefficient and depends on the property values of the fluid, the imposed flow field, the geometry of the system and the temperature difference. The heat transfer is therefore a quantity that is highly specific for a particular system.

Radiation Heat Transfer

Convective transmission of thermal energy requires the presence of fluid. On the other hand, heat transfer by radiation occurs by the transmission of photons or electro waves and does not require the presence of an intervening medium. The rate at which a surface-area emits radiant energy is represented by the following equation

$$q \;=\; A\varepsilon\sigma\left(T^4_{surface}\right) \tag{2.27}$$

The radiation emission rate of a substance is therefore proportional to the fourth power of its absolute temperature. The contribution of radiation to heat transfer is thus not significant at low temperatures but it becomes predominant at the temperature levels encountered in pyrometallurgical processing.

Mass Transfer

The differential mass transfer equations can also be derived by expressing mathematically the conservation of mass (of the species) over an infinitesimal fluid volume. If it is assumed that the diffusion flux due to the gradient of the species is negligible and the rate of accumulation of the species is zero, the equation can be expressed as

$$\left(\frac{\partial N_{specie} \cdot A_M}{\partial_x} + \frac{\partial N_{specie} \cdot A_M}{\partial_y} + \frac{\partial N_{specie} \cdot A_M}{\partial_z} \right) + \left(A_M \cdot R_{specie} \right) = 0 \quad (2.28)$$

Rate of desulphurisation reaction

Upon injection of calcium carbide into carbon rich metal, it partially decomposes to form calcium vapour and graphite (Talballa, 1976):

$$CaC_2 \Leftrightarrow \uparrow Ca_{(g)} + 2C_{(s)} \qquad\qquad\qquad (2.29)$$

The calcium vapour diffuses through the reaction product layer of calcium sulphide and residual graphite and reacts with sulphur transported through the hot metal boundary layer outside the particle. It forms calcium sulphide at the surface of the calcium carbide particle adjacent to liquid metal.

The overall desulphurisation reaction involves the following postulated steps:

❑ Mass transfer of sulphur through the boundary layer to the calcium particle surface
❑ Thermal decomposition of calcium carbide
❑ Diffusion of calcium vapour through the micro pores of the reaction product layer to the outer surface of the calcium carbide particle
❑ Chemical reaction of calcium with sulphur takes place at the interface of the calcium carbide particle and liquid hot metal

For high temperature metallurgical reactions, the chemical reaction rate is generally very fast. This means that the 3rd and 4th step in the above-

mentioned hypothesis are fast enough to ensure that they will not be rate limiting and can therefore be omitted.

Rate of mass transfer of sulphur through a hot metal boundary layer

The molar flow of sulphur from the bulk hot metal phase to the surface of the particle may be expressed as

R_S = (mass transfer coefficient)×(surface area)×(driving force)   (2.30)

For a spherical object the mathematical statement of the above-mentioned equation is

$$R_{S,bl} \quad = \quad k_p \cdot 4\pi r_O^2 \cdot \left(C_S^{pl} - C_S^{ip} \right)$$
(2.31)

It can be seen that the driving force for diffusion is the concentration gradient of sulphur between the plume and the surface of the calcium carbide particle. The phenomena of mass transfer between spherical particles surrounded by fluid can be described by the dimensionless group, which is used to correlate the mass transfer.

$$\text{Sherwood} \quad = \quad \text{function}\left(\text{Reynolds}_{[Re]}, \text{Schmidt}_{[Sc]}, \text{Grashoff}_{[Gr]}\right) \quad (2.32)$$

For the condition of forced convection (Gr = 0), the correlation for the mass transfer from a spherical particle can be expressed as

$$Sh \quad = \quad 2 + B \cdot Re_{particle}^{0.50} \cdot Sc_{particle}^{0.33}$$
(2.33)

where B is constant which falls in the range 0.3 – 1.0.

For the agitated system Sano et al (Sano, 1974), in their study of mass transfer to solid particles, proposed a correlation for dimensionless mass transfer coefficients by using Kolmogoroff's theory of local isotropy in agitated systems. Kolmogoroff's theory of local isotropy is used to account for the influence of the local turbulent flow field on mass transfer of a particle:

$$Sh = \frac{k_P d_P}{D_S} = 2 + 0.4 \left(\frac{\varepsilon d_P^4}{v^3} \right)^{\frac{1}{4}} Sc^{\frac{1}{3}} \tag{2.34}$$

where ε is given by

$$\varepsilon = \left(U_P - U_l \right) g \tag{2.35}$$

The phenomena of mass transfer between bubbles surrounded by fluid can be described by using the same dimensionless group as in Equation 2.34.

For the condition of forced convection (Gr = 0), the correlation for the mass transfer from a large spherical-cap bubble can be expressed as

$$Sh = 1.28 \left(Re_{bubble} \cdot Sc_{bubble} \right)^{\frac{1}{2}} \tag{2.36}$$

This equation can be combined with the equation for the rising velocity of spherical-cap bubbles (Equation 2.23) to yield the following simple expression for the mass transfer coefficient

$$k_b = 1.08 g^{\frac{1}{4}} D_S^{\frac{1}{2}} d_b^{-\frac{1}{4}} \tag{2.37}$$

Diffusion of calcium vapour through the product layer

The molar flow of calcium vapour through the reacted shell of calcium sulphide can be expressed as

$$R_{Ca} = -D_{Ca,eff} \cdot \left(\frac{4\pi r_o r_i}{r_o - r_i} \right) \cdot \left(C_{Ca}^{ip} - C_{Ca}^{r_i} \right) \qquad (2.38)$$

At steady-state conditions these two steps occur at the same rate and it is through this approach, together with mathematical manipulation, that an equation incorporating the two above-mentioned transfer mechanisms are combined to form an integrated overall rate expression.

$$R_{S,total} = -\left(\frac{\left(C_S^{pl} - C_{S,i} \right)}{\left(\left(\frac{1}{k_P \cdot 4\pi r_o^2} \right) + \left(\frac{r_o - r_i}{D_{Ca,eff} \cdot 4\pi r_o r_i} \right) \right)} \right) \qquad (2.39)$$

STATISTICAL ANALYSIS

The purpose of the following section is to formulate the basic concepts associated with regression analysis and to express ways to assess the appropriateness of the subsequent model.

Regression Analysis

Regression is the study of relationships among variables. The purpose of regression is to predict, or estimate, the value of one variable from known values of other variables related to it. In order to make

estimations, the important predictors influencing the output variable of the process must be identified. One of the most important tasks in a regression study is to determine which variables are influential indicators, which are of mediocre importance and also which predictors are redundant with other variables (Younger, 1979). Thus, a predictor variable is one that is used to estimate some characteristics or response variable. Beyond merely identifying which variables can be used to estimate the value of another variable, the methods of regression can also be used to describe the manner in which variables are related through the use of important statistical tools.

Predicting a change over time, on the other hand, is not achieved through regression analysis. Rather, it requires time series analysis where the prime focus is not to identify variables that carry information about other variables but to extrapolate from present to future conditions. Time series, also referred to as a 'process' (Kanjilal, 1995), is therefore defined as a sequence of observations on a variable of a process.

The desulphurisation process under investigation in this report is a batch process. This implies that subsequent data cannot be perceived as time series data. It does however not exclude the use of multiple regression analysis techniques or use of hierarchical or multi-layer models like neural networks utilised in non-linear modelling and the following section will elaborate on some of the fundamental concepts of regression analysis.

Fundamentals of Regression Analysis

In most processes, the value of a certain dependent variable might be affected by several independent variables, but without further investigation, one will not know which variables will indeed be the strong

predictors of the response- or dependent variable. Data is therefore collected on all predictors (k-predictors) and their response, together with the help of multiple linear regression techniques are used to eliminate those predictors that are not effective.

The Linear Regression Model

Linear regression analysis is concerned with the specification of the nature of the relationship and the determination of the values of the coefficients in a regression function (Parsons, 1978).

First consider the simplest case of a linear model of the form (Aldrich, 2002)

$$\mathbf{y} = \mathbf{X}\beta + \mathbf{e} \tag{2.40}$$

where $\mathbf{y}$ is an n x 1 response vector, $\mathbf{X}$ is an n x m matrix of data (i.e. n observations on m variables), with rank m, β is a m x 1 vector of parameters, and e is an n x 1 random vector with independent, identically and normally distributed elements.

The error term is composed of two general kinds of errors i.e.

❑ model error, or 'lack of fit', which implies that all the important predictors are not taken into consideration or that the relationship is not precisely specified and

❑ random error, which is unpredictable and uncontrollable.

This is equivalent to the model $E(\mathbf{y}) = \mathbf{X}\beta$, with

$$\mathbf{y} = \begin{bmatrix} Y_1 \\ Y_2 \\ \vdots \\ Y_n \end{bmatrix}, \ \mathbf{X} = \begin{bmatrix} 1 & x_{11} & x_{21} & \cdots & x_{m1} \\ 1 & x_{12} & x_{22} & \cdots & x_{m2} \\ \vdots & \vdots & \vdots & \cdots & \vdots \\ 1 & x_{1n} & x_{2n} & \cdots & x_{mn} \end{bmatrix} \text{and } \beta = \begin{bmatrix} \beta_o \\ \beta_1 \\ \vdots \\ \beta_m \end{bmatrix} \tag{2.41}$$

Estimation of model parameters

If $E(\mathbf{y}) = \mathbf{X}\beta$ and $E[(\mathbf{y} - \mathbf{X}\beta)(\mathbf{y} - \mathbf{X}\beta)^T] = \mathbf{V}$, and $\mathbf{V}$ is known, it is possible to obtain the least squares estimate of β, without having to make further assumptions with regard to the distribution of $\mathbf{y}$. This is accomplished by minimizing

$$\mathbf{S} = (\mathbf{y} - \mathbf{X}\beta)^T \mathbf{V}^{-1} (\mathbf{y} - \mathbf{X}\beta) \qquad (2.42)$$

That is

$$\partial \mathbf{S}/\partial\beta = -2\mathbf{X}^T\mathbf{V}^{-1} (\mathbf{y} - \mathbf{X}\beta) = \mathbf{0} \qquad (2.43)$$

or

$$\mathbf{b} = (\mathbf{X}^T\mathbf{V}^{-1}\mathbf{X})^{-1}\mathbf{X}^T\mathbf{V}^{-1}\mathbf{y} \qquad (2.44)$$

provided that the matrices can be inverted. If the elements of $\mathbf{y}$ are independent, and have a common variance, then

$$\mathbf{b} = (\mathbf{X}^T\mathbf{X})^{-1} \mathbf{X}^T\mathbf{y} \qquad (2.45)$$

The fitted regression model is then

$$\mathbf{y} = \mathbf{X}\mathbf{b} \qquad (2.46)$$

The above-mentioned regression function (Equation 2.40) merely states the conceptual framework of the problem. It is a way of saying that a problem is being investigated in which there is an imperfect linear relationship between variables. Unfortunately the exact values of $\beta_0,...,$ β_m can never be known but the primary goal is still to get a handle on this underlying correlation between the variables. The desulphurisation data under investigation will therefore be used to get numerical estimates of the parameters in order to approximate the value of $\mathbf{y}$ from $\mathbf{X}$. Certain

key aspects concerning the significance and accuracy of the related predictors will be touched upon.

Useful descriptive statistics

At this point it is useful to digress briefly to introduce some notations that will be helpful in future sections.

❑ *Corrected sum of squares of the predictors (X)*

$$S_{XX} = \frac{n\sum_{i=1}^{n} X_i^2 - \left(\sum_{i=1}^{n} X_i\right)^2}{n} = \sum_{i=1}^{n}\left(X_i - X_{average}\right)^2 \qquad (2.47)$$

❑ *Corrected sum of squares of the response ($\hat{Y}$)*

$$S_{YY} = \frac{n\sum_{i=1}^{n} Y_i^2 - \left(\sum_{i=1}^{n} Y_i\right)^2}{n} = \sum_{i=1}^{n}\left(Y_i - Y_{average}\right)^2 \qquad (2.48)$$

❑ *Corrected sum of cross products (X·$\hat{Y}$)*

$$S_{XY} = \frac{n\sum_{i=1}^{n} X_i Y_i - \left(\sum_{i=1}^{n} X_i\right)\left(\sum_{i=1}^{n} Y_i\right)}{n} = \sum_{i=1}^{n}\left(X_i - X_{average}\right)\left(Y_i - Y_{average}\right) \qquad (2.49)$$

❑ Covariance between two variables X and Y (a measure of the extent to which the two variables act alike)[Parson, p.615 & 616 / Younger, p.42]

$$Cov_{X,Y} = \left(\frac{S_{X,Y}}{n}\right) \qquad (2.50)$$

Sum of squares and mean squares

It is important to find a measure of the variability of the actual values, Y, provided by the data, around the average values, $\hat{Y}$, predicted by the regression equation.

Mean Square of Regression (MSR)

For the case of k independent variables in the regression function, the formula

$$MSR = \frac{\sum_{i=1}^{k} b_i S_{X_i Y}}{k} \qquad (2.51)$$

calculates the variance of the response or dependent variable, $\hat{Y}$, due to changes in *only* the independent variables, X_1 through to X_k. The quantity is called the mean square regression (MSR) and does not account for the total variance in the independent variable.

Mean Square of Error (MSE)

For the case of k independent variables in the regression function, the formula

$$s_{xy}^2 = \frac{S_{YY} - \sum_{i=1}^{k} b_i S_{X_i Y}}{n - (k+1)} = \frac{\sum_{i=1}^{n} \left(Y_i - \hat{Y}_i\right)^2}{n - (k+1)} = MSE \qquad (2.52)$$

calculates the error variance, or a value also referred to as the mean square due to error (MSE). In other words, Equation 2.46 measures the average squared amount that the actual value differs from the predicted values as the result of error. At this point however, it is very important to note that s_{xy}^2 does also not account for the total variability in the response variable, but measures variability *after* it has been taken into account that $\hat{Y}$ varies with the independent variables, X_1 through to X_k.

Degrees of freedom (DF)

The quantity $n - (k + 1)$ in the denominator in Equation 2.46 is called degrees of freedom and the reason for the inclusion of $n - (k + 1)$, instead of just n is owing to the fact that we want s_{xy}^2 to be an unbiased estimator of the error variance. This implies that s_{xy}^2 tends neither to overestimate nor to underestimate the error variance and is accurate on the average.

Sum of Square of Regression (SSR)

The numerator in Equation 2.51 represents a quantity called the sum of squares of the regression (SSR)

$$SSR = \sum_{i=1}^{k} b_i \, S_{X_i Y} \qquad (2.53)$$

Sum of Square of Error (SSE)

The numerator in Equation 2.52 represents a quantity called the sum of squares of the error (SSE)

$$SSE \; = \; S_{YY} - \sum_{i=1}^{k} b_i \, S_{X_i Y} \qquad\qquad (2.54)$$

Sum of Squares of the Total (SST)

The first term of the right-hand side of Equation 2.50 denotes a quantity known as the sum of squares of the *total* (SST) variance detected in the independent (response) variable as a result of variance due to regression *and* error.

$$SST \; = \; S_{YY} \qquad\qquad (2.55)$$

The F - Statistic

F is the ratio of the MSR to the MSE

$$F \; = \; \frac{MSR}{MSE} \qquad\qquad (2.56)$$

The numerator of F measures the relationship (regression) between the response variable and the independent variables, while the denominator measures the variation in the response variable due to error. Thus F compares variation in $\hat{Y}$ owing to its relationship with the independent variables to variation in $\hat{Y}$ due to error.

Analysis of Variance (ANOVA)

All of these statistical expressions can be shown nicely in their respective roles if the F-statistic is calculated by means of an analysis of variance table (ANOVA). As the name implies, the table analyses the variation in $\hat{Y}$ into its component parts – one part due to its relationship with X_1 through to X_k and one part due to error. The universal outline of the ANOVA table for a multiple regression is:

Table 2.1 Analysis of variance

SOURCE	Sum of Squares (SS)	Degrees of Freedom (DF)	Mean Square (MS)	F
Regression	$\sum_{i=1}^{k} b_i S_{X_i Y}$	k	$\dfrac{\sum_{i=1}^{k} b_i S_{X_i Y}}{k}$	$\dfrac{MSR}{MSE}$
Error	$S_{YY} - \sum_{i=1}^{k} b_i S_{X_i Y}$	$n - (k+1)$	$\dfrac{S_{YY} - \sum_{i=1}^{k} b_i S_{X_i Y}}{n - (k+1)}$	
Total	S_{YY}	$n - 1$		

Although the multiple regression has been analysed, it will be beneficial to look at the question of relationship from different viewpoint by exploring the correlation between the variables.

Fundamentals of Correlation Analysis

In regression analysis, the independent variable is treated as predetermined and the objective is the specification of the regression function describing the relationship between the independent and dependent variable. The objective of correlation analysis, on the other hand, is to evaluate the extent to which variables covary in a linear

fashion (Parsons, 1978). By correlation is therefore implied the degree of linear association or relationship, that is, to what extent the variables behave alike or vary together (covary). Put another way, two variables are said to be correlated when a change in the value of one of the variables tends to be associated with a consistent corresponding change in the value of the other.

To a large extent, measures of correlation tell us the same thing as measures obtained in the study of regression but the value lies in their ability to measure the same thing in a slightly different way.

The main differences between the two analysis techniques are as follows:

❑ Unlike regression analysis, where the independent variable(s) can be predetermined, both the independent and the dependent variables are presumed to be random variables in correlation analysis.

❑ Regression analysis as a measure of strength depends on the unit of measurement, whereas correlation analysis does not.

❑ Correlation analysis is interested in determining the degree to which two variables are related and not in predicting one from the other.

Coefficient of Determination

The question therefore arises as to what percentage of variation in the dependent variable can be explained by the independent variables (X_1 through to X_k) together and how this percentage is evaluated. With k independent variables having an influence on the response variable, the multiple coefficient of determination is a measure of the extent to which these variables are correlated. This quantity can be formulated as follows

$$r^2 = 1 - \frac{SSE}{SST} = \frac{SSR}{SST} = \frac{\sum_{i=1}^{k} b_i S_{X_i Y}}{S_{YY}} \qquad (2.57)$$

As can be seen from the Equation 2.57, the coefficient of determination can be calculated from the ANOVA table. Owing to its calculation method, the value of the coefficient of determination is always positive, thereby neglecting to indicate whether the influence is direct or indirect. When the strength, as well as the direction of the relationship is required, another measure called the multiple coefficient of correlation is used.

Multiple Coefficient of Correlation

An alternative measure frequently employed as an index of the degree of correlation between variables is an abstract number known as the coefficient of correlation and its calculation is closely linked to the covariance between variables as seen in Equation 2.44.

$$Cov_{X,Y} = \left(\frac{S_{X,Y}}{n} \right) \qquad (2.50)$$

Not unlike regression analysis, the problem with the covariance as a measure of the strength of a relationship is that its magnitude is influenced by the units of the measurement of the variables. To eliminate the influence of units of measurement, the deviations are expressed in standard deviation units. The resulting standardised covariance is referred to as the coefficient of correlation.

$$r = \frac{Cov_{X,Y}}{\sqrt{\frac{S_{XX}}{n}} \cdot \sqrt{\frac{S_{YY}}{n}}} \qquad (2.58)$$

Initially it might be thought that the use of the symbol r for the coefficient of correlation could cause confusion owing to the fact that the symbol r^2 has previously been utilised to refer to the coefficient of determination. This is not the case however, as both coefficients are alternative measures for evaluating the strength of the linear relationship and are related in the following fashion

$$r = \sqrt{r^2} \qquad\qquad (2.59)$$

Therefore, given the coefficient of determination, the coefficient of correlation can be obtained by taking the square root of r^2.

Principal Component Analysis

Principal Component Analysis (PCA) is a technique for mapping multidimensional data into lower dimensions with minimal loss of information (Aldrich, 2002). PCA linearly transforms a set of variables into a substantially smaller set of uncorrelated variables containing most of the information of the original set of variables. These derived variables that maximise the variance accounted for in the original set of variables are referred to as principal components. In this way it reduces the dimensionality of the variable space.

Apart from being a useful technique to reduce the dimensionality of the variable space, principal component analysis can also be used to visualize multivariate data sets, so that outlying or atypical observations can be detected.

In contrast to direct methods in which multivariate observations are transformed in such a way so as to enable the observations to be depicted graphically in a direct form, geometrical configurations of multivariate observations can also be constructed, whereupon the 'best' 2-D subspace to view the data can be found, and the data can be projected into this 2-D subspace for visualization and interpretation.

Mathematical perspective (Aldrich, 2002)

In general it can be supposed that a (m x 1) vector $\mathbf{x}^T = (x_1, x_2, ... x_m)$ of variables is observed on each of n independent samples or units, which gives rise to an (n x m) matrix of observations with elements x_{ij}, (i = 1, 2, ... n and j = 1, 2, ... m). Moreover, the m values observed on the i'th unit or sample can be denoted by $\mathbf{x}_i$. The mean of the j'th variable in the sample is then $x_{avg,j} = 1/n\Sigma_{i=1}^n x_{ij}$. The sample mean *vector* is $\mathbf{x}_{avg}^T = (x_{avg,1}, x_{avg,2}, ... x_{avg,m})$. The variance of the j'th variable is given by $s_{jj} = [1/(n-1)]\Sigma_{i=1}^n(x_{ij}-x_{avg,j})^2$, while the covariance between the j'th and k'th variables is given by $s_{jk} = [1/(n-1)]\Sigma_{i=1}^n(x_{ij}-x_{avg,j})(x_{ik}-x_{avg,k})$. These variances and covariances are represented by the *sample covariance matrix* $\mathbf{S}$, which has s_{jk} as the (j,k)'th element, that is $\mathbf{S} = [1/(n-1)]\Sigma_{i=1}^n(\mathbf{x}_i - \mathbf{x}_{avg})(\mathbf{x}_i - \mathbf{x}_{avg})^T$ or in terms of matrix notation

$$\mathbf{S} = \text{cov}(\mathbf{X}) = \mathbf{X}^T\mathbf{X}/(n-1) \tag{2.60}$$

where the columns of $\mathbf{X}$ have been mean centred. If the columns of $\mathbf{X}$ have been autoscaled to zero mean and unit variance, $\mathbf{S}$ is also the correlation matrix ($\mathbf{R}$) of $\mathbf{X}$.

With principal component analysis, the matrix $\mathbf{X}$ is decomposed into the sum of the outer products of two vectors, viz.

$$X = TP^T = t_1p_1^T + t_2p_2^T + t_3p_3^T + ... + t_kp_k^T + ... E \qquad (2.61)$$

The index k is less than or equal to the smallest dimension of the data matrix, i.e. $k \leq min(n,m)$. The p_j vectors are the eigenvectors of the covariance matrix S (Equation 2.60) and the t_j are the score vectors representing the relationships between the samples, that is

$$Sp_j = \lambda_jp_j \qquad (2.62)$$

This implies that the derivation of principal components is based on the successive projection of lines through the m-dimensional space, as indicated in Figure 2.8, so that the variance of the projections of the n points in the space onto these lines is maximal at each instance. It can be shown that a line in a space can be represented by a vector p of unit length, which means that per definition $p^Tp = \Sigma_{j=1}^{m}p_j^2 = 1$. It is thus algebraically possible to define the principal components to be the linear combination $p_i = p_i^TX$ of the original variables that maximizes the value of $p_i^TSp_i$, subject to the constraint that $p_i^Tp_i = 1$.

The loading of the k'th original variable x_k on the j'th principal component p_j is defined by $p_{jk}(\lambda_j)^{1/2}$, where $p_j^T = (p_{j1}, p_{j2}, ... p_{jm})$. The *score* of the i'th individual or sample point on the j'th principal component p_j is defined as $t_{ij} = p_j^Tx_i = p_{j1}x_{i1} + p_{j2}x_{i2} + ... + p_{jm}x_{im}$ (j = 1, 2, ... m).
Note that because the (t_i,p_i) pairs are extracted in descending order according to the associated eigenvalues λ_i, the first pair captures the largest amount of variation in the data that can possibly be captured by a linear factor, while each subsequent pair captures the largest amount of the variation of the data not captured by the preceding pairs (that is after subtracting $t_ip_i^T$ from X).
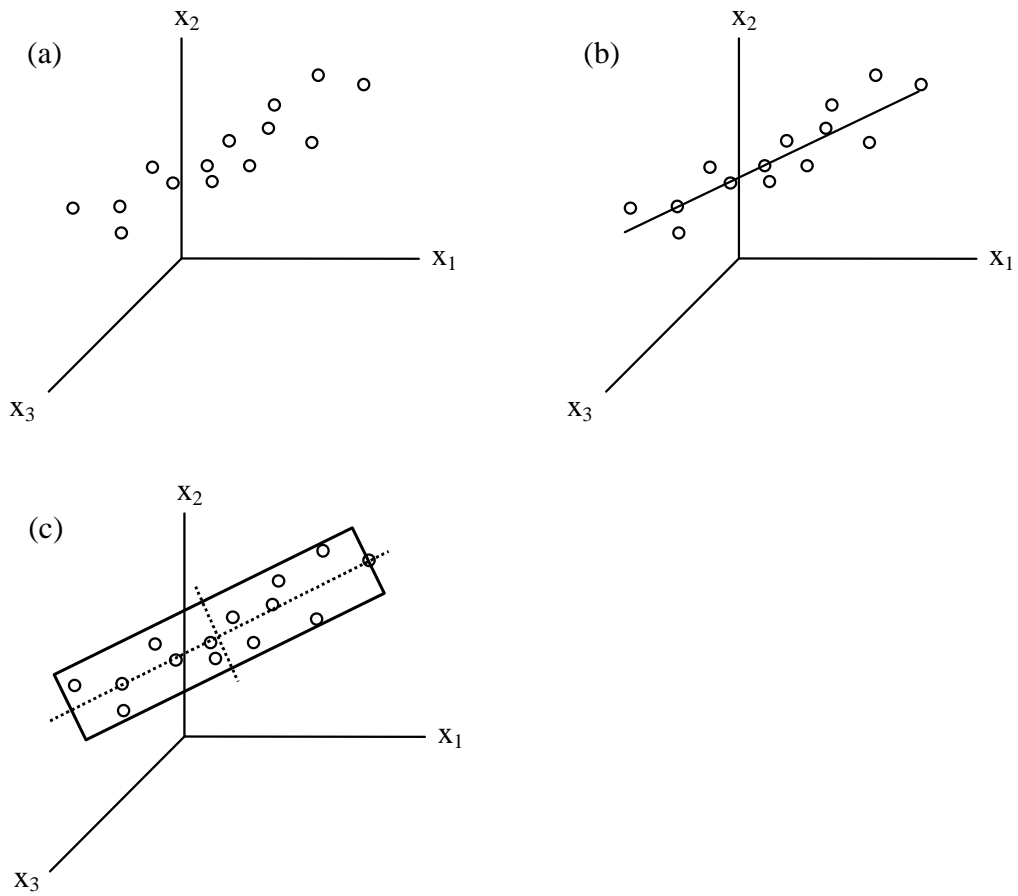
Figure 2.8 Geometric representation of the steps in principal component analysis, showing (a) the data points in the observation space, (b) the first principal component, (c) the plane defined by the first two principal components

3. DATA EXPLORATION

PLANT DATA

The current benchmark at the Saldanha Steel Liquid Iron Desulphurisation section (LID) is to desulphurise all Corex metal with a sulphur value of more than 0.04 weight percent. When a tapped ladle from the Corex exceeds this criterion, it is sent to the LID section for desulphurisation. In the past the required CaC_2 injection time (at constant flowrate) was determined through the use of a custom designed mathematical model embedded within the plant's control loop. That particular model has since been abandoned for an "operators' instinct" approach, relying on experience and gut feel to perform the desulphurisation, thereby leaving ample room for improvement and optimisation of the current process.

The operators use the following values as "rule-of-thumb" when desulphurising (Laas, 2002):

Table 3.1 Operators instinct: Calcium carbide addition and corresponding injection times

Initial sulphur content [weight %]	CaC$_2$ addition [kg]	Injection time at flowrate of 0.5 kg/s
> 0.1 wt% S	add 380 to 300 kg	12.7 – 10 minutes of lancing
> 0.08 wt% S	add 300 to 250 kg	10 – 8.3 minutes of lancing
> 0.065 wt% S	add 250 to 180 kg	8.3 – 6 minutes of lancing
> 0.045 wt% S	add 180 to 150 kg	6 – 5 minutes of lancing

Saldanha Steel made LID data available for the benefit of this project. Before exploration of the data could commence, the data was checked and filtered for any unrealistic values and discrepancies brought on by

practical process restrictions and human error. The revised dataset contained three disturbance variables, one manipulated variable and two controlled variables and comprised out of 1523 rows of data. Each row of data represents a single batch desulphurisation run performed in an individual ladle, making it impossible for data contained in consecutive rows to be perceived as time series data. It did however not preclude data exploration through the use of multiple regression analysis techniques.

RESULTS - MULTIPLE LINEAR REGRESSION

The purpose of regression is to predict, or estimate, the value of one variable from known values of other variables related to it. In order to make predictions, the important predictors influencing the output variable of the process must be identified and their individual impact quantified.

Table 3.2 Variable types

Variable	Unit	Description	Type of Variable
Tonnes	kg	Mass of molten iron in the ladle	Disturbance
BeginSul	wt%	Initial concentration of sulphur in the metal	Disturbance
EndSul	wt%	Final sulphur concentration after desulphurisation	Controlled
BeginTemp	°C	Temperature of melt before desulphurisation	Disturbance
EndTemp	°C	Temperature of melt after desulphurisation	Controlled
InjTime	min	Desulphurising agent (CaC_2) injection time	Manipulated

Table 3.2 identifies the various role-playing variables. Injection time (InjTime) was specified as the dependent variable ($\hat{Y}$), with the other five

variables acting as predictor variables. Through the use of *SPSS for Windows* ©, a preliminary multiple regression analysis was performed on the data, generating the following results.

Regression Coefficient Estimates

Table 3.3 Regression coefficient estimates

		Unstandardized Coefficients	Standardized Coefficients
Model		b	beta
0	(constant)	4	
X_1	Tonnes	5e-05	0.209
X_2	BeginTemp	4e-02	0.588
X_3	EndTemp	-4.16e-02	-0.592
X_4	BeginSul	60.6	0.750
X_5	EndSul	-114.8	-0.420

The subsequent multiple regression equation has the form

$$\text{InjTime} = 4 + 5e\text{-}05X_1 + 4e\text{-}02X_2 - 4.16e\text{-}02X_3 + 60.6X_4 - 114.8X_5 \qquad (3.1)$$

with the objective being the forecasting of the optimum CaC_2 injection time required given specific input values of the five predictors.

Any multiple regression analysis therefore starts off by "solving" the problem and generating a proposed model. Based on some solutions predicted by the intermediate model, further analysis will be performed and the equation revised if necessary.

At this point it is interesting to note that the absolute value of the standardised coefficient denominations in Table 3.3 quantifies the individual impact of each of the independent variables on the outcome

of the model. The independent variable with the largest absolute value standardised coefficient value, BeginSul, thus has the biggest influence on the CaC_2 injection time. More on the significance of the standardised coefficients in Section 3.3.1..

Analysis of Variance (ANOVA)

The predicted values of the dependent variable as proposed by the model were measured against the actual values of the independent variable as provided by Saldanha Steel and the variance between them analysed. The results can be seen in Table 3.4

Table 3.4 Analysis of variance

Model		Sum of Squares	df	Mean Square	F
1	Regression	6028.9	5	1205.7	260.3
	Error	7024.6	1517	4.6	
	Total	13053.6	1522		

With F = 260.3 implying that the variation due to regression is an estimated 260.3 times as great as the variation due to error.

Multiple Coefficients of Determination and Correlation

With the multiple regression analysed, it is valuable to investigate the correlation between the variables. The coefficient of determination and correlation is provided in Table 3.5.

Table 3.5 Coefficients of determination and correlation

Model	r	r^2
1	0.680	0.462

With the multiple coefficient of determination, r^2, calculated from ANOVA values (see Equation 2.53) it can be said the combined variation in the five predictors accounted for 46.2% of the variation in the dependent variable (InjTime). A positive coefficient of correlation, r, indicated a direct relationship between the dependent variable and the five predictors.

Outliers

Although the original data set was checked for any unrealistic values and discrepancies brought on by practical process restrictions and human error, it was still not clear whether or not the scatter of the remaining data utilised in the regression coefficient estimates was uniform. The scatter of the data often provides valuable information about possible influential observations (data points) and outliers that can have a negative impact on the regression equation. Data scatter can be investigated by utilising a range of techniques.

Residual plotting

When comparing the target or actual values with the predicted values of the intermediate model the difference in value between these two data sets are called the unstandardised residuals. A basic plot of standardised residuals (Figure 3.1) can provide helpful information about outliers and influential observations.

Figure 8. Standardised Residual Plot
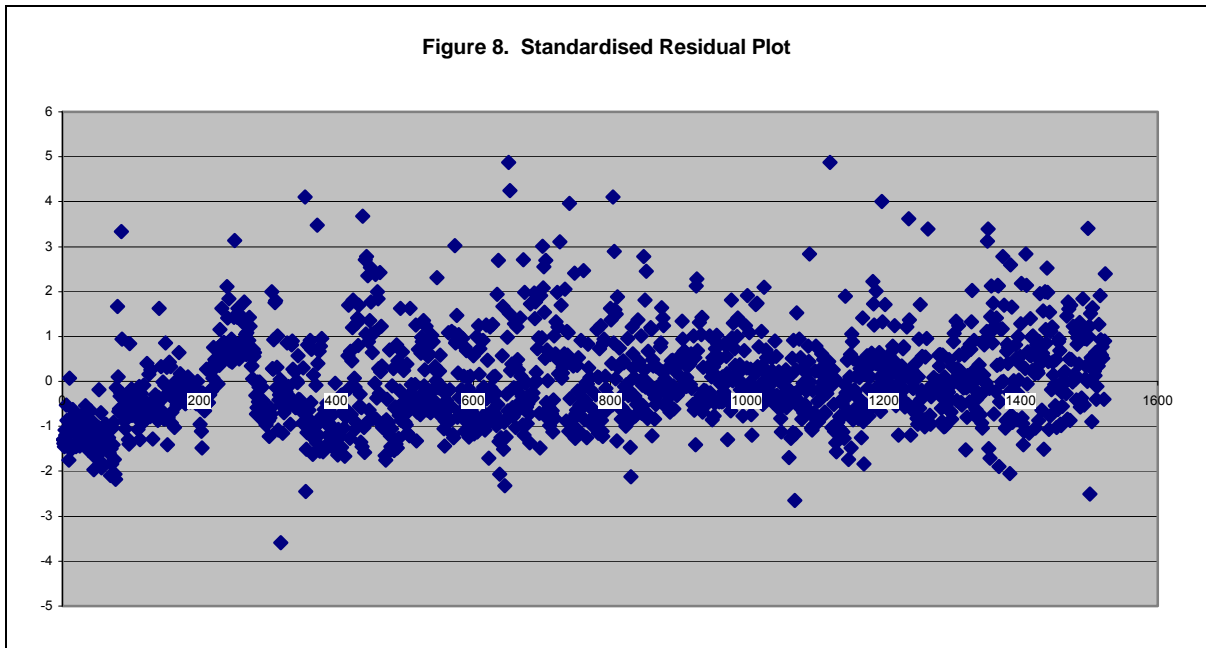
Figure 3.1 Standardised residual values

A few of the predicted values differ substantially from the target values – some even as much as five standard deviations from zero. It is considered standard practice to consider a potential outlier as a point with a residual of three standard deviations or more from zero. Through the use of data filtering techniques the observations corresponding to above-mentioned criterion were identified.

Through residual plotting it also became apparent that the data gathered during the crucial "start-up" phase of the plant in February 1999 (roughly the first 300 data points as indicated on Figure 3.1) was erratic and contained potentially influential observations that could have a negative effect on the predictive abilities of the proposed model.

Studentised Residual Plotting

Another way of analysing the observations is by plotting the studentised residuals. The standardised residuals differ from the studentised residuals only in the way in which the standard deviation is computed. For a 98% confidence level in the data set, the upper and lower limits of the residuals were set at $\pm$ 2.326, with all data points falling outside these ranges identified as plausible influential observations or outliers.

Figure 9. Studentised residual plotting
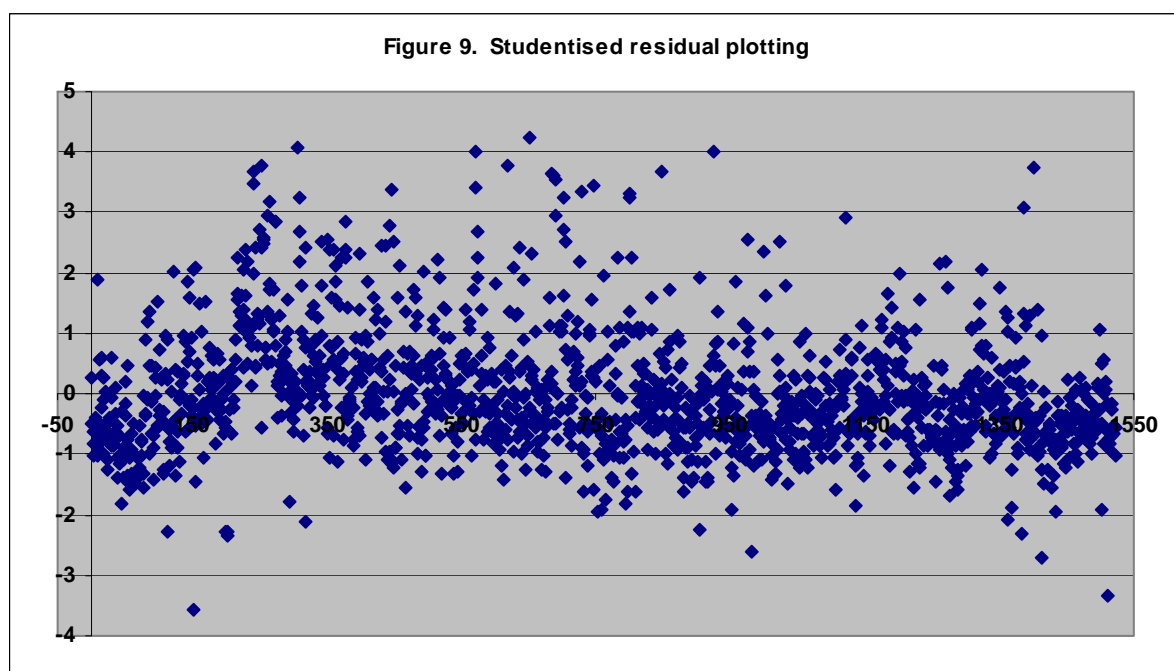
Figure 3.2 Studentised residual values

Cook's Distances

Yet another method of identifying outliers is by comparing the Cook's distances (Figure 3.3). These distances are a summary measure of the influence of a single observation, based on the total changes in all other residuals when the observation is deleted from the parameter estimation

process, as well as the observation's distance from the other observations (leverage) (Aldrich, 2002). The bigger the distance, the bigger the influence of the observation and all observations with Cook distances of more than 0.03 were identified as potential outliers.
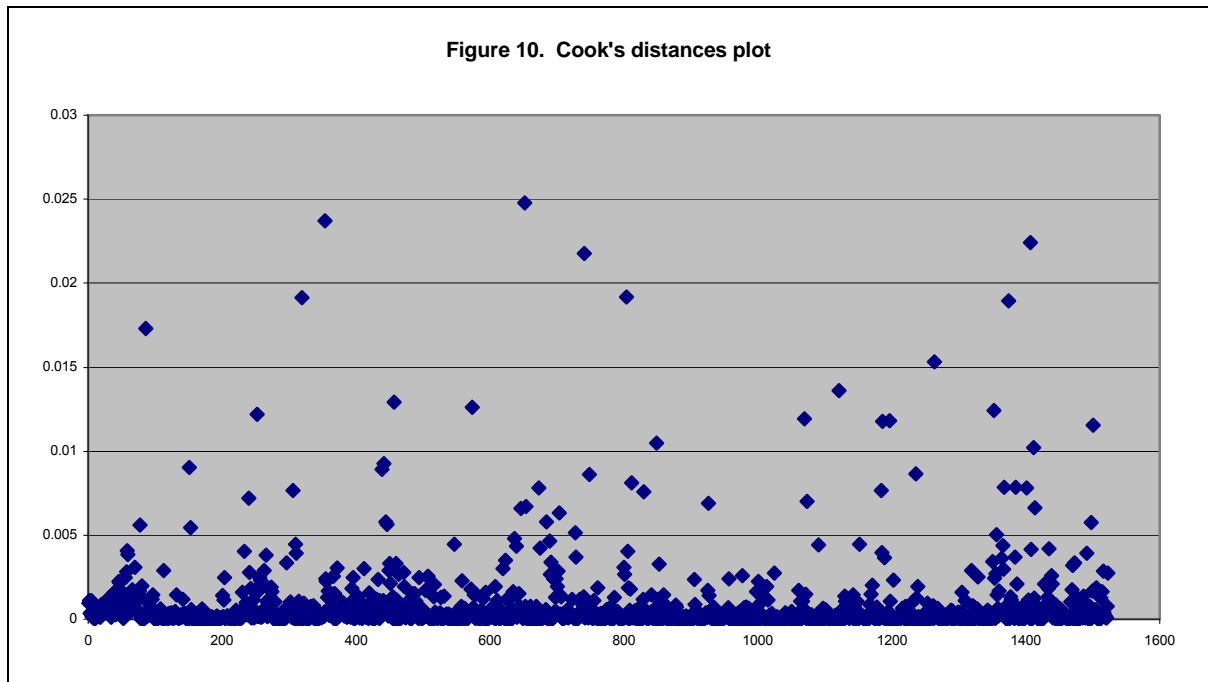
Figure 3.3 Cook's distances

Mahalanobis Distances

Mahalanobis distances (Figure 3.4) measure the difference between the value of the specific observation and the mean of the other observations. If this result is very different from the others for a specific observation, it means that the entire regression equation could be shifted appreciably because of this particular observation. The bigger the distance, the bigger the influence of the observation and all observation distances greater than 19 were identified.

Figure 11. Mahalanobis distances plot
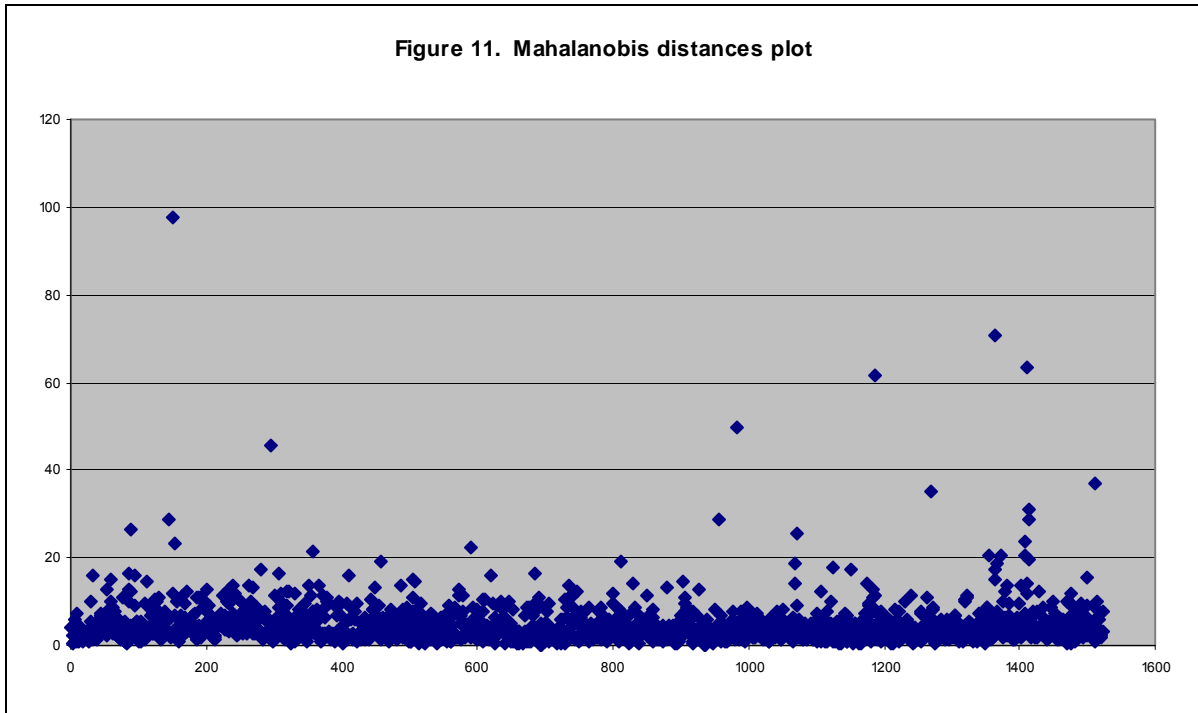
Figure 3.4 Mahalanobis distances

Observations identified as outliers by merely one of these four techniques were retained as functional data points. Twenty-eight individual data points however, were identified as influential observations by more than one of these identifying techniques and eliminated from the data set.

RESULTS – FINAL MULTIPLE LINEAR REGRESSION

The new data set contained 1495 rows and multiple regression analysis performed on the new data revealed the following results as depicted in Table 3.6.

Regression Coefficient Estimates

Table 3.6 Regression coefficient estimates – Without outliers

Model		Unstandardized Coefficients	Standardized Coefficients	Collinearity Statistics	
		b	beta	Tolerance	VIF
0	(constant)	3.83			
X_1	Tonnes	5.E-05	0.219	0.936	1.069
X_2	BeginTemp	4.3E-02	0.661	0.044	**22.836**
X_3	EndTemp	-4.5E-02	-0.666	0.045	**22.456**
X_4	BeginSul	64.5	0.812	0.711	1.406
X_5	EndSul	-122.7	-0.461	0.738	1.355

The revised multiple regression equation has the form

$$InjTime = 3.82 + 5e\text{-}05X_1 + 4.3e\text{-}02X_2 - 4.5e\text{-}02X_3 + 64.5X_4 - 122.7X_5 \quad (3.2)$$

As mentioned earlier, the absolute values of the standardised coefficients (beta) provide important insight into the importance of each independent variable on the linear model and these numerical values supply almost all the necessary information to perform a rough sensitivity analysis. In this case it is the sulphur content in the ladle before desulphurisation with a value of 0.812 that has the biggest influence in determining the outcome of the model, with the independent variable with the smallest absolute value standardised coefficient having the least amount of influence on the outcome of the linear model. It would therefore seem logical to assume that the two temperature variables have the second biggest influence of the model. It is however important to consider the results of a collinearity diagnostics analyses before instilling complete confidence in the regression coefficients as being the most effective indicator of model sensitivity.

Collinearity Diagnostics

When certain independent variables in the data set are highly correlated, it is difficult to separate the distinctive effects of each predictor on the dependent variable. In the case where the correlation coefficient between two independent variables are perfect (singularity), the regression coefficients become uncertain and vague and little or no meaning can be attached to their particular values. In the case of less perfect collinearity, the regression coefficients can be estimated, but less and less meaning can be attached to their value as the degree of collinearity increases.

Tolerance is a statistic used to determine how much the independent variables are linearly related to one another (multicollinear). In other words, the proportion of a variable's variance not accounted for by other independent variables in the equation. A variable with very low tolerance contributes little information to a model, and can cause computational problems.

Variance Inflation Factor (VIF) is the reciprocal of the tolerance. As the variance inflation factor increases, so does the variance of the regression coefficient, making it an unstable estimate. Large VIF values are therefore an indicator of multicollinearity and it can clearly be seen from Table 3.6 that the VIF values for the two temperature variables (BeginTemp & Endtemp) are extremely high compared to the other independent variables. This means that the regression coefficient values of these two variables are not necessarily a clear indication of the variables' influence on the regression model and can therefore not completely be trusted.

Table 3.7 Pearson correlations

	InjTime	Tonnes	BeginTemp	EndTemp	BeginSul	EndSul
InjTime	1	0.106	-0.087	-0.131	0.555	-0.097
Tonnes	0.106	1	0.214	0.202	-0.165	-0.029
BeginTemp	-0.087	0.214	1	**0.977**	-0.334	-0.274
EndTemp	-0.131	0.202	**0.977**	1	-0.330	-0.245
BeginSul	0.555	-0.165	-0.334	-0.330	1	0.477
EndSul	-0.097	-0.029	-0.274	-0.245	0.477	1

The assumption of a high degree of collinearity between the two temperature variables is further substantiated by a particularly high Pearson correlation value of 0.977 in Table 3.7. Pearson correlation is a measure of linear association between two variables. Values of the correlation coefficient range from -1 to 1. The sign of the coefficient indicates the direction of the relationship and its absolute value indicates the strength, with larger absolute values indicating stronger relationships. It is important to realise though that a high simple correlation between two variables is a sufficient, but not a necessary condition for multicollinearity. Multicollinearity can still be a major problem, even when the correlation between variables appears to be low.

Results - Analysis of Variance (ANOVA)

Revised results based on the filtered data set is summarised in Table 3.8.

Table 3.8 Analysis of variance – Without outliers

Model	Sum of Squares	Mean Square	F
Regression	6566.1	1313.2	360.7
Residual	5420.9	3.6	
Total	11986.9		

After filtering the relevant outliers from the data set, the F – statistic value increased by 100 points with the variation due to regression now an estimated 360.7 times as great as the variation due to error.

Multiple Coefficients of Determination and Correlation

The coefficient of determination increased from 0.426 to 0.548. The variation in the 5 predictors together now account for 54.8 % of the variation in the injection time value.

Table 3.9 Coefficients of determination of correlation – Without outliers

Model	r	r^2
	0.740	0.548

How large must r^2 be?

Is r^2 = 0.548 interpreted as weak, moderate or strong? Since $0 < r^2 < 1$, and since $0.548 \cong 0.50$, one might say that an r^2 of 0.548 indicate a moderately weak relationship. However, as mentioned earlier, it means that the 5 predictors by themselves explain 54.8 % of the total variability in dependent variable, leaving only 45.2 % of the variability to be explained by *all other possible predictors* together. While the interpretation of how strong is strong is rather subjective, it can therefore be argued that if *all the other possible predictors* are able to influence the dependent variable and explain its variability, r^2 = 0.548 for five predictors indicates a moderately strong relationship.

Principal Component Analysis

Through principal component analysis the set of variables was linearly transformed into a smaller set of uncorrelated variables containing most of the information of the original set of variables.

Table 3.10 Principal component analysis

Comp	Initial Eigenvalues			Extraction Sums of Squared Loadings		
	Total	% of Variance	Cum %	Total	% of Variance	Cum %
1	2.507	41.785	41.785	2.507	41.785	41.785
2	1.341	22.351	64.136	1.341	22.351	64.136
3	1.019	16.990	81.126	1.019	16.990	81.126
4	o.923	15.386	96.512			
5	o.188	3.131	99.644			
6	2.138E-02	0.356	100.000			

Three principal component factors were extracted from the data. In Table 3.10 it can be seen that these three factors account for more than 81 % of the variance in the data thereby reducing the dimensionality of the problem to three. This then allows for the visualisation of multivariate data sets, so that unusual trends of observations can be detected.
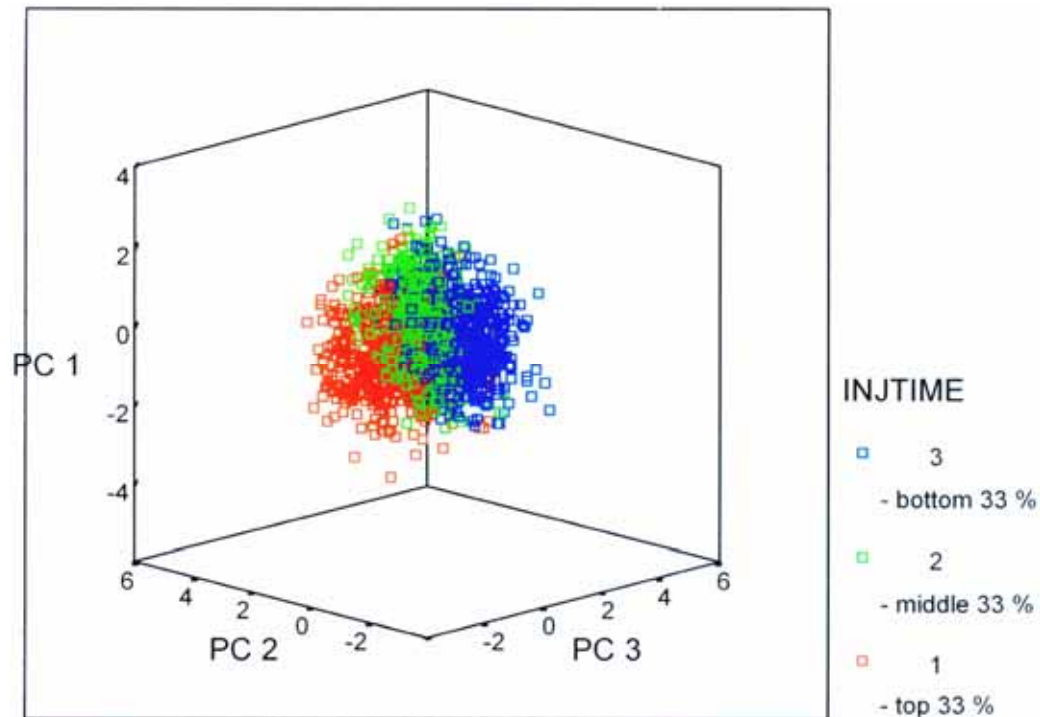
Figure 3.5 Principal component analysis

A three dimensional plot was generated by utilising the principal component factors. The data was labelled with the values of the predicted dependent variable (*InjTime*) generated by the model. The top 33 % of the dependent variable values are labelled in red, the middle 33 % with green and the bottom 33 % of the values are labelled in blue. The plot quite clearly identifies three distinct areas, indicating to the genuine validity of the multiple regression model.

RESULTS – NON-LINEAR MODELLING

A standard backpropogation network was also employed to model the filtered data from the previous section. A standard software package, Qnet for Windows ©, was utilised and the network structure that yielded the highest correlation between target output and network output generated the following results

Table 3.11 Backpropogation neural network model output

```
Number of Layers:              3

Input Layer:
       Nodes:                  5
       Transfer Function:      Linear
Hidden Layer:
       Nodes:                  10
       Transfer Function:      Sigmoid
Output Layer:
       Nodes:                  1
       Transfer Function:      Sigmoid

Connections:                   FULL

Training Information:
       Iterations:             10 000
       Training Correlation:   0.76306
       Training Determination: 0.58226
       Test Correlation:       0.76546
       Test Determination:     0.58593
       Momentum Factor:        0.8

       Training Patterns:      1279
       Test Patterns:          200
       Inclusion Method:       RANDOM
```

Average Contribution of Input Node on Output

Input Node	Output Node	Percent Contribution
1 - Tonnes	1	8.70
2 - BeginTemp	1	20.87
3 - EndTemp	1	24.71
4 - BeginSul	1	30.45
5 - EndSul	1	15.26

The neural network produced a coefficient of determination of 0.5823. This substantiated the results generated through multiple linear regression that the variances in the five predictors account for roughly 55% of the

variances in the dependent variable. Note that the sulphur content at the onset of desulphurisation (BeginSul) once again has the biggest contribution on the network output providing a 30.45 % contribution.

The output values generated were graphically compared with the target values and are depicted in Figure 3.6.
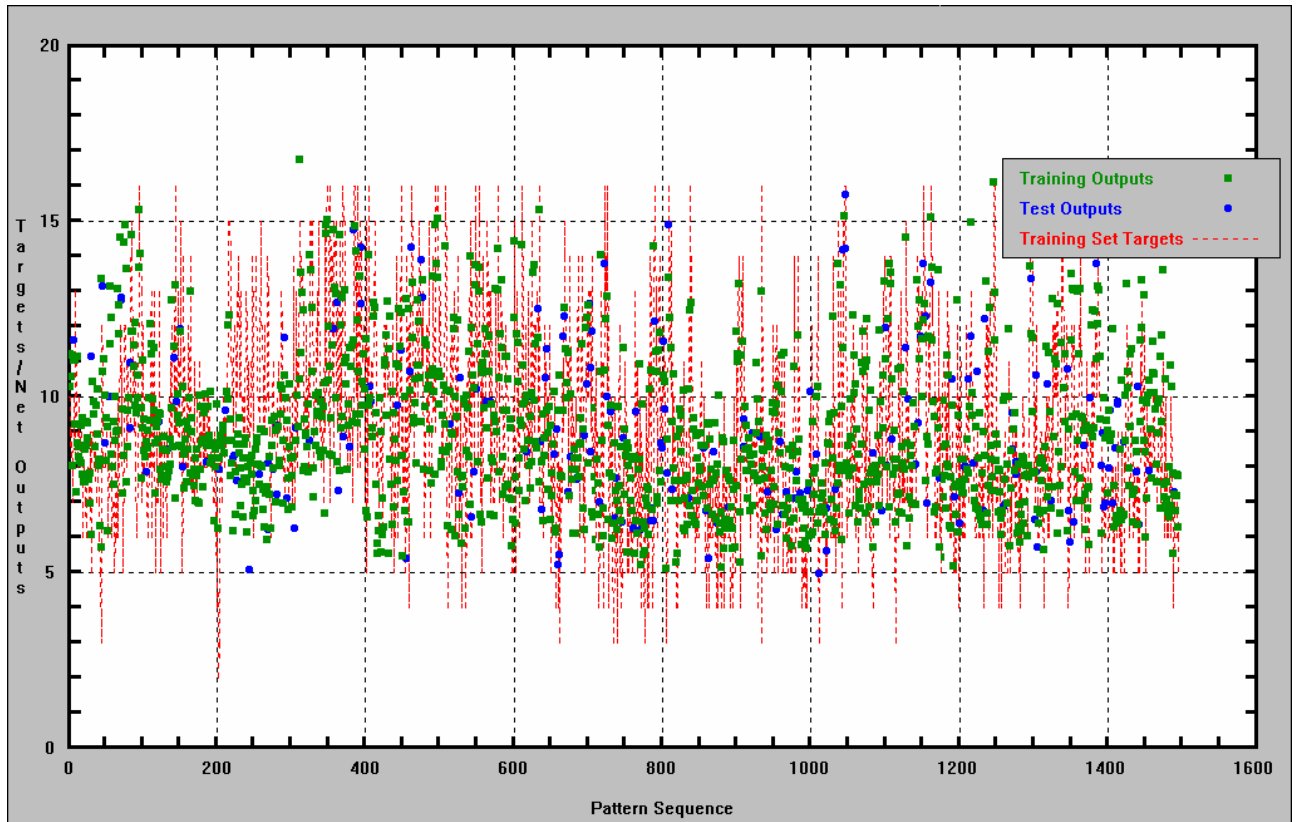
Figure 3.6 Target values vs. Output values

SUMMARY

Although the empirical modelling approach clearly succeeds in capturing the underlying patterns of the problem as well as providing an indication of the sensitivity of the manipulated variables on changes in the disturbance and controlled variables, a total empirical approach would be insufficient. It is only through a combination of semi-empirical

and fundamental modelling that the desulphurisation process can be more lucidly defined, accounting for, if only in part, the other 45% variance in the dependent variable.

4. FUNDAMENTAL MODELLING

Introduction

In order to therefore gain a better understanding of the fundamental principles and kinetics governing the desulphurisation process at Saldanha Steel, a kinetic model is presented. Coupled with experimental work, the model provides a quantitive understanding of the CaC_2 injection procedure together with improved insight as to the influence of those critical variables controlling the process and those utilised in subsequent optimising procedures.

The model calculates the velocities, temperatures and compositions of the gas, liquid and solid phases in the rising plume during desulphurisation, as well as the contribution of the topslag (carry-over slag & flux) towards the desulphurisation process. Desulphurisation of the liquid iron occurs in the ascending plume and at the top slag/metal interface.

Figure 4.1 Schematical representation of the physical phenomena in the rising plume

Figure 4.1 schematically shows the physical phenomena within the plume of a horizontally injected calcium carbide desulphurisation process. Two jets containing a mixture of calcium carbide and nitrogen issue from the lance tip. On exit the jets expand very rapidly and penetrate only a short distance into the metal (Oryall, 1976) before rising vertically. In conjunction with rapid expansion, the jets in the iron penetrate extensively behind the nozzle giving the impression that the jets were

injected from a vertical rather than a horizontal nozzle, thereby creating one combined plume.

At the point of momentum dissipation, the gas and powder partially separate, with the gas forming large spherical cap bubbles. The diameter of these bubbles depends on the carrier gas flowrate and the outer diameter of the lance orifice (Guthrie, 1978). The calcium carbide powder may remain inside the carrier gas bubbles or end up in the liquid iron. The percentage of particles associated with the bubbles is a parameter that plays a vitally important role in the modelling of the process.

The calcium carbide particles, which come into contact with liquid metal, are heated rapidly to reach the plume temperature. At this temperature, calcium carbide is partially decomposed to form graphite and calcium vapour (Talballa, 1976). The calcium vapour diffuses through the reaction product layer, comprising of mostly CaS, to react with sulphur at the surface of particles. Meanwhile the carrier gas flow rate controls the rate of liquid recirculation in the ladle and assures that fresh sulphur-rich liquid metal is pumped into the plume where the desulphurisation reactions occur.

Once the calcium carbide particles reach the surface they are incorporated into the topslag and continue desulphurising through topslag-metal reactions.

The present study is therefore concerned with the development of a one-dimensional steady state model for the momentum, heat and mass transfer in an ascending gas-liquid-powder plume for the conditions relevant to the Saldanha Steel desulphurisation injection process, along with a model accounting for the contribution of topslag (carry over as well as reagent flux) to the overall desulphurisation rate.

Model for single CaC$_2$ particle desulphurisation

To develop a model that will represent calcium carbide desulphurisation in the plume, the transport and chemical reaction steps are divided into two separate steps (Chiang, 1991).

A model for the diffusion processes that occur through the product layers of calcium carbide and graphite that accumulate on the surface of each calcium carbide particle

The phenomena occurring at the inside and on the surfaces of injected calcium carbide particles may be explained based on the experiments and mechanism proposed by Talballa (Talballa, 1976). In these experiments, calcium carbide decomposes to form calcium vapour and a layer of graphite a high temperatures. The calcium vapour reacts with the sulphur in the iron to form a layer of calcium sulphide over the graphite layer. It is through these thick layers of graphite and calcium sulphide that the decomposed calcium vapour has to diffuse in order to reach the reaction interface on the surface of the particle. In order to model the rate of diffusion of calcium vapour through these product layers around a single calcium carbide particle, the following assumptions were made

- All calcium carbide particles are spherical
- Calcium sulphide and graphite layers form topochemically on the surface of the particle
- Mass transfer resistance due to the chemical reaction rates are negligible and the chemical rates of desulphurisation and calcium carbide decomposition are fast
- The effective diffusivity of calcium vapour through the product layers is constant

❑ The calcium carbide diffusion in quasi-steady state is slow enough in order to assume steady state diffusion fluxes

The calculation of the effective diffusivity of calcium vapour is presented elsewhere (Chiang, 1991). It was shown by Chiang that the diffusivity of a calcium carbide vapour through the product layer around the calcium carbide particle was approximately 7×10^{-7} m2/s.

A model for the transport processes that bring sulphur-rich liquid into the plume and through the boundary layers around the particles.

Momentum, heat and mass transfer principles play a vital role in the rate at which sulphur-rich liquid is pumped into the plume (entrainment) and the model relies on all three of these important principles to help account for the overall desulphurisation process within the plume.

Along with a good understanding of the relevant transport phenomena within the plume, good insight into the affected boundary layers around the particles and the bubbles is also required. Before addressing the specific boundary layer concerns one must first analyse and define the overall calcium carbide desulphurisation mechanism within the plume:

Overall calcium carbide desulphurisation mechanism

The overall calcium carbide desulphurisation mechanism is postulated to involve the following individual steps

Step 1: Mass transfer of sulphur through the boundary layer to the calcium carbide particle surface

Step 2: Thermal decomposition of calcium carbide

Step 3: Diffusion of calcium vapour through the micro pores of the reaction product layer to the outer surface of calcium carbide

Step 4: Chemical reaction of calcium with sulphur takes place at the interface of the calcium carbide particle and liquid hot metal

For high temperature metallurgical reactions, the chemical reaction rate is generally very fast and as mentioned in Section 4.2.1.1, desulphurisation and calcium carbide decomposition reactions reach equilibrium almost instantaneously. Therefore step 2 and step 4 are fast enough to ignore.

That leaves step 1 and step 3 and in order to evaluate the individual resistance contribution of both steps to the overall calcium carbide desulphurisation reaction, the rate of calcium diffusion was compared with the rate of diffusion of sulphur through the boundary layer around each particle:

The rate of sulphur diffusion can be expressed as follows

$$R_{S,bl} \quad = \quad k_p \cdot 4\pi r_O^2 \cdot \left(C_S^{pl} - C_S^{ip} \right) \tag{4.1}$$

For a 75µm particle located inside the iron and with a sulphur mass transfer coefficient of 7.5×10^{-4} m/s, the rate of sulphur transfer through the hot metal boundary layer around the calcium carbide particle is 1.8×10^{-10} mol/s.

For an effective calcium diffusivity of 7×10^{-7} m²/s (see Section 4.2.1.1) and the assumption that the product layer radius is half the particle radius ($r_i = \frac{1}{2}r_o$), the rate of calcium diffusion can be calculated by the following formula (Fogler, 1992)

$$R_{Ca} = -D_{Ca,eff} \cdot \left(\frac{4\pi r_o r_i}{r_o - r_i} \right) \cdot \left(C_{Ca}^{ip} - C_{Ca}^{r_i} \right) \qquad (4.2)$$

and is approximately 6×10^{-8} mol/s.

This means that rate of calcium transfer through the product layer around the particle is some 300 times greater than the sulphur transfer through the hot metal boundary layer. Consequently, under the present conditions, calcium transfer provides negligible resistance to the overall mass transfer and is therefore rapid enough not to be rate controlling. That means that step 3 can also be ignored.

That leaves the mass transfer of sulphur through the boundary layer to the calcium carbide particle surface as the only rate-controlling step needing to be considered in a model for single calcium carbide desulphurisation in the plume. The following additional assumptions were made before development of the model could commence (Chiang, 1987).

Model assumptions

❑ The total concentration of calcium vapour is constant at the temperature of interest (Talballa, Tojan, 1976)

❑ The initial chemical composition of the particles are constant throughout their volume and the excess C and CaO do not participate in the reaction (Farias, Irons, 1985b)

❑ Due to the low solubility of calcium in the carbon-rich hot metal and the fast reaction rate of calcium vapour with sulphur, the reaction site is assumed to be at the carbide/hot metal interface (Farias, Irons, 1985b)

Mathematical Formulation

The rate at which sulphur diffuses through the boundary layers to the particles depends entirely on whether or not the particles are located on the bubble interface or in the liquid itself. Both particle positions will represent very different boundary conditions, resulting in dissimilar modelling strategies. Through analysis of Saldanha Steel data by the author it was apparent that the actual utilisation of calcium carbide particles were between 30 – 35% of that expected from Equation 1.1 (see Appendix C.4). It was therefore important for any mass transfer equation to be able to account for this phenomenon.

An equation representing the desulphurisation reaction of the calcium carbide particles in the liquid melt is given by

$$\frac{d(1-f)\theta_p U_p C_p \alpha_{pl}}{dZ} \quad = \quad J_l\left(C_S^{pl} - C_S^{ip}\right) \qquad (4.3)$$

with α_{pl} representing the extent (utilisation) of the reaction and J_l depicting a combined mass transfer function

$$J_l \quad = \quad \frac{6 \cdot \theta_p k_p (1-f) A_{pl}}{d_p} \qquad (4.4)$$

Owing to the use of carrier gas at elevated flowrates, the liquid iron in the vessel is at a highly agitated state and the subsequent mass transfer coefficient must duly reflect this occurrence. The turbulent mass transfer coefficient to spheres in liquids that represent the relevant conditions was therefore obtained from the following formula (Sano, 1974)

$$k_p = \frac{D_s}{d_p}\left(2 + 0.4\left(\frac{\varphi d_p^4}{\nu^3}\right)^{1/4}\left(\frac{\mu}{\rho_l D_s}\right)^{1/3}\right)$$ (4.5)

with

$$\varphi = \left(U_g - U_l\right)g$$ (4.6)

A second equation representing the extent (utilisation) of the desulphurisation reaction of the calcium carbide particles associated with the bubbles is given by

$$\frac{d\theta_p f U_g C_p \alpha_{pg}}{dZ} = J_2\left(C_s^{pl} - C_s^{ib}\right)$$ (4.7)

with

$$J_2 = \frac{6 \cdot \theta_g k_b A_{pl}}{d_b}$$ (4.8)

Due to the difference in structure and owing to lack of solubility of calcium carbide (Irons, 1999) in liquid iron, Irons assumed that the particles associated with the bubbles are not situated on the outside but on the inside of the bubble surface. For sulphur to reach the calcium carbide particles situated inside the bubble, it will have to diffuse through the boundary layer around the bubble. The turbulent mass transfer coefficient value relevant to spherical-cap bubbles was taken from the proposed correlation by Calderbank (Szekely, 1971)

$$k_b = 1.08 g^{0.25} D_s^{0.5} d_b^{-0.25}$$ (4.9)

Plume momentum transfer equations

As the horizontally-injected jets created through the lancing procedure rapidly expand to form a combined plume, the gas and powder is partially separated. At the point of momentum dissipation, the gas and the powder experience a force upward due to buoyancy and a force downward due to drag. The bubbles created by the carrier gas will rise considerably faster than the liquid, thereby excluding the use of any mixture models. The liquid itself experiences a force that is equal but opposite to the drag force on the gas together with the particles and the reason why the liquid recirculation rate is a function of the carrier gas and reagent flowrates. The liquid is therefore accelerated towards the top of the ladle and will move up with the gas and the particles, ensuring that fresh sulphur-rich liquid metal is entrained into the reaction zone of the plume.

Three separate momentum equations have been written for the three phases, in which the velocities of the solid, gas and liquid phases can be calculated. The equations were formulated based on certain key assumptions, some of which have already been mentioned in Section 2.6.2.1.2.

Model assumptions

❑ Conditions are at steady state, effectively cancelling out the accumulation segment in the original momentum equation
❑ The flow is one-dimensional, along the axis of the plume (Farias, Irons, 1986)
❑ Liquid entrainment into the plume is controlled by drag forces only (Farias, Irons, 1986)

- After initial formation, the plume diameter remains constant (Farias, 1985a)
- Gas and powder concentrations are low enough that single particle drag coefficients can be used and bubble-bubble and particle-particle interactions can be ignored (Farias, Irons, 1985a)
- Viscous forces have been ignored (Farias, Irons, 1985a)
- The bubble diameter is a function of carrier gas flowrate and orifice diameter and considered to be constant during rising (Oryall, Brimacombe, 1976)
- All variables and properties are averaged across the plume diameter (Farias, Irons, 1985a)
- The fraction of particles entrapped inside the bubbles remain constant throughout the process (Farias, Irons, 1985a)

Mathematical formulation

The bubbles comprise out of a mixture of gas and a certain fraction of the calcium carbide particle that is associated with the bubbles. The mixture density of the bubbles can be written as

$$\rho_m = \theta_g \rho_g + f \theta_p \rho_p \qquad (4.10)$$

The conservation of mass in the bubble and the powder in the liquid can be expressed by the following equations

$$\frac{d(\rho_m U_g A_{pl})}{dZ} = 0 \qquad (4.11)$$

$$\frac{d(1-f)\theta_p \rho_p U_p A_{pl}}{dZ} = 0 \qquad (4.12)$$

with the clear understanding that within the control volume the liquid mass is not conserved because liquid is entrained into the plume owing to the drag from the bubbles and particles (Streeter, Wylie, 1979).

The momentum balance for each phase per unit volume of plume can be written with functions for buoyancy and drag forces operating on each phase (Farias, 1986)

$$\frac{d\rho_m U_g^2 A_{pl}}{dZ} \;=\; F_{gp}^B - F_{gp-l}^D \tag{4.13}$$

$$\frac{d(1-f)\theta_p\rho_p U_p^2 A_{pl}}{dZ} \;=\; F_p^B - F_{p-l}^D \tag{4.14}$$

$$\frac{d\theta_l\rho_l U_l^2 A_{pl}}{dZ} \;=\; F_{gp-l}^D + F_{p-l}^D \tag{4.15}$$

The buoyancy forces for the gas and powder in the bubbles and the powder in the liquid respectively are

$$F_{gp}^B \;=\; (\rho_l - \rho_m)\theta_g g A_p \tag{4.16}$$

$$F_p^B \;=\; (1-f)(\rho_l - \rho_p)\theta_p g A_p \tag{4.17}$$

The corresponding drag functions were developed as the product of the drag force on a single particle or bubble and the number of particles and bubbles present in the plume control volume. For the gas and powder in the bubble it was assumed that the powder merely changes the apparent density of the bubble, not the nature of the boundary layer.

$$F_{gp-l}^{D} = \frac{0.75 \rho_l C_{Dg} (U_g - U_l)^2 \theta_g A_p}{d_b} \qquad (4.18)$$

$$F_{p-l}^{D} = \frac{0.75 \rho_l C_{Dp} (U_p - U_l)^2 (1-f) \theta_p A_p}{d_p} \qquad (4.19)$$

The prime concern is therefore to establish the net forces acting on the particle and the gas and hence to determine its relative velocity with respect to the fluid. A vital parameter required for these calculations is the dimensionless drag coefficient or friction factor. The drag coefficient is a function of the shape of the particle or bubble and the Reynolds number of the investigated object.

$$Re_{object} = \frac{d_{object} \cdot u_{relative} \cdot \rho_{liquid}}{\mu_{liquid}} \qquad (2.21)$$

The movement of the calcium carbide particles in the liquid iron was found to be in the Newton Law Region ($500 < Re_{object} < 2 \times 10^5$). Within this region the drag coefficient remains constant at a value of $C_D \approx 0.44$. For large spherical-cap bubbles rising in stationary liquids, the drag coefficient reaches a constant value of $C_D \approx 2.66$ (Lin, 1995).

Examination of the expressions for the drag forces acting on the particle and the bubble (Equations 4.18 and 4.19) show that the viscosity of the liquid does not appear in the equations. The physical reason for this is that the total force acting on the objects is made up of two components - one due to viscous forces and the other due to inertial forces. At low values of the Reynolds number ($Re < 5$) the viscous force is predominant and the viscosity value will be utilised, whereas for large values of the Reynolds number ($Re > 2 \times 10^5$) the inertia forces are far more important and viscous forces can be ignored.

The carrier gas density is a function of temperature and pressure

$$\rho_g = \frac{P_{atm} + \rho_l g (H - Z)}{R T_g}$$ (4.20)

and will decrease as the gas rises in the plume. Despite the decreasing ferro-static head the bubble size is assumed to remain constant during rising, which implies bubble break-up (along with increasing gas volume fractions) within the plume.

Bubble size is a function of the carrier gas flowrate and orifice diameter. The volume of the bubbles was calculated by using the following empirical correlation (Irons, 1978)

$$V_b = 0.083 \cdot QR^{0.867} \cdot D_o^{0.435}$$ (4.21)

Initial conditions

With regard to initial conditions when solving the model, the extremely rapid expansion of the jet (Oryall, 1976) makes it fair to assume that the plume reaches maximum diameter at $Z = 0$. The initial liquid velocity at $Z = 0$ can be estimated by using the average recirculation velocity (Sano, 1983)

$$U_{l\text{-ini}} = \frac{1.17 \left(Q_{gm} g H A_{pl}^2 \right)^{0.339}}{\frac{\pi}{4} \left(D_L^2 - D_p^2 \right)}$$ (4.22)

with Q_{gm} representing the gas flow rate at the bulk liquid temperature and mean pressure

$$Q_{gm} = \frac{MFRG}{\left[\dfrac{\left(P_{atm} + \rho_l gZ\right)}{\left(300R_{eng}\right)}\right]}$$

(4.23)

Due to the substantial density difference between the carrier gas and the molten iron, the subsequent buoyancy force will be dominant enough to assume that the initial velocity of the bubble will be close to terminal.

$$U_{Terminal} = 1.02\left(\frac{gd_b}{2}\right)^{\frac{1}{2}}$$

(4.24)

Taking into account that the bubbles will move at a velocity relative to the flow of liquid, the initial bubble velocity is calculated as follows

$$U_{g-ini} = U_l + 1.02\left(\frac{gd_b}{2}\right)^{\frac{1}{2}} = U_l + U_{Terminal}$$

(4.25)

The diameter of the bubble is calculated by utilising Equation 4.21

$$d_b = \left(\frac{6 \cdot V_b}{\pi}\right)^{\frac{1}{3}}$$

(4.26)

and the initial velocity of the CaC$_2$ particles in the liquid iron is set equal to the initial velocity of the liquid iron itself.

$$U_{l-ini} = U_{p-ini}$$

(4.27)

The particles associated with the bubbles will travel at the same speed as the bubbles.

The gas volume fraction in a submerged air jet, injected horisontally into mercury, has been measured under non-reactive conditions (Oryall, 1976). The measurements revealed that the jets expanded extremely rapidly upon discharge from the nozzle with an initial expansion angle of 155 degrees. Along with rapid expansion it was also found that the jet penetrated extensively behind the nozzle, creating almost the same effect as a vertically injected nozzle. Although the volume fraction of the carrier gas at the orifice can be as high as 90 percent, it was shown that rapid liquid entrainment will ensure that the fraction of gas inside the plume will decrease to less that 10 percent within as little as 8 cm above the orifice. For this reason the volume fractions of the three phases were defined as simple functions of the various velocities, mass flow rates and plume area and their initial values determined through the following equations

$$\theta_g = \frac{MFRG}{\left(\rho_g U_{g-ini} A_{pl}\right)} \qquad\qquad (4.28)$$

$$\theta_p = \left(\frac{MFRP \cdot f}{\left(\rho_p U_{g-ini} A_{pl}\right)}\right) + \left(\frac{MFRP \cdot (1-f)}{\left(\rho_p U_{p-ini} A_{pl}\right)}\right) \qquad (4.29)$$

$$\theta_l = 1 - \left(\theta_g + \theta_p\right) \qquad\qquad (4.30)$$

Plume heat transfer equations

For heat transfer, it was assumed that the important heat transfer mechanisms in the plume were radiation from liquid to particles inside

the bubble (G_1), convection from the liquid to the particles in the liquid (G_2), convection from the liquid to the bubbles (G_3) and convection from the gas to the particles inside the bubbles (G_4) (Farias, 1985).

Four separate heat transfer equations have been written, making a clear distinction between the particles associated with the liquid and the particles associated with the bubbles. With these equations the temperatures of these four phases were calculated as a function of the vertical distance from the bottom of the plume.

Model assumptions

❑ There is no exchange of mechanical and thermal energy, thus only thermal energy balances need to be considered (Farias, Irons, 1985a)

❑ Although the mechanism of diffusion (random transfer of fluid molecules) contributes to convection transfer, the dominant contribution is generally made by the bulk motion of fluid particles with the diffusion effect being negligible (Incropera, 1990)

❑ Viscous dissipation is ignored (Farias, Irons, 1985a)

❑ Forced convection is assumed, thereby eliminating the need to consider temperature gradients brought on by internal density variations (Farias, Irons, 1985a)

❑ The specific heat capacity and thermal conductivity values of all phases do not vary significantly with pressure or temperature and were therefore kept constant at the bulk liquid temperature (Farias, Irons, 1985a)

❑ The heat of wetting the solids is negligible (Farias, Irons, 1985a)

❑ Internal temperature gradients within the calcium carbide particles are ignored (Farias, Irons, 1985a)

- ❏ Conduction of heat radially and axially is negligible in comparison to that of convective transport (Farias, Irons, 1985a)
- ❏ The cooling effect of the lance is negligible
- ❏ The entrained liquid is at the bulk bath temperature (Farias, Irons, 1985a)

Mathematical Formulation

With these assumptions the heat flow rate balances per unit volume of plume were written for the four phases (Farias, Irons, 1985a)

Liquid phase

$$\theta_l \rho_l U_l Cp_l \frac{dT_l}{dZ} = -G_1\left(T_l^4 - T_{pg}^4\right) - G_2\left(T_l - T_{pl}\right) - G_3\left(T_l - T_g\right) + \rho_l Cp_l T_{bulk} \frac{d\theta_l U_l}{dZ}$$

(4.31)

Particles in the liquid

$$(1-f)\theta_l \rho_p U_p Cp_p \frac{dT_{pl}}{dZ} = G_2\left(T_l - T_{pl}\right)$$

(4.32)

Particles in the gas

$$f\theta_p \rho_p U_g Cp_p \frac{dT_{pg}}{dZ} = G_1\left(T_l^4 - T_{pg}^4\right) + G_4\left(T_g - T_{pg}\right)$$

(4.33)

Gas phase

$$\theta_g \rho_g U_g Cp_g \frac{dT_g}{dZ} = G_3\left(T_l - T_g\right) - G_4\left(T_g - T_{pg}\right)$$

(4.34)

For the radiation mechanism the particles were assumed to behave as grey bodies with a radiation shape of one with the radiation heat transfer function defined as follows (Chiang, 1987)

$$G_1 = \frac{\left(\dfrac{V_p\, f\theta_p\, \sigma}{A_p}\right)}{\left(\dfrac{f\theta_p\, d_b}{\left((\theta_g + f\theta_p)d_p\, \varepsilon_l\right)} + \dfrac{1}{\varepsilon_p} - 1\right)} \qquad (4.35)$$

For convection to the particles in the liquid the heat transfer function can be calculated by employing the following equation

$$G_2 = \frac{A_p\, h_p\, (1-f)\theta_p}{V_p} = \frac{6 \cdot h_p\, (1-f)\theta_p}{d_p} \qquad (4.36)$$

where the heat transfer coefficient h_p was obtained from the Ranz-Marshall correlation for spheres under forced convection conditions

$$h_p = \frac{kc_l}{d_p}\left(2 + 0.6Re_p^{0.5}\, Pr_l^{0.33}\right) \qquad (4.37)$$

with Re_p defined by Equation 2.21.

For convection to the gas bubbles the heat transfer function is

$$G_3 = \frac{6 \cdot h_b\, \theta_g}{d_b} \qquad (4.38)$$

with the heat transfer coefficient obtained from the penetration theory applied to gas phase resistance (Chiang, 1987)

$$h_b \;=\; \left[\frac{4 \cdot \rho_g Cp_g kc_g \left(U_g - U_l \right)}{\pi d_b} \right] \qquad (4.39)$$

Finally, for the convection to the particles in the gas it was assumed that the particles were dispersed within the bubble and travelled at the terminal velocity

$$G_4 \;=\; \frac{6 \cdot h_{gp} \cdot f \cdot \theta_p}{d_p} \qquad (4.40)$$

where

$$h_{gp} \;=\; \frac{kc_g}{d_p} \left(2 + 0.6 Re_{gp}^{0.5} Pr_g^{0.33} \right) \qquad (4.41)$$

Initial Conditions

The temperature of CaC_2 and nitrogen at the bottom of the jet (Z = 0) are assumed to be 25°C. The liquid temperature at the bottom of the plume is assumed to be the same as the liquid bulk temperature.

Plume mass transfer equations

Taking into consideration that all previous assumption still applies, the model for the overall sulphur balance in the plume is formulated based on the original, as well as the following additional assumptions.

Model Assumptions

- The diffusion flux as a result of the sulphur gradient in the plume is negligible
- The calcium carbide particles after travelling through the plume are absorbed by the top slag
- The calcium carbide desulphurisation is confined to the plume

Mathematical Formulation

The overall rate of desulphurisation in the plume is described by formulating the conservation equation of sulphur at steady-state, over a control volume unit

---

Convective transfer of sulphur   +   Entrained transfer of sulphur   +   Desulphurisation = 0

With the desulphurisation segment represented by Equation 4.3 to 4.9, the remaining terms of the above-mentioned sulphur balance can be written in differential form (Chiang, 1991).

$$\frac{dC_S^{pl} U_l A_{pl} \theta_l}{dZ} = \frac{dC_S^{b} U_l A_{pl} \theta_l}{dZ} - J_1\left(C_S^{pl} - C_S^{ip}\right) - J_2\left(C_S^{pl} - C_S^{ib}\right) \qquad (4.42)$$

Initial Conditions

With reference to boundary conditions, the sulphur concentration in the liquid at the bottom of the plume (Z = 0) is assumed to have the same

value as that of the bulk sulphur concentration in the liquid. The initial sulphur content of the CaC_2 particle is assumed to be zero at $Z = 0$.

Plume desulphurisation rate

In the present model the rate of desulphurisation in the plume can be determined through the reduction in sulphur content and the residence time of the CaC_2 particles in the liquid. As will be seen in Section 6.1.3 of this study, the contribution of the CaC_2 particles associated with the bubbles towards the desulphurisation reaction is insignificant and its residence times are not considered.

$$\frac{dC_S^b}{dt} = \frac{C_{S,t}^{pl} - C_{S,(t+t_{Res})}^{pl}}{t_{Res}} \qquad (4.43)$$

DEVELOPMENT OF MODEL - TOPSLAG

After the calcium carbide particles reach the surface they are incorporated into the topslag and continue desulphurising through slag-metal reactions, thereby increasing the overall utilisation of reagent. Certain key parameters exert substantial influence on the topslags' contribution towards the overall desulphurisation potential of the system.

Sulphur distribution ratio (L_S)

The sulphur distribution ratio is a measure of the thermodynamic ability of the slag to contain sulphur. It takes into account the effect of the various components of the slag on the activities of the sulphur and oxygen ions in the metal-slag system that has a direct influence on the

sulphur distribution ratio. In turn the activities of sulphur and oxygen in the metal-slag system is a function of the composition of the slag.

Amount of slag

During the desulphurisation process, the injected calcium carbide reagent becomes part of the topslag, thereby contributing to the ever-increasing amount of topslag. An increased amount of topslag will result in an increase in the topslag's ability to desulphurise liquid iron (Seshadri, 1997). Also of critical importance is the amount of carry-over slag contributed to the process via the Corex, even before desulphurisation commences (Engell, 1988). These parameters are accounted for in model presented in the following section.

Mathematical Formulation

The total contribution of the topslag to the rate of desulphurisation can be expressed as (Seshadri, 1997)

$$
\frac{dC_S^b}{dt} = -\left[\frac{10 \cdot \rho_l \cdot K_{ms} \cdot A_{ts}}{M_{Sul} \cdot METWT}\right]\left[\frac{M_{Sul} \cdot C_S^b}{10} - \rho_l\left[\frac{\left(\frac{METWT \cdot M_{Sul}}{10 \cdot \rho_l}\right)\left(C_{S,i} - C_S^b\right) + M_{ts(t=0)}\left(\%S\right)_o}{L_S\left(M_{ts(t=0)} + MFRP \cdot t\right)}\right]\right]
$$

(4.44)

where

$$
K_{ms} = \beta \cdot \left(D_S \frac{Q'}{A_{ts}}\right) \quad \text{where,} \quad Q' = \frac{QR \cdot T}{273}
$$

(4.45)

and β equal to a value of 500.

MODEL SOLUTION

Together Equation 4.3 to 4.43 constitute the complete mathematical formulation of momentum, heat and mass transfer of sulphur for calcium carbide desulphurisation in the plume. After all the necessary substitutions and mathematical manipulations (product rule) had been completed, the system was represented by a set of ten stiff, coupled, first-order differential equations for the three phase velocities, the temperatures of the liquid, gas and particles associated with the liquid and the bubbles, the sulphur concentration in the plume and the utilisation of the particles in the liquid and in the bubbles (Polking, 1995). The relevant equations are represented in matrix format (Constantinides, Mostoufi, 1999)

$$[M] \cdot [N] = [Q] \tag{4.46}$$

or in detail

$$
\begin{bmatrix}
1 & 0 & 0 & 0 & 0 & 0 & 0 & 0 & 0 & 0 \\
0 & 1 & 0 & 0 & 0 & 0 & 0 & 0 & 0 & 0 \\
0 & 0 & 1 & 0 & 0 & 0 & 0 & 0 & 0 & 0 \\
0 & 0 & 2T_l - T_{bl} & 0 & 0 & 0 & U_l & 0 & 0 & 0 \\
0 & 0 & 0 & 0 & 0 & 1 & 0 & 0 & 0 & 0 \\
0 & 0 & 0 & 0 & 1 & 0 & 0 & 0 & 0 & 0 \\
0 & 0 & 0 & 1 & 0 & 0 & 0 & 0 & 0 & 0 \\
0 & 0 & C_{pl} - C_b & 0 & 0 & 0 & 0 & U_l & 0 & 0 \\
0 & \alpha_{pl} & 0 & 0 & 0 & 0 & 0 & 0 & 0 & U_p \\
\alpha_{pg} & 0 & 0 & 0 & 0 & 0 & 0 & 0 & U_g & 0
\end{bmatrix}
\cdot
\begin{bmatrix}
U_g \\
U_p \\
U_l \\
T_g \\
T_{pg} \\
T_{pl} \\
T_l \\
C_{pl} \\
\alpha_{pg} \\
\alpha_{pl}
\end{bmatrix}
=
\begin{bmatrix}
F1 \\
F2 \\
F3 \\
F4 \\
F5 \\
F6 \\
F7 \\
F8 \\
F9 \\
F10
\end{bmatrix}
\tag{4.47}
$$

with the value of F1 being shown as an example.

F1 represents the righthand side of the first manipulated equation describing the velocity of the carrier gas flow in the ladle as a function of distance (U_g).

$$F1 \quad = \quad \left[\frac{F_{pg}^{B} - F_{pg-I}^{D}}{2\rho_m U_g A_p} \right] \qquad (4.48)$$

A MATLAB program incorporating all the obligatory equations, together with the rate equation of topslag desulphurisation (Equation 4.44 to Equation 4.45) so as to obtain the overall rate of desulphurisation during injection was designed in order to perform the required desulphurisation calculations, as well as in-depth sensitivity analysis on key parameters.

For MATLAB to solve the subscribed set of ordinary differential equations, further mathematical manipulation involving elementary matrix calculations was required and the 10 × 1 matrix ($[N]$) comprising of the ten variables in question needs be expressed as follows:

$$[N] = [M]^{-1} \cdot [Q] \qquad (4.49)$$

with the quantity $[M]^{-1}$ representing the inverse of the 10 × 10 matrix

$$[M]^{-1} = \begin{bmatrix} 1 & 0 & 0 & 0 & 0 & 0 & 0 & 0 & 0 & 0 \\ 0 & 1 & 0 & 0 & 0 & 0 & 0 & 0 & 0 & 0 \\ 0 & 0 & 1 & 0 & 0 & 0 & 0 & 0 & 0 & 0 \\ 0 & 0 & 0 & 0 & 0 & 0 & 1 & 0 & 0 & 0 \\ 0 & 0 & 0 & 0 & 0 & 1 & 0 & 0 & 0 & 0 \\ 0 & 0 & 0 & 0 & 1 & 0 & 0 & 0 & 0 & 0 \\ 0 & 0 & \dfrac{T_b}{U_l} & \dfrac{1}{U_l} & 0 & 0 & 0 & 0 & 0 & 0 \\ 0 & 0 & \dfrac{C_{pl}U_gU_lU_p - C_bU_gU_lU_p}{U_gU_l^2U_p} & 0 & 0 & 0 & 0 & \dfrac{1}{U_l} & 0 & 0 \\ \dfrac{\alpha_{pg}}{U_g} & 0 & 0 & 0 & 0 & 0 & 0 & 0 & 0 & \dfrac{1}{U_g} \\ 0 & \dfrac{\alpha_{pl}}{U_p} & 0 & 0 & 0 & 0 & 0 & 0 & \dfrac{1}{U_p} & 0 \end{bmatrix} \quad (4.50)$$

Finally $[N]$ can be presented in a format suitable for MATLAB calculations, with the relevant source code for the MATLAB program shown in Appendix B.

$$[N] = \begin{bmatrix} U_g \\ U_p \\ U_l \\ T_g \\ T_{pg} \\ T_{pl} \\ T_l \\ C_{pl} \\ \alpha_{pg} \\ \alpha_{pl} \end{bmatrix} = \begin{bmatrix} F1 \\ F2 \\ F3 \\ F7 \\ F6 \\ F5 \\ \left(\dfrac{F4}{U_l} + \dfrac{F3\left(T_{bl}U_g^3U_lU_p^2 - T_lU_g^3U_lU_p^2\right)}{U_g^3U_l^2U_p^3} \right) \\ \left(\dfrac{F3\left(C_{pl}U_gU_lU_p - C_bU_gU_lU_p\right)}{U_gU_l^2U_p} + \dfrac{F8}{U_l} \right) \\ \left(\dfrac{F10}{U_g} + \dfrac{F1\cdot\alpha_{pg}}{U_g} \right) \\ \dfrac{F9}{U_p} - \dfrac{F2\cdot\alpha_{pl}}{U_p} \end{bmatrix} \quad (4.51)$$

The next section will be devoted to the validation of the proposed model.

5. MODEL VALIDATION

The most important step in mathematical model development is the verification of subsequent solutions. The predictions of the model have to be compared with experimental measurements (Ilegbusi, 2000) and possible discrepancies resolved by critically examining both

❑ the accuracy of measurements, and
❑ the appropriateness of the assumptions made.

These experimental measurements may be obtained using physical models, pilots, or actual data obtained in real manufacturing systems. In this study actual data obtained in a real manufacturing environment was utilised and provided by Saldanha Steel.

PARAMETER FITTING AND MODEL TESTING

Subject to actual process conditions as set out in Table 5.1, it was calculated that the final sulphur value in the iron after desulphurisation at the LID section at Saldanha Steel would be equal to an average value of **0.036 wt%**. The authentic data set utilised to determine the value in question could be found in Appendix C.1.

Table 5.1 Default parameters

Parameter	Parameter value (with 95% confidence levels)
Initial sulphur value in the iron	0.077 ($\pm$ 0.0017) wt%
Mass of iron in ladle	95035 ($\pm$ 506) kg
Injection depth	2.2 m (below the surface)
Carrier gas flowrate	0.014 m^3/s (840 litre/min)
Particle parameter position	0.7
Calcium carbide flowrate	0.51 ($\pm$ 0.023) kg/s
Reagent injection time	7.9 ($\pm$ 0.46) minutes

These values provided the base case needed to estimate the parameters and ultimately test the validity of the proposed desulphurisation model. While the aforementioned values remained constant throughout the training phase, the plume diameter, a particularly flexible parameter, was employed as a parameter-fitting tool.

Parameter Fitting

The diameter of the plume was very difficult to establish experimentally. Bearing in mind that the shape of the plume is cylindrical (Farias, 1986), a good approximation of the plume diameter could be found by monitoring the break-through diameter of the carrier gas area on the surface of the topslag during desulphurisation. It was established that the diameter of the break-through area fluctuated within certain experimental limits (See Table 5.2).

Table 5.2 Plume break-through diameter

Parameter	Upper limit [m]	Lower limit [m]
Plume diameter	2.4	1.5

By making use of the experimental values depicted in Table 5.2, the model was trained repeatedly with various plume diameter values from within the allowable region until a calcium carbide injection time of 7 minutes and 54 seconds (as produced by the model and also depicted in Table 5.1) coincided with a final sulphur value in the iron of 0.036 wt%. A plume diameter of 1.7 m provided the most accurate model calibration. This particular plume parameter was subsequently fixed at a value of 1.7 m and utilised in all succeeding model calculations.

Model Testing

With the training and parameter-fitting phase of the modelling process complete, the comparative prediction strength of the model was verified through testing with different sets of industry values.

Conditions A

Subject to another set of industrial conditions defined in Table 5.3, the final sulphur value in the iron after desulphurisation at the LID section at Saldanha Steel was equal to **0.041 wt%**, with the data set found in Appendix C.2.

Table 5.3 Industrial conditions A

Parameter	Parameter value
Initial sulphur value in the iron	0.067 wt%
Mass of iron in ladle	94960 kg
Injection depth	2.2 m (below the surface)
Calcium carbide flowrate	0.3 kg/s
Reagent injection time	8.2 minutes

With these values providing the input parameters to the model, a solution predicting the final sulphur value after 8.2 minutes of desulphurisation was generated and the result depicted in Figure 5.1.
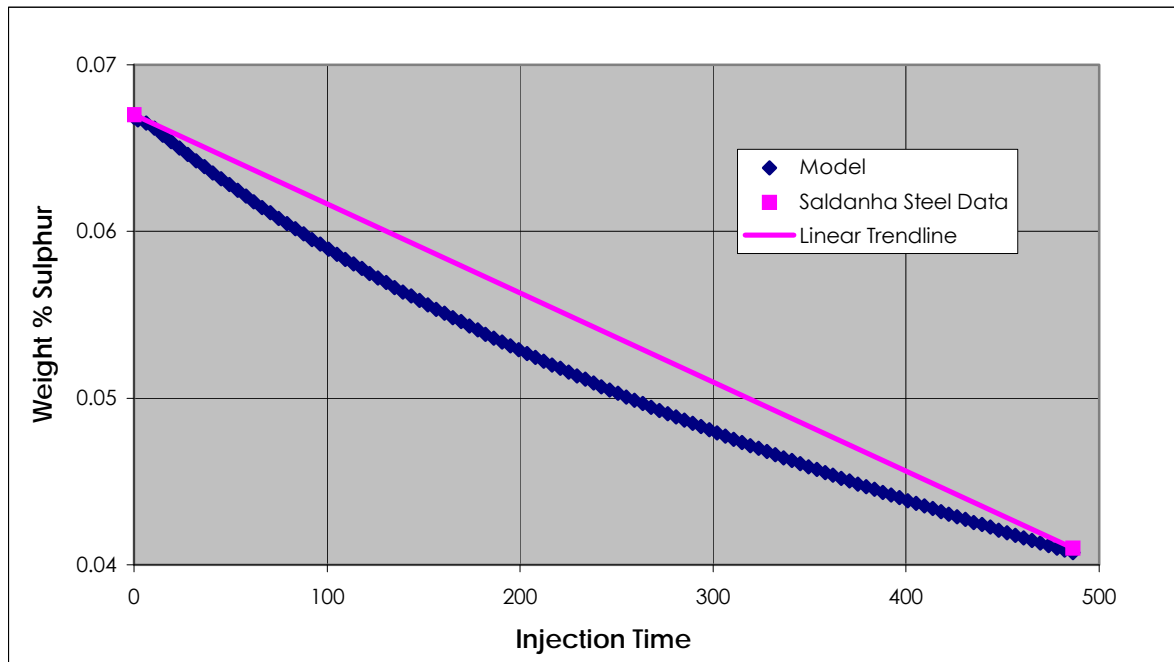
Figure 5.1 Conditions A: Industrial data compared to desulphurisation model results

At Saldanha Steel, as mentioned in Section 1.2, a representative sample of the iron can only be taken before and after calcium carbide injection. This is reflected in the fact that an actual desulphurisation run is only presented by two data points – one at the start and one at the end of the process. The proposed model solution however, not only supplies the final thermodynamic outcome but also provides valuable insight into the dynamic path of the desulphurisation process.   A more detailed discussion of model results can be seen in Chapter 6.

A comparative summary between the experimental and predicted average final sulphur concentrations in Table 5.4 shows excellent agreement between the two values.

Table 5.4 Industrial conditions A: Prediction strength

Parameter	Experimental	Model	Accuracy [%]
Final sulphur value [wt %]	0.041	0.0407	99.2 %

The accuracy of the prediction is calculated by utilising the following formula:

$$\text{Accuracy} \quad = \quad \left[1 - \left(\text{abs} \left| \frac{\text{Exp}_{value} - \text{Model}_{value}}{\text{Exp}_{value}} \right| \right) \right] \cdot 100 \qquad (5.1)$$

Conditions B

A third set of industrial conditions is defined in Table 5.5. An increase in liquid iron mass will cause an inevitable increase in the depth of injection owing to the fact that the desulphurisation lance at Saldanha Steel can, in the current mechanical set-up, only be lowered to one particular level (see Section 6.3.1).

The final sulphur value in the iron after desulphurisation at the LID section at Saldanha Steel was equal to **0.032 wt%**, with the data set depicting the conditions found in Appendix C.3.

Table 5.5 Industrial conditions B

Parameter	Parameter value
Initial sulphur value in the iron	0.063 wt%
Mass of iron in ladle	113133 kg
Injection depth	2.62 (below the surface)
Calcium carbide flowrate	0.51kg/s
Reagent injection time	8 minutes

A solution predicting the average final sulphur value after 8 minutes of desulphurisation was generated and the results are depicted in Figure 5.2.
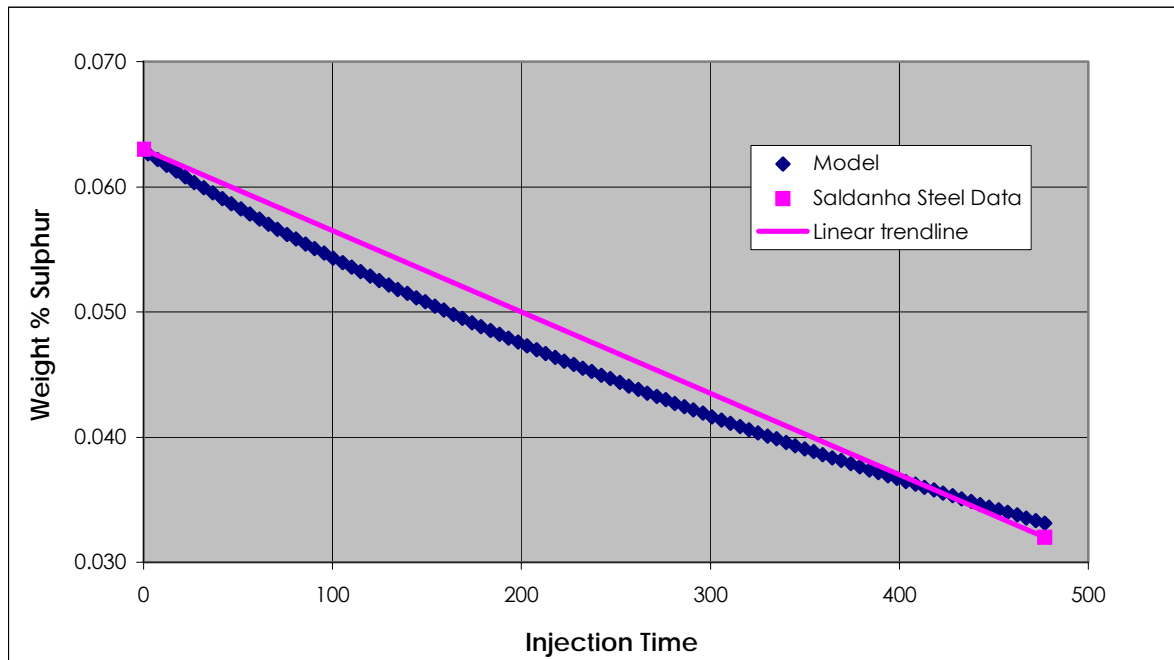
Figure 5.2 Conditions B: Industrial data compared to desulphurisation model results

A comparison between the experimental and predicted values, as seen in Table 5.6, once again confirms exceptional conformity between the two values.

Table 5.6 Industrial conditions B: Prediction strength

Parameter	Experimental	Model	Accuracy [%]
Final sulphur value [wt %]	0.032	0.0331	96.6 %

What makes the results of these two tests even more significant is the fact that the model sustains a very high level of predictive accuracy given large differences in reagent flowrate. Sensitivity analysis shown in Chapter 6, Section 6.2.2, will show that changes in the flowrate of the

desulphurising agent resulted in the most substantial changes in final sulphur concentration (the rate of desulphurisation). It is this capacity to facilitate these changes while still maintaining a high level of precision that instils confidence in the ability of the model.

PARTICLE POSITION

During the injection process the jets will expand very rapidly, with the gas and powder partially separating at the point of momentum dissipation. The calcium carbide powder may remain inside the carrier gas bubble or outside in the liquid iron. The fraction of particles associated with each phase plays a decisive role in the process, with the success of any proposed desulphurisation injection model inadvertently linked to the correct assessment of this influential parameter. In order to examine the impact of such a potentially sensitive parameter on the outcome of the model, three different particle-liquid contact patterns were simulated in combination with the default industrial conditions defined in Table 5.1, with the subsequent results are illustrated in Figure 5.3.
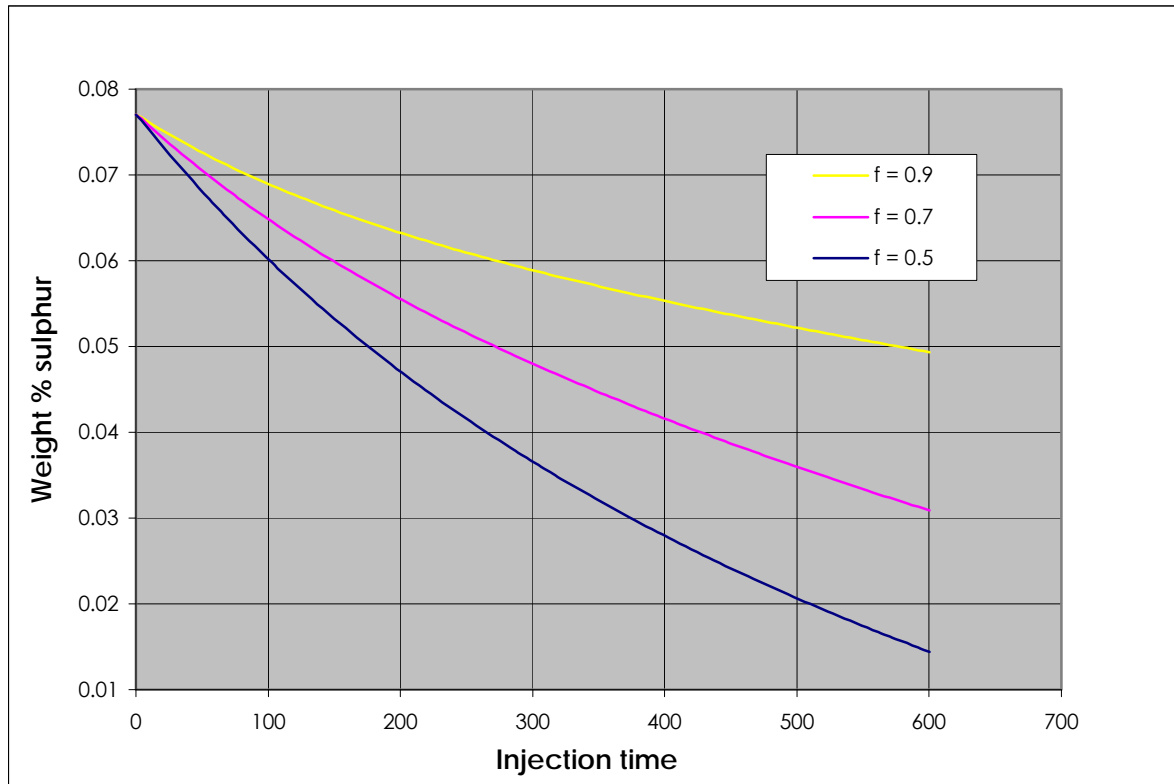
Figure 5.3 Variation in required desulphurisation injection times as a function of various f - values

By associating 50% of the calcium carbide particles with the liquid, the sulphur concentration in the ladle drops to a level of 0.05 weight percent exactly 7 minutes faster than the same system with only 10% of the calcium carbide particles associated with the metal. This once again underlines the fact that it is imperative for the choice of the particle position parameter (f) to reflect the system under investigation as accurately as possible.

The **actual** overall calcium carbide particle **utilisation** after desulphurisation given the default parameters at Saldanha Steel is 32.5 % of that expected from the following reaction

$$CaC_2 + S_{(\%inFe)} \quad \Leftrightarrow \quad CaS + 2C \qquad\qquad (5.2)$$

with the pertinent stoichiometric calculations validating the statement found in Appendix C.4. This utilisation value incorporates desulphurisation reactions taking place in the plume and in the topslag.

Figure 5.4 however, depicts the average **model-generated utilisation** of the calcium carbide particles as a result of 7.8 minutes of injection desulphurisation in **only the plume** at various particle position parameter values.
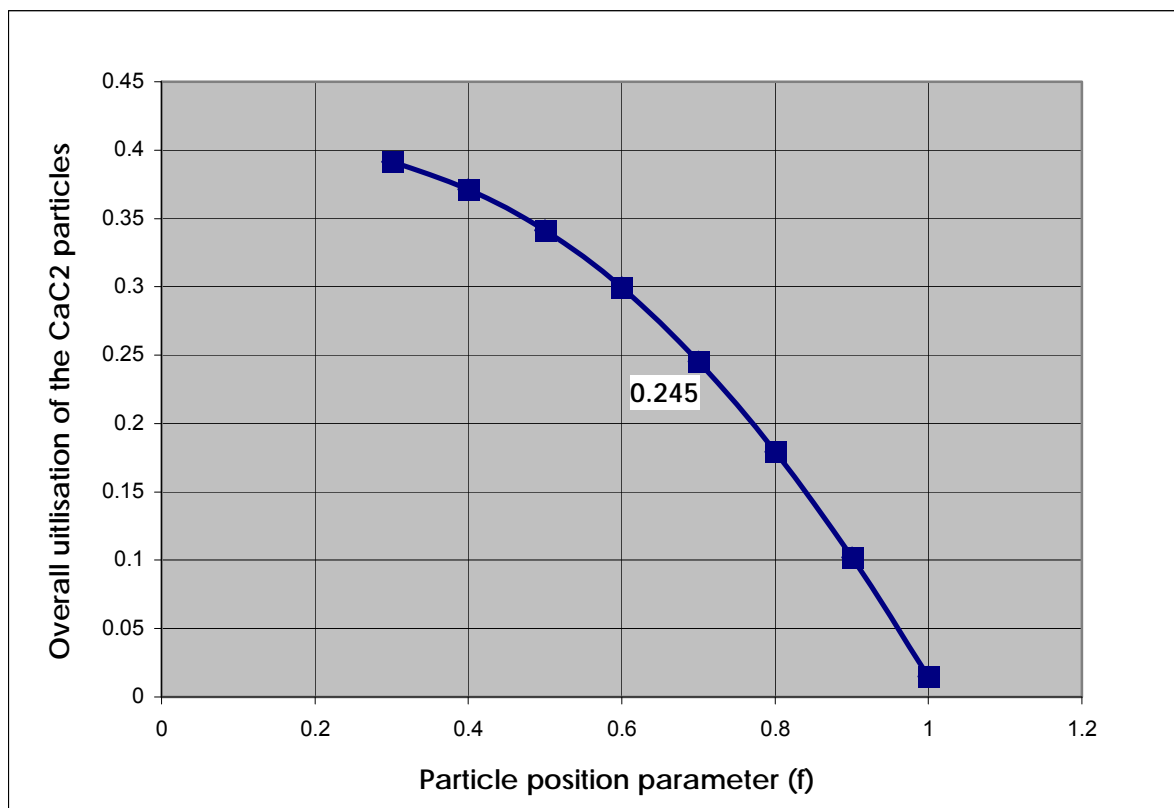
Figure 5.4 Average utilisation values of CaC2 particles in the plume as a function of f after 7.8 minutes of injection

At a particle position parameter value of 0.7, the proposed model shows a calcium carbide particle utilisation of 24.5 percent (in the plume alone). When combined with subsequent utilisation of calcium carbide in the topslag (8.8 percent), the average particle utilisation at a particle

position parameter value of 0.7 amounts to 33.3 percent of that expected from Equation 5.2. The concurring calculations can be found in Appendix C.5.

Table 5.7 Overall model utilisation

	Model	Actual	Accuracy
Overall CaC$_2$ utilisation	33.3 %	32.5 %	97.5%

The comparative results summarised in Table 5.7 supports the findings of Chiang *et al*, who proposed that during the injection process, 20 to 40 percent of the particles enter the melt with the remainder being positioned on the inside of the carrier gas interfaces. It is owing to the excellent agreement between the actual and the theoretical values found at a particle position parameter value of 0.7, that this particular value was used as the default value in all subsequent modelling exercises. For the complete summary of the model parameters, along with the required geometric measurements, material properties of the solid, gas and liquid phase and other essential values utilised in the model, consult Appendix A.

Although the results in the subsequent section are specific to a particular scenario, it still provides invaluable information and insights into the important variables and parameters playing a role in injection desulphurisation processes in general, along with the influence that changing parameters can have on the outcome of the procedure.

6. RESULTS AND DISCUSSION

A quasi-steady state, one-dimensional three phase model for the momentum, heat and mass transfer in an ascending gas-liquid-powder plume for the conditions relevant to the Saldanha Steel desulphurisation injection process has been developed. This has been done in conjunction with a model accounting for the contribution of topslag (carry over as well as reagent flux) to the overall desulphurisation rate and the following section will represent the generated results in detail.

The desulphurisation model provides valuable process insight into two very distinct and different aspects of the desulphurisation process. It has the ability to provide information concerning the velocity, temperature and utilisation profile of all three phases within the plume itself, as well as the capacity to monitor the sulphur concentration in the melt for the duration of the injection process.

In the following sections particular attention will be given to the model's analising ability in this regard, as well as investigating the manipulated, disturbance and control variables and their influence on the desulphurisation process as a whole. Unless stated otherwise, all results were generated by utilising the default industrial parameters seen in Table 6.1.

Table 6.1 Default parameters

Parameter	Parameter value (with 95% confidence levels)
Initial sulphur value in the iron	0.077 ($\pm$ 0.0017) wt%
Mass of iron in ladle	95035 ($\pm$ 506) kg
Injection depth	2.2 m (below the surface)
Carrier gas flowrate	0.014 m^3/s (840 litre/min)
Particle parameter position	0.7
Calcium carbide flowrate	0.51 ($\pm$ 0.023) kg/s
Reagent injection time	7.9 ($\pm$ 0.46) minutes

PLUME PROFILE

The model has the ability to generate information concerning the state of the three phases as a function of the vertical distance it is moving up and away from the bottom of the plume, thus creating a virtual "snapshot" of the conditions within the plume at a certain time.

Velocity profile

Figure 6.1 shows the velocity profiles of the three different phases within the plume as a function of the vertical distance from the bottom of the plume during the last second of operation.
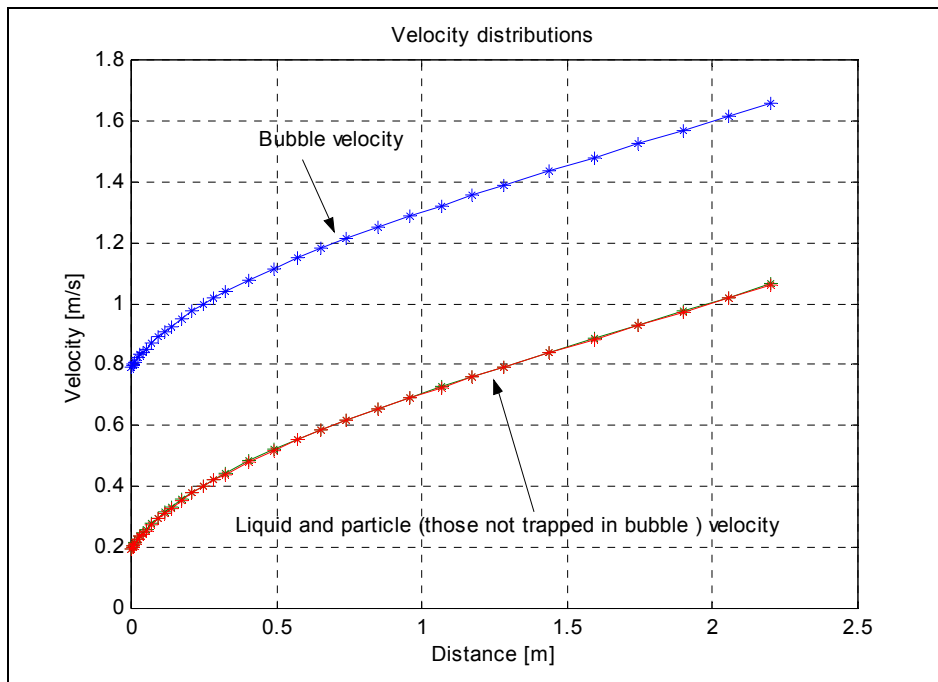
Figure 6.1 Velocity profile of the desulphurisation plume

The initial velocity of the liquid phase at the bottom of the plume is equal to the recirculation velocity within the ladle (Equation 4.22) and it is this particular parameter that indirectly determines the initial velocity of the carrier gas bubbles with respect to the ladle. Owing to the extremely large density difference between the gas and liquid phase, the buoyancy force acting on the bubble will be dominant enough to assume that the initial velocity of the bubble will be close to it's terminal velocity in the liquid melt (Equation 4.24). The initial velocity value of the gas phase as depicted in Figure 6.1 is therefore the cumulative value of the terminal velocity of the bubble in liquid iron at the current conditions, together with the recirculation velocity of the liquid. As can be seen in Figure 6.1, this difference in velocity between the two phases remains constant throughout the depth of the plume.

Upon momentum dissipation of the jets, some of the calcium carbide particles enter the liquid melt while the rest of the particles remain

trapped inside the gas bubbles. The rising velocity of the particles associated with the melt as measured against the velocity of the liquid, can be determined by utilising Stokes law (Szekely, 1971). This particular velocity however is small and virtually indistinguishable from the bulk liquid motion and will seemingly be travelling at the same speed as the bulk liquid. Owing to this reason, Figure 6.1 only seems to be indicating two out of a possible three velocity profiles, bearing in mind that the particles associated with the bubbles remain trapped inside the bubble and will travel at the same speed as the bubbles.

Temperature profile

Figure 6.2 shows the temperature profiles of the gas, liquid, particles in the melt and inside the bubbles.
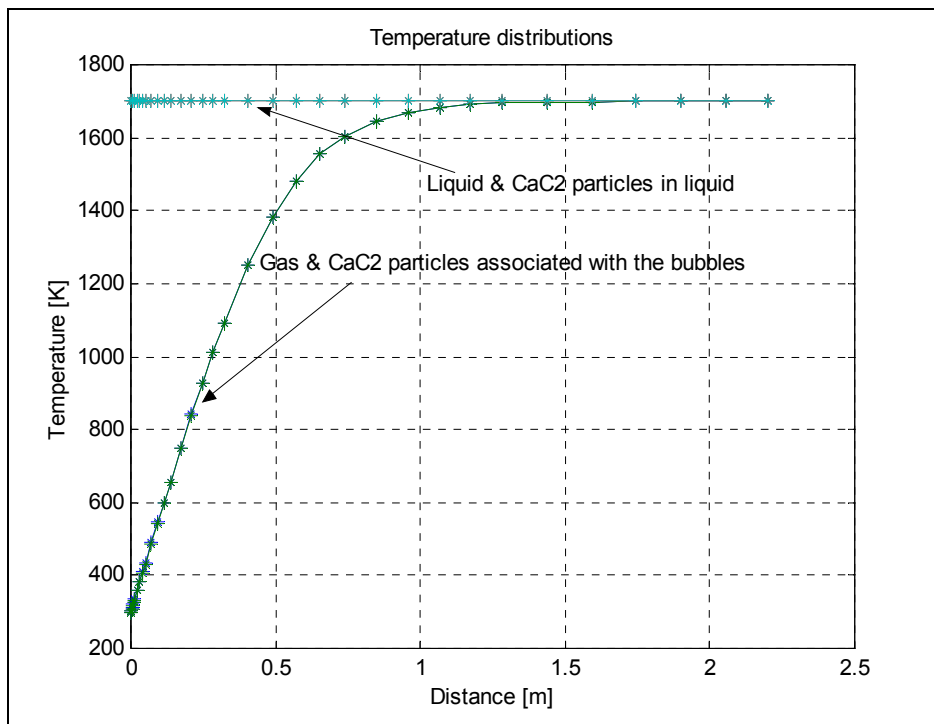
Figure 6.2 Temperature profile of the desulphurisation plume

Upon injection the temperature of the particles and the gas is at room temperature. For that reason a slight drop in liquid melt temperature at the bottom of the plume is expected (Figure 6.3), which is partially recovered as liquid is entrained into the plume.

At Saldanha Steel the average diameter of the calcium carbide particles is 75 microns and owing to its particularly small size, the particles inside the melt are heated almost instantaneously to the bulk metal temperature. The temperature profile of the particle inside the melt will therefore coincide with the temperature profile of the liquid in the ladle. Two heat transfer mechanisms were identified as being responsible for heating the particles inside the bubbles. The first is radiation from the bulk liquid to the particles and the second one is convection from the gas inside the bubble to the particles. The latter of these two mechanisms is the most dominant, thus allowing the temperature of the particles inside the bubble to increase only as fast as the temperature of the gas inside the bubbles. The gas inside the bubbles reaches liquid bulk temperature at a distance of 1.25 m above the bottom of the plume (Figure 6.2).
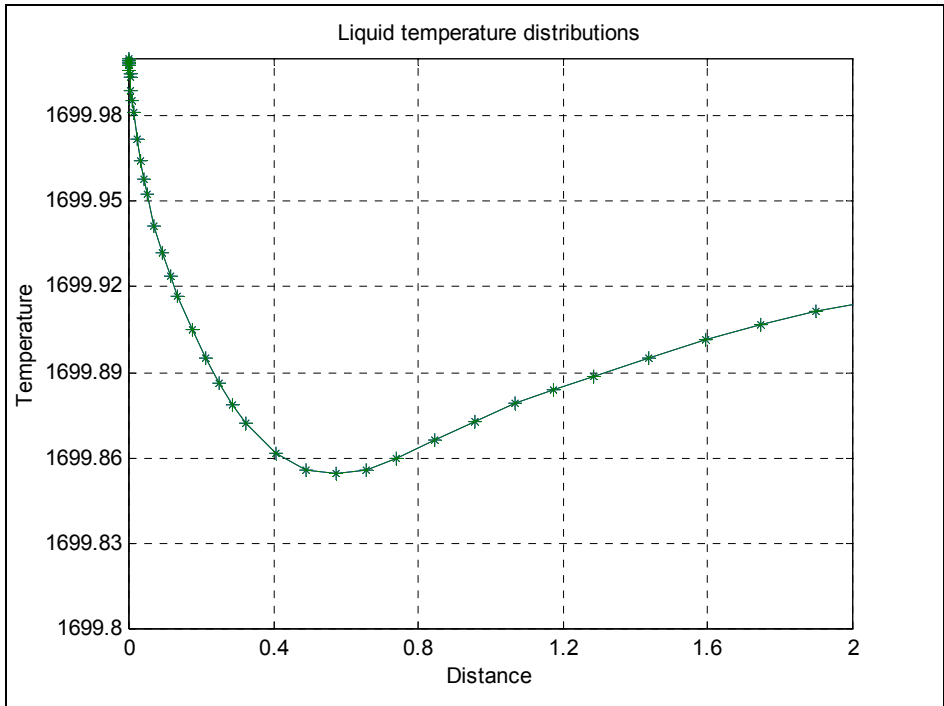
Figure 6.3 Temperature profile of the bulk liquid

Utilisation profile

Figure 6.4 shows the utilisation profiles of the particles in the melt and the particles associated with the bubbles.
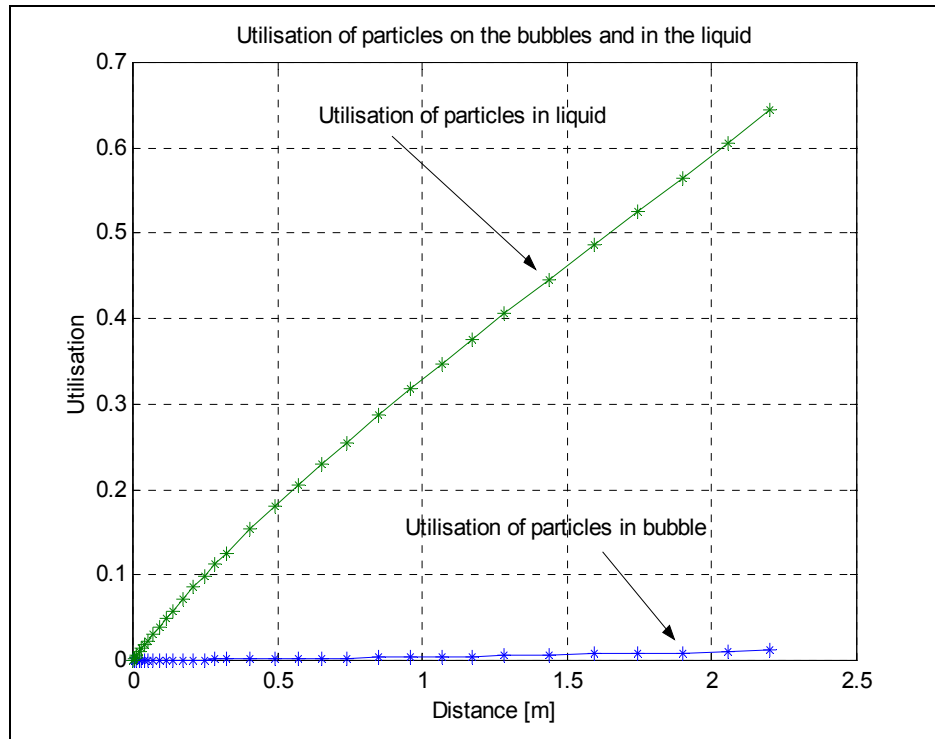
Figure 6.4 Utilisation profile of the desulphurisation plume

The particles in the melt quite clearly have far superior desulphurisation potential, with as much as 65 percent of the particle converted to calcium sulphide upon entry into the topslag. The particles associated with the bubbles however have very little positive impact on the process with only as little as 1 percent of the particles' desulphurisation potential utilised. The reason for this can be seen in Figure 6.5.
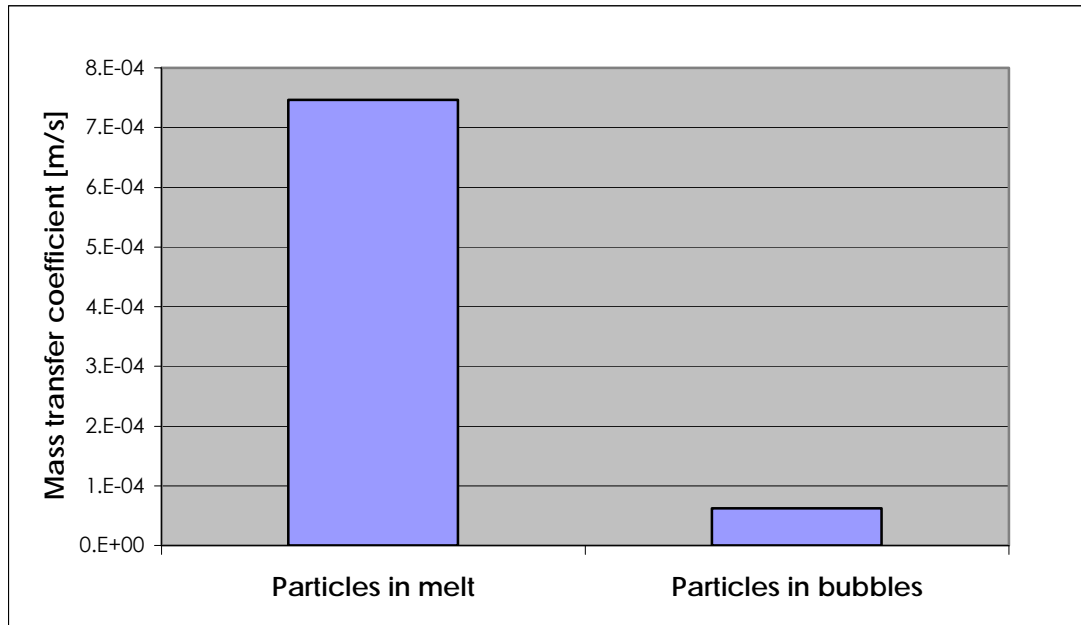
Figure 6.5 Mass transfer coefficient of particles in the melt and particles associated with the bubbles

For the sulphur in the melt to react with the calcium gas at the reaction interface of the calcium carbide particle, it only has to diffuse through the boundary layer around the particle. Through Equation 4.5, the turbulent mass transfer coefficient to particles in the melt was found to be 7.46×10^{-4} [m/s]. For sulphur to reach the calcium carbide particles situated inside the bubble however, it will first have to diffuse through the boundary layer around the bubble. By utilising the turbulent mass transfer coefficient equation proposed for spherical-capped bubbles (Equation 4.9), the mass transfer coefficient to the surface of these bubbles was found to 6.17×10^{-5} [m/s]. With the latter mass transfer coefficient more than one order of magnitude less than the former, the contribution of the particles inside the bubbles towards desulphurisation will inevitably be substantially lower.

The total average utilisation of the calcium carbide particles associated with both phases can be calculated as follows

$$\alpha_{Total} = \alpha_{pl}(1-f) + \alpha_{pg}f \qquad\qquad (6.1)$$

Through careful analysis of the above-mentioned equation, the importance of the choice of the particle position parameter value (f) once again becomes unmistakably evident. Even a relatively insignificant change in f could drastically alter the total utilisation value of the reagent.

EFFECT OF THE MANIPULATED VARIABLES

It is well known that the chemical reactions in most high temperature metallurgical refining systems are very fast. It was shown in Section 4.2.1.2 that under these conditions, the rate of calcium carbide desulphurisation is controlled by the transport of sulphur to the reaction interface. Whether the control lies solely in the steps of mixing; mass transfer of sulphur in the hot metal or mixed control by both these steps, depends mainly on the carrier gas and reagent flowrates and as a result, the injection depth.

Carrier gas flowrate

The carrier gas not only delivers the desulphurising agent into the metal, but in the absence of any mechanical stirring, the carrier gas also fulfils the role of stirring agent. The Saldanha Steel desulphurisation plant utilises nitrogen gas as their reagent carrier. Various nitrogen flowrates were modelled and the results are depicted in Figure 6.6.
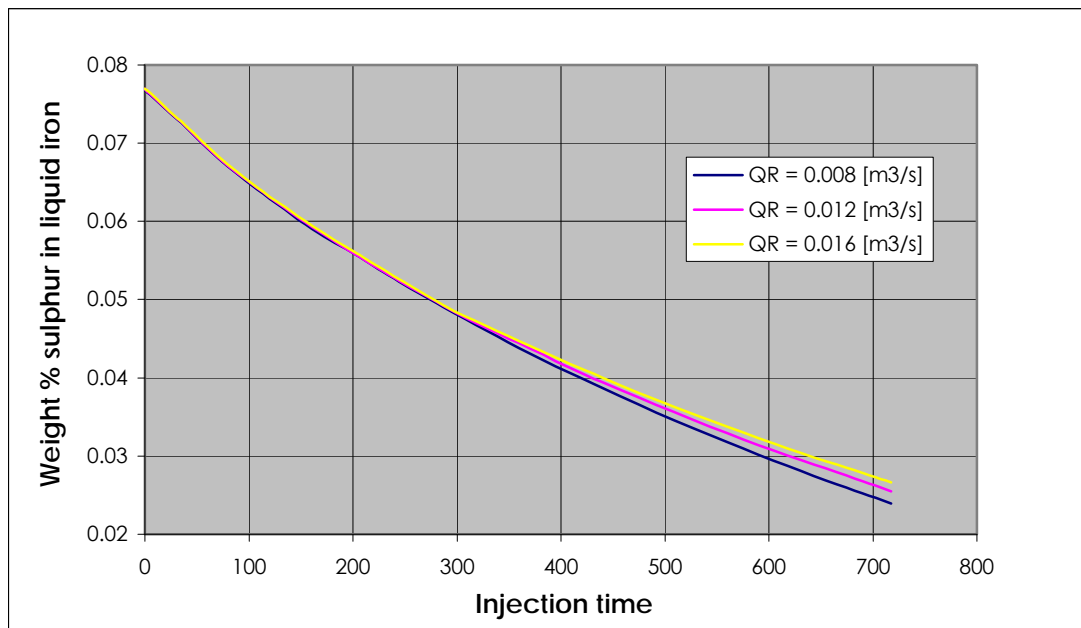
Figure 6.6 Variation in required desulphurisation injection times as a function of various carrier gas flowrates

At double the carrier gas flowrate, no significant disparity in injection time required to reach the desired sulphur level, was observed. The rate of desulphurisation and therefore the final concentration of the sulphur in the melt (0.036 wt%) is actually influenced by two competing factors as far as the carrier gas flowrate is concerned:

❑ As the carrier gas flowrate increases, so too will the recirculation velocity of the ladle (Equation 4.22). An increase in liquid velocity will cause a decrease in residence time of both the particles in the melt and the bubbles. Even though the bubbles reach terminal rising velocity almost immediately, their velocity relative to the ladle is a function of liquid recirculation velocity. The less time the calcium carbide particles spend in the plume, the less effective the desulphurisation result will become. Due to this subsequent decrease in residence time, the rate of desulphurisation within the plume will reduce.

❑ On the other hand, as the carrier gas flowrate increases, so will the agitation rate of the melt. These phenomena will result in an increase in the topslag desulphurisation rate. The additional stirring will cause the topslag-metal interface renewal rate to be boosted, thus avoiding its premature saturation and resulting in higher sulphur mass transfer coefficient inside the boundary layers. The desulphurisation rate will increase along with the mass transfer coefficient as seen in Equation 4.45.

The negative desulphurisation effect in the plume brought on by the decreased calcium carbide residence time however, is the slightly more dominant role-player, explaining the slight increase in overall injection time required at higher carrier gas flowrates.

The "required injection time" refers to the time it will take, given the default industrial parameters, for the sulphur content in the iron to drop to 0.036 weight percent.

Reagent flowrate

Of all the various desulphurisation parameters tested with the model, it was the alterations made to the calcium carbide flowrate that resulted in the most substantial changes in the required injection rate.
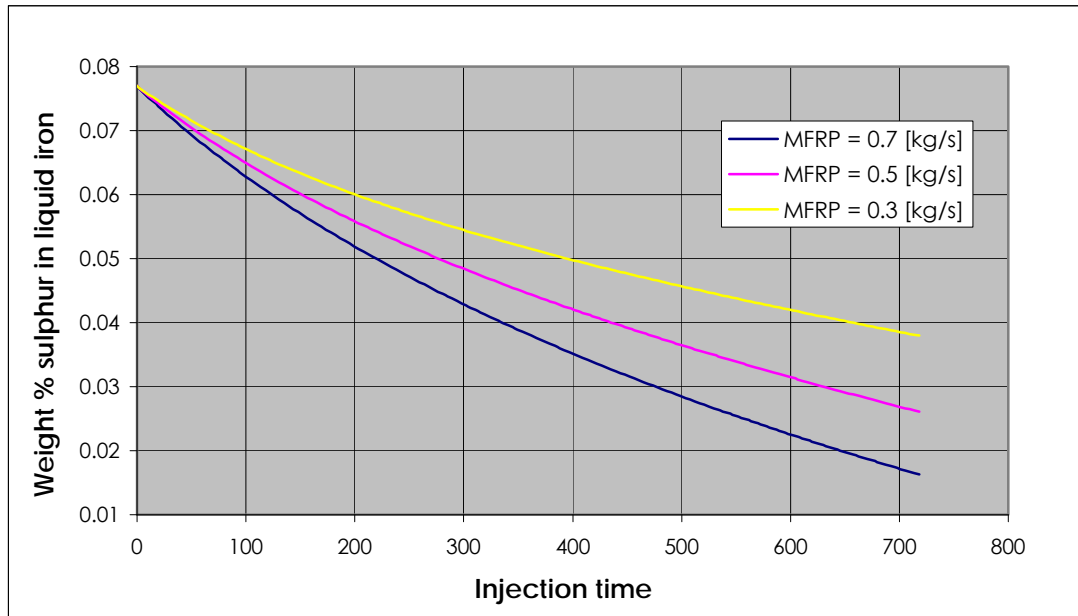
Figure 6.7 Variation in required desulphurisation injection times as a function of various reagent mass flowrates

By slightly more than doubling the reagent flowrate from 0.3 kg/s to 0.7 kg/s, the required injection time was cut by more than 5 minutes. The reason for such a significant change in the rate of desulphurisation can be found in the substantial difference in utilisation between particle in the melt and particles associated with the bubbles. Upon entering the topslag, the particles associated with the bubbles hardly participate in the process, with only about 1 percent of their desulphurisation potential utilised. In sharp contrast, the particles trapped in the melt has a 65 percent conversion rate (Figure 6.4). Assuming that the particle position parameter value remains at 0.7, any increase in the reagent flowrate will result in a sharp increase in the amount of calcium carbide in the melt. With such a high conversion rate, along with subsequent increases in the overall interfacial area between reagent and metal available for the relevant reactions, the desulphurisation benefits are bound to be considerable.

By far the biggest influence on the liquid recirculation velocity is the buoyancy force created by the bubbles of the carrier gas. When only the reagent flowrate is increased, the difference in liquid velocity is negligible and can be ignored. If anything, the liquid velocity will slightly decrease: A rise in calcium carbide flowrate will result in greater particle load on the bubbles, which will bring about an escalation in the density of the gas-powder mixture (ρ_m). According to Equation 4.16, this will cause the buoyancy force created by the bubbles to decrease somewhat and the liquid recirculation velocity to follow suit. The increase in overall interfacial reaction-area due to a boost in reagent flowrate therefore remains the fundamental motivation for the sizeable improvement in the desulphurisation rate.

Although a rise in reagent flowrate will bring about a consequential increase in the amount of calcium carbide utilised, the possible financial implications of such an action is insignificant compared to the subsequent savings that could come about with a decrease in required injection time. These and other financial implications as a result of suggested changes in the current desulphurisation process will be fully discussed in Section 6.4.

Injection depth

Three different injections depths were modelled and the results are depicted in Figure 6.8.
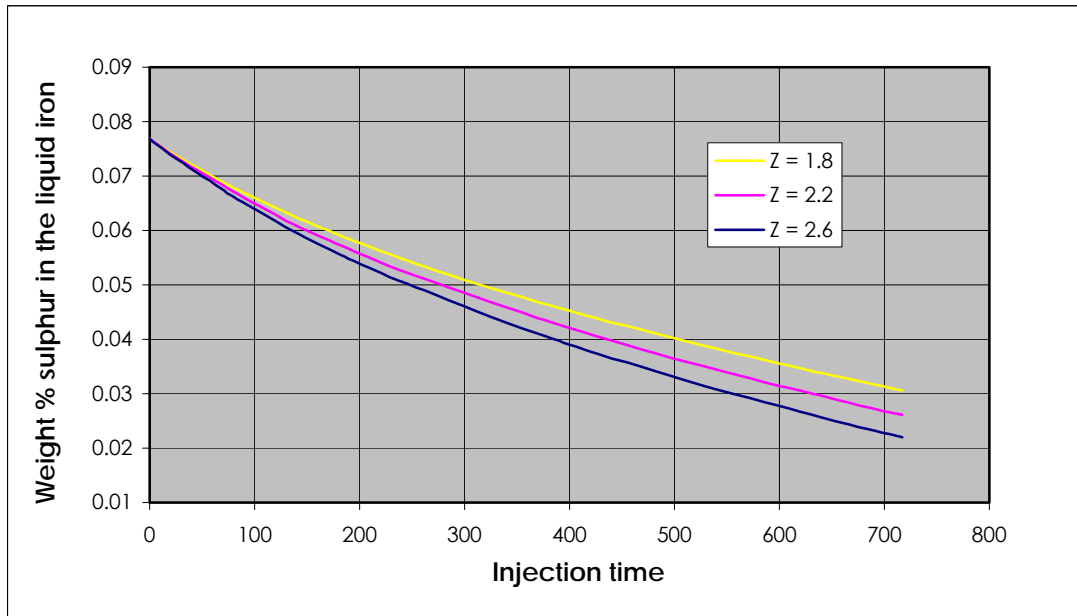
Figure 6.8 Variation in required desulphurisation injection times as a function of various injection depths

Although not as influential as a change in calcium carbide flowrate, a change in the injection depth of the desulphurising agent has a substantial effect on the process. Once again the rate of desulphurisation and therefore the final concentration of the sulphur in the melt is influenced by two opposing factors:

❑ As can be seen from Equation 4.22, an increase in injection depth will result in an increase in the recirculation velocity of the liquid – an occurrence connected to a subsequent decrease in reagent particle residence time.

❑ However, the residence time of the particles and the gas will in fact increase due to the extra travelling distance through the melt, notwithstanding the ensuing increase in recirculation velocity. Therefore, upon increasing the depth of injection (lowering the lance) there will be an ensuing decline in the injection time necessary to reach the required sulphur concentration prescribed by Saldanha Steel. As can be seen from Figure 6.8, a 0.8 m injection depth increase will result in a decreased injection time of two minutes.

The various parameters contained in the following sections are determined even before desulphurisation commences and cannot be controlled directly. Their values are produced and generated as a result of blast furnace conditions, slag concentrations and ore mineralogy.

Initial mass of iron

The current desulphurisation procedure at Saldanha Steel does not allow for a deliberate adjustment in injection depth. The lance is routinely lowered to a standardised level and a change in the initial mass of the liquid iron in the ladles will automatically induce a change in the injection depth. Figure 6.9 demonstrates the different injection times required at various ladle tonnages, while routinely compensating for the inevitable change in injection depth.
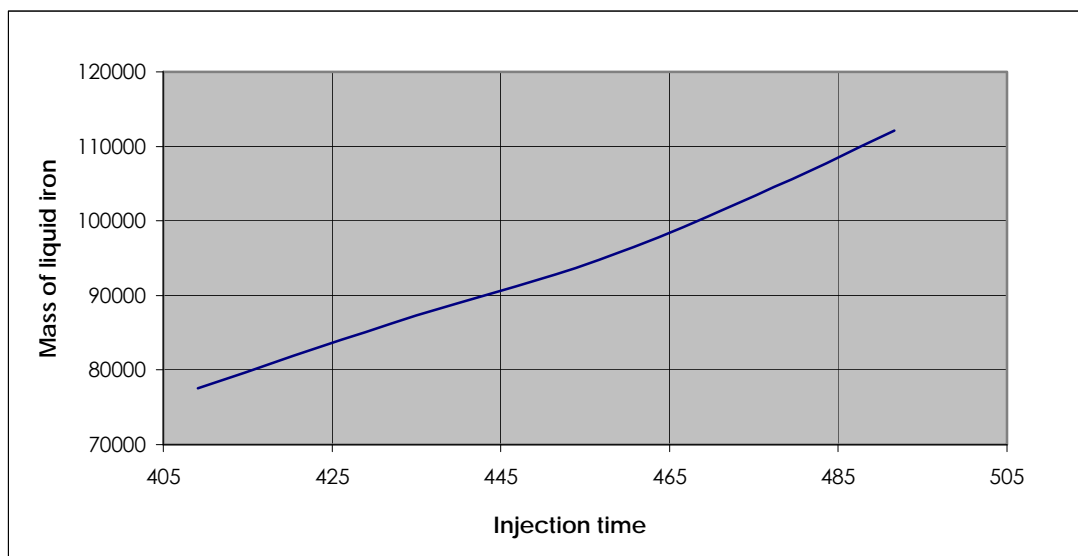
Figure 6.9 Variation in desulphurisation injection time as a function of various initial metal masses

Depending on Corex conditions, the amount of iron in the ladles can vary substantially and a 20-ton decrease in initial metal load can decrease injection time by up to one minute. Less iron implies less sulphur and this will result in the desulphurisation reaction at the topslag-metal interface creating a larger sulphur concentration gradient, ensuring that the rate of desulphurisation is increased. Less iron will however also involve a decrease in the injection depth, thereby counteracting the increase in the desulphurisation rate brought on as a result of the larger desulphurisation gradient.

Although the initial mass of the melt cannot be considered a manipulated variable but indeed a disturbance variable, a clear understanding of the ensuing changes brought on as result of its variance, is important if the process is going to be successfully controlled.

Reagent particle diameter

The average particle diameter of the calcium carbide reagent has a profound effect on the desulphurisation process. Eighty percent of all the calcium carbide particles utilised at Saldanha Steel has an average diameter smaller than 75 microns. While still keeping the reagent flowrate constant at a value of 0.5 kg/s, a 20-micron decrease in this particle diameter will result in a decrease of two minutes on the required injection time.
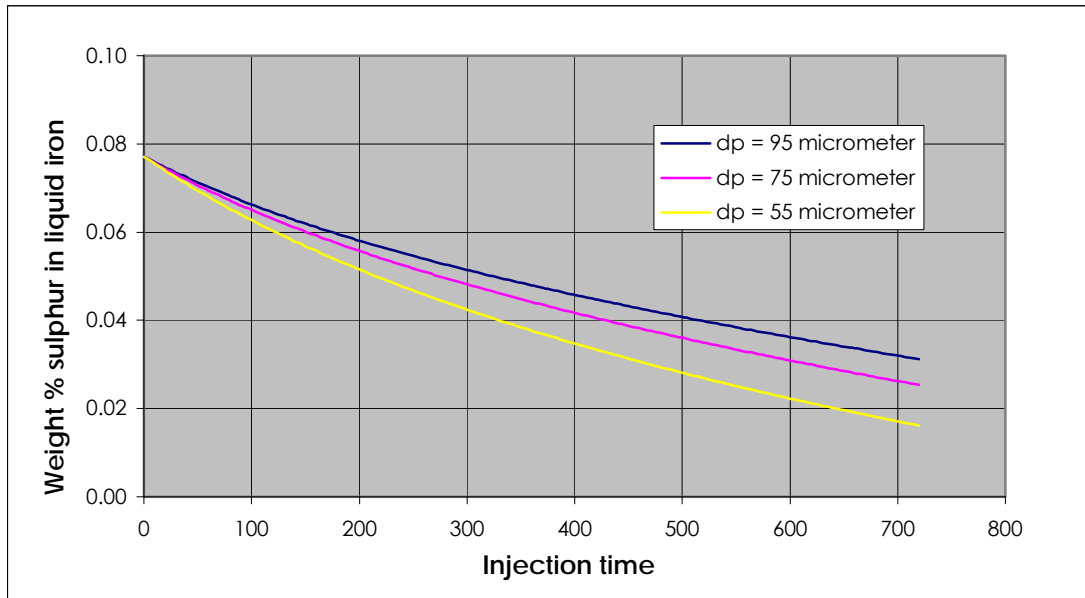
Figure 6.10 Variation in desulphurisation injection time as a function of various reagent particle sizes

This occurrence can be explained in terms of surface area: The proposed decrease in the average particle diameter will result in a 35% rise in the total surface area available for the desulphurisation reaction (See Figure 6.11).
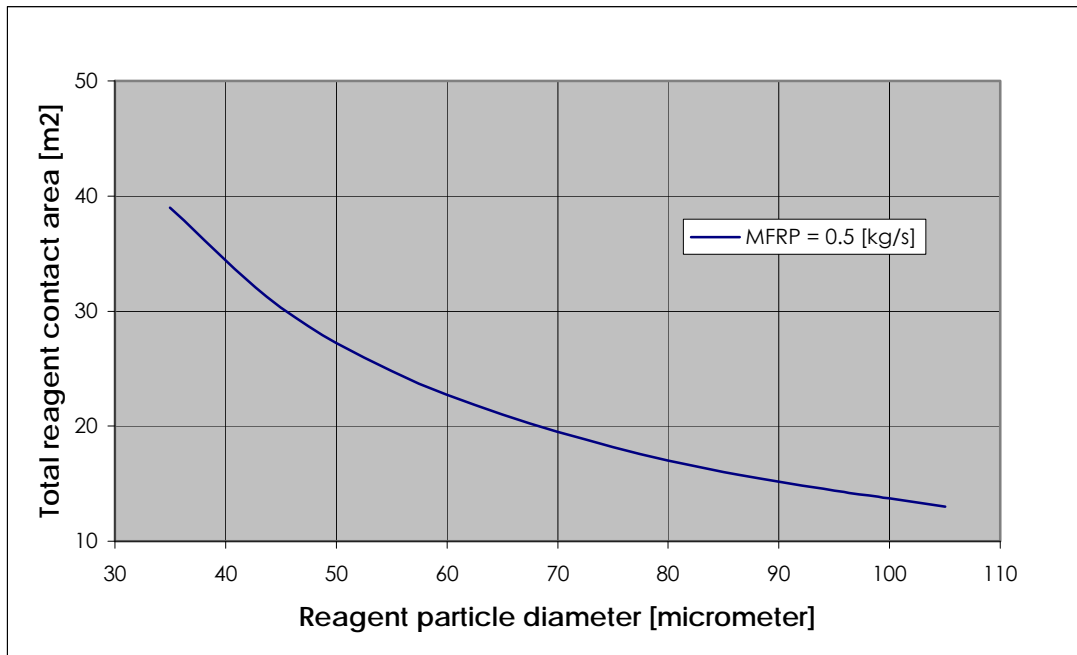
Figure 6.11 Variation in total reaction surface area as a function of various reagent particle diameters

With such substantial consequences a reality, prior knowledge and constant monitoring of the calcium carbide and its particle size distribution are of vital importance.

Initial sulphur concentration

Although it is quite obvious that less initial sulphur in the liquid melt will result in a decrease in the required injection time, it is the disparity between the various desulphurisation rates depicted in Figure 6.12 that is of particular interest.
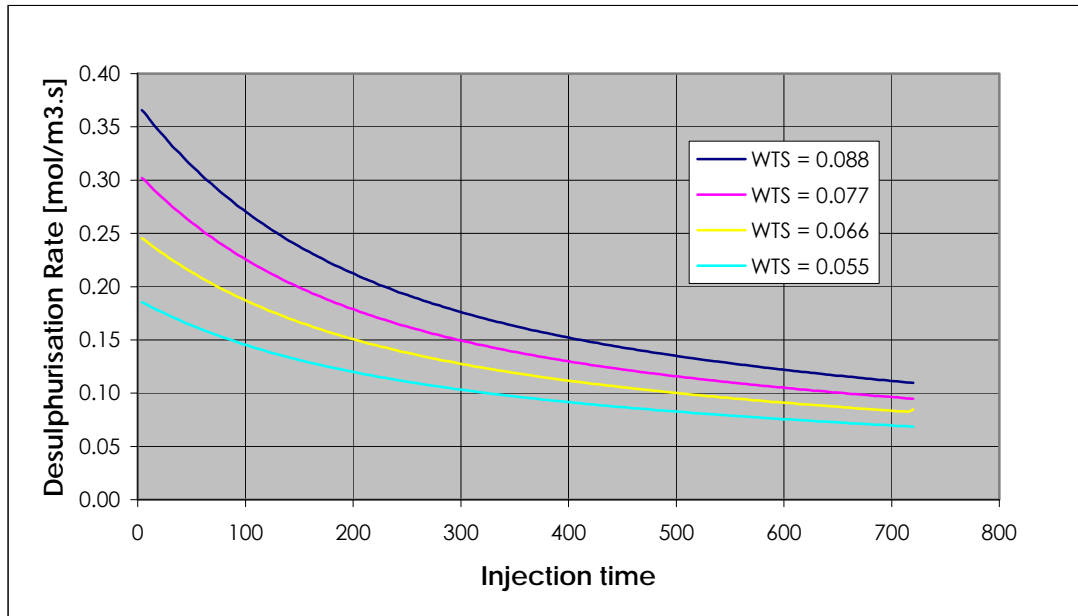
Figure 6.12 Variation in desulphurisation injection time as a function of the desulphurisation rate

At initial sulphur levels of around 0.088 weight percent, early desulphurisation rates can be as much as double when compared to the desulphurisation rates of iron with an initial sulphur value of 0.055 weight percent or less. As can be deduced from the last two term on the right hand side of Equation 4.42, a higher initial sulphur level (C_S^{pl}) will result in an increased sulphur concentration gradient within the iron, which in turn boosts the overall desulphurisation rate. On the other hand, given the higher initial values, sulphur will subsequently be removed at a much more rapid rate, with the ensuing concentration gradient decreasing slightly faster. This allows the desulphurisation rates to converge as the injection process continues.
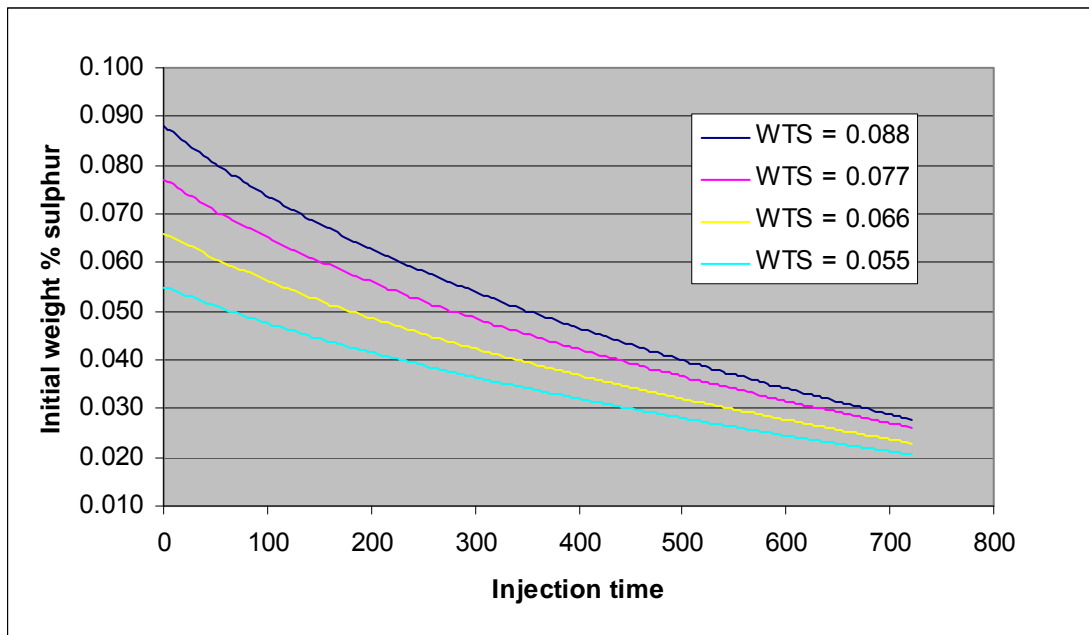
Figure 6.13 Variation in desulphurisation injection time as a function of the initial concentration of sulphur

Given the default parameters, the proposed desulphurisation model predicts that a liquid melt at Saldanha Steel containing 0.055 weight % sulphur would require 300 seconds of calcium carbide injection to lower the sulphur level to the obligatory 0.036 weight percent. That points to a 0.019 weight percent difference in sulphur concentration between the start and the finish of the desulphurisation procedure. The ensuing injection time required to remove almost **triple** that value (0.052 weight percent sulphur) only amounts to roughly **double** the above-mentioned injection time (570 seconds). This discrepancy is a direct consequence of the disparity in concentration gradients and these findings are experimentally validated when compared with the "rule-of-thumb" addition-guidelines (Table 3.1) currently employed by the operators at the Saldanha Steel plant. The comparative results are graphically shown in Figure 6.13.
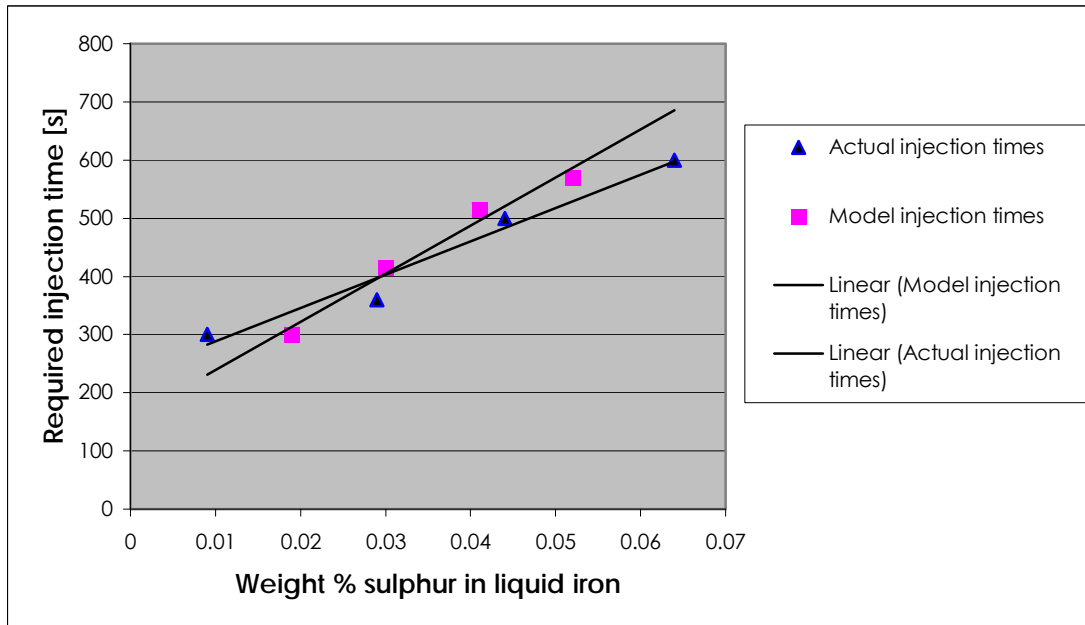
Figure 6.14 Comparison between model and experimental values between injection times as a function of various initial sulphur concentrations in the liquid iron

Amount of carry-over slag

Carry-over slag is defined as that portion of slag that was associated with the preceding processing step, in this case the Corex plant.
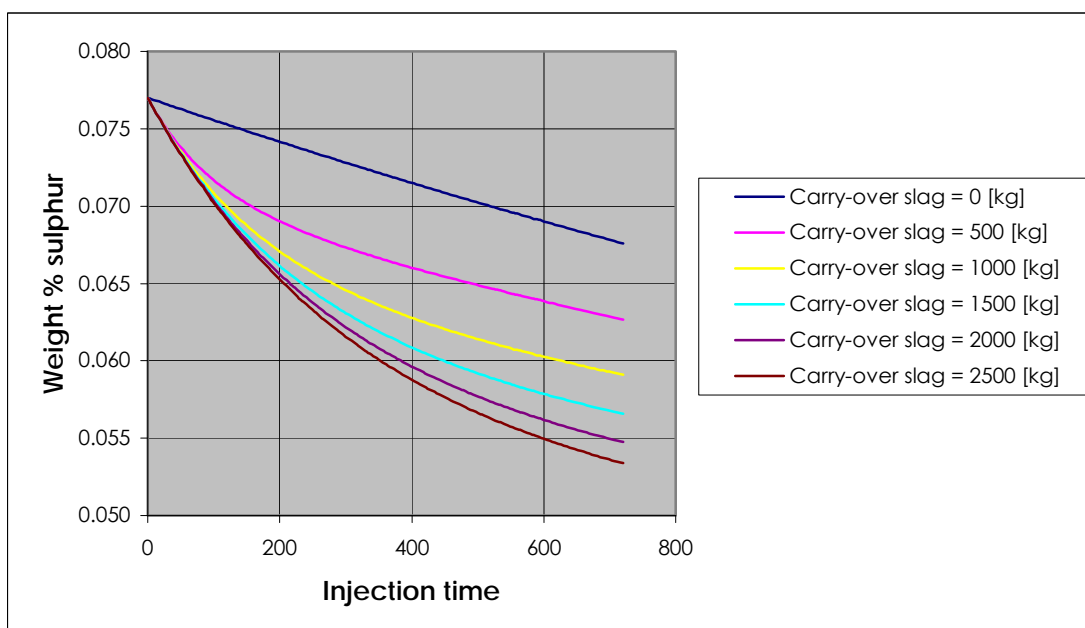
Figure 6.15 *Variation in the desulphurisation injection time as a function of various carry-over slag masses*

In the present model, a variation in the amount of carry-over slag will result in a change of the topslags' ability to desulphurise. Although Figure 6.14 depicts the overall sulphur change in the system as a result of topslag and plume involvement together, it essentially only reflects the contribution of the topslag towards the final sulphur concentration.

The average amount of carry-over slag associated with each tapped ladle at Saldanha Steel is 1000 kg with a concentration of 1.24 weight % sulphur (Laas, 2002). In the unlikely event that no carry-over slag is tapped from the melter-gasifier, the exact same melt would require 3 additional minutes of injection in order to reach the desired sulphur level of 0.036 weight percent. On the other hand, by increasing the carry-over slag to a value as high as 2500kg, the required injection time can only be reduced by less than one minute. An optimum carry-over slag volume needs to be indentified that minimises required injection time, while still curbing the amount of inclusions entering the ConArc through excess carry-over slag.

It is also important to remember that once the melter-gasifier has filled a ladle with molten iron, exposure to the atmosphere will ensure that an inevitable cooling process will commence. The protective layer brought on as a result of the carry-over slag will help decrease the rate of temperature loss (along with oxidation of the steel), resulting in consequential financial savings. These and other financial implications are discussed in the following section.

COST ESTIMATION

All chemical plants are built to make a profit and an estimate of the cost of proposed changes to any process is needed before the profitability of a project can be assessed. Cost estimation though is a specialised subject in its own right and a complete financial project evaluation is not within the scope of this report. It is however important to make some quick, rough, cost estimates concerning the desulphurisation process at Saldanha Steel in order to put the much emphasised required injection time into perspective.

Liquid iron in a ladle can loose between 150 – 300 °C between the tapping of the Corex and charging of the steelmaking furnace (ConArc), even without being desulphurised. A detailed process description from Corex to the steelmaking furnace (ConArc), clarifying, amongst other things, the exact reasons for such dramatic loss in temperature, can be found in Appendix F. Table 6.2 presents a summary of the findings.

Table 6.2   Liquid iron temperature loss from Corex to ConArc without considering desulphurisation.

Process step	Reason for temperature loss	Temperature loss	Cumalative temp
Corex ready for tapping	N/A		Approximately 1500 °C
Tapping	Runner exposed to atmosphere	50 – 100 °C	1450 – 1400 °C
	Contact to ladle refractory bricks	50 – 100 °C	1350 – 1400 °C
Waiting in line at the LID section	Ladle exposed to atmosphere	16 °C per hour	1300 – 1350 °C after three hours
Charging the Conarc	Extreme exposure to atmosphere	50 – 100 °C	1250 – 1300 °C

During the desulphurisation process the iron in the ladle car looses 4.3 °C for every minute of injection (or 260 °C per hour). This rate of cooling was determined experimentally and detailed results can be seen in Appendix F. With the temperature losses identified in Table 6.2, as well as the losses associated with the desulphurisation injection process, the temperature of subsequent batches of iron **charged** into the ConArc can be as low as 1200 – 1300°C.

The steel produced in the ConArc must be **tapped** at a temperature of 1640 °C. Inside the ConArc, the charged melt therefore has to be reheated in order to reach the required tapping temperature. The heat comes in the form of chemical energy during the blowing phase and a combination of chemical and electrical energy during the arcing phase. Electrical energy is supplied via the graphite electrodes and is usually the largest energy contributor in arc refining operation.

The electrodes deliver the power to the furnace in the form of an electric arc between the electrodes and the furnace charge. Depending on the quality of the slag foam, the effective energy transfer from the electrodes to the charge can vary between 85% for good quality foam to as low as 63% for below average quality foam (Laas, 2002). Table 6.3 sums up the implied electrical energy price tag attached to the reheating procedure of a ConArc charge.

Table 6.3 Costs associated with reheating of the ConArc furnace

Conarc effectiveness [%]	Mass of charge in Conarc [tons]	Energy requirements [kWh/°C]	Unit cost [R/kWh]	Cost to increase Conarc temp by 1°C
85	210	57	0.12	R6.90
63	210	87	0.12	R10.50

In the preceding sections of this chapter, decreases in the required injection times were proposed as a result of a series of sensitivity analyses performed on a variety of process variables. When it is considered that Saldanha Steel desulphurises an average of two ladles every day, the above-mentioned energy consumption information, as well as the subsequent financial implications, becomes apparent.

Table 6.4 and 6.5 reflect the costs involved when the furnace is operating at 63 % and 85 % effeciency respectively.

Table 6.4 Furnace costs involved when operating at 63 % efficiency

Variable		Proposed change	Unit	Injection time saving [seconds]	ConArc power saving per year [Rand]
Manipulated	Carrier gas flowrate	Increase from 0.008 → 0.012	m³/s	Negligible	**Negligible**
	Reagent flowrate	Increase from 0.3 → 0.7	kg/s	320	**(R167,600) R76,600**
	Injection depth	Increase from 1.8 → 2.6	m	115	**R 128,600**
Disturbance	Initial mass of iron	Decrease from 100 → 80	ton	60	**R 67,100**
	Reagent diameter	Decrease from 75 → 55	μm	125	**R 139,700**
	Carry-over slag A	Increase from 0 → 1 000	kg	200	**R 223,700**
	Carry-over slag B	Increase from 1 000 → 2 500	kg	50	**R 55,800**

Table 6.5 Furnace costs involved when operating at 85 % efficiency

Variable		Proposed change	Unit	Injection time saving [seconds]	ConArc power saving per year [Rand]
Manipulated	Carrier gas flowrate	Increase from 0.008 → 0.012	m³/s	Negligible	**Negligible**
	Reagent flowrate	Increase from 0.3 → 0.7	kg/s	320	**(R109,800) R18,800**
	Injection depth	Increase from 1.8 → 2.6	m	115	**R 107,825**
Disturbance	Initial mass of iron	Decrease from 100 → 80	ton	60	**R 56,200**
	Reagent diameter	Decrease from 75 → 55	μm	125	**R 117,200**
	Carry-over slag A	Increase from 0 → 1 000	kg	200	**R 187,600**
	Carry-over slag B	Increase from 1 000 → 2 500	kg	50	**R 46,800**

Apart from tangible pecuniary savings, the reduction in production turn-around time can also be tremendously beneficial – especially at such an integrated plant like the one found at Saldanha Bay.

It must however be said that these proposed process adjustments could come at a price:

- A 0.4 kg/s increase in the reagent flowrate might reduce the injection time by 320 seconds, but will also bring about the use of an extra 38 kg of calcium carbide reagent with every ladle. At R3400 per ton, the additional calcium carbide will decrease proposed savings per annum to R76,600 and R18,800 respectively. *Note that all the other savings depicted in Table 6.4 and 6.5 incorporate the subsequent reagent savings as a result of decreased injection time.* It should also be considered that the present model proposes single-particle interaction coefficients. By increasing the reagent loading to a point where this assumption becomes improbable, the prediction could be rendered untrustworthy. Reagent overloading could also result in coupled reagent flow (Farias, 1985), an occurrence that cannot be accounted for within the scope of this study.
- An increase in injection depth simply implies that the lance must be lowered into the melt, thereby exposing an extra 0.8 m of the lance to the melt. Some lances are only equipped to handle a fixed injection depth and some potential erosion problems can arise. The current injection depth at Saldanha Steel is fixed and the capital investment required to enable depth-control on the lance has also not been assessed.
- A decrease in the initial mass of the iron results in a decrease in the per annum throughput of the plant!

- With size reduction being such an energy intensive process, finer calcium carbide particles could bring about an increase in the purchasing price of the desulphurisation agent.
- The addition of impurities (other than sulphur) that comes with the increase in carry-over slag, might create refining problems if the necessary precautions are not taken to prohibit the transfer of additional slag while charging the ConArc.

It must therefore be stated that values in Tables 6.4 and 6.5 are tentative figures at best, but goes a long way in highlighting the potential advantages a reduction in injection time could have on the operating cost of the desulphurisation process at Saldanha Steel.

In the hypothetical event that all of the ladles will have to be desulphurised (an average of 24 per day), Table 6.4 and Table 6.5 will look a whole lot different:

Table 6.6 Furnace costs involved when operating at 63 % efficiency (24 ladles a day)

Variable		Proposed change	Unit	Injection time saving [seconds]	ConArc power saving per year [Rand]
Manipulated	Carrier gas flowrate	Increase from 0.008 → 0.012	m³/s	Negligible	**Negligible**
	Reagent flowrate	Increase from 0.3 → 0.7	kg/s	320	**(R 2.01m) R 0.92m**
	Injection depth	Increase from 1.8 → 2.6	m	115	**R 1.54m**
Disturbance	Initial mass of iron	Decrease from 100 → 80	ton	60	**R 0.81m**
	Reagent diameter	Decrease from 75 → **55**	μm	125	**R 1.68m**
	Carry-over slag A	Increase from 0 → **1 000**	kg	200	**R 2.68m**
	Carry-over slag B	Increase from 1 000 → **2 500**	kg	50	**R 0.67m**

Table 6.5 Furnace costs involved when operating at 85 % efficiency (24 ladles a day)

Variable		Proposed change	Unit	Injection time saving [seconds]	ConArc power saving per year [Rand]
Manipulated	Carrier gas flowrate	Increase from 0.008 → 0.012	m³/s	Negligible	**Negligible**
	Reagent flowrate	Increase from 0.3 → 0.7	kg/s	320	**(R 1.32m) R 0.23m**
	Injection depth	Increase from 1.8 → 2.6	m	115	**R 1.29m**
Disturbance	Initial mass of iron	Decrease from 100 → 80	ton	60	**R 0.67**
	Reagent diameter	Decrease from 75 → 55	μm	125	**R 1.41m**
	Carry-over slag A	Increase from 0 → 1 000	kg	200	**R 2.25m**
	Carry-over slag B	Increase from 1 000 → 2 500	kg	50	**R 0.56m**

7. CONCLUSIONS

The character of research is such that a project is never considered fully completed – the refinement of new and existing processes, in order to increase efficiency, is indeed the most important task of the engineer and scientist. It is the purpose of this chapter to present the most significant conclusions drawn from this investigation and based on these conclusions, subsequent recommendations regarding future research.

LITERATURE REVIEW

In Chapter 2 it was revealed that the conditions for removal of sulphur from the melt is at an optimum immediately after being tapped from the blast furnace and is achieved through the use of specialised injection techniques. It was shown that desulphurisation of the reduced melt occurs in two distinct regions namely the ascending plume of injected calcium carbide particles and the topslag-metal interface consisting of both the injected flux and some carry-over slag from the blast furnace.

A survey of the literature concerning the desulphurisation injection process disclosed a growing trend towards a more fundamental understanding of the actual process, with additional emphasise placed on the reaction kinetics within the injection plume itself. Although most of the kinetic models described in the literature provided constructive insight into general desulphurisation trends, no single model could accurately describe injection situation specific to the Saldanha Steel plant. The development of an expert kinetic desulphurisation model was therefore warranted.

DATA EXPLORATION

Chapter 3 focussed on the empirical modelling of the actual Saldanha Steel plant desulphurisation data and found that the data did not represent a change over time, thus precluding the use of linear transfer function models. It did however not preclude the use of multiple regression analysis and after extensive filtering of the relevant data, it was found that variation in the five most influential process predictors, together accounted for 54.8% of the variation in the independent variable, resulting in a coefficient of correlation equal to 0.74. A standard backpropogation network employed to model the same data, together with a principal component analysis, substantiated the results and pointed towards the validity of a the multiple regression model. Although the empirical modelling approach succeeded in encapsulating some of the underlying patterns of the Saldanha Steel desulphurisation process, it was concluded that a total empirical approach was inadequate and underlined the need for a much more fundamental modelling methodology.

FUNDAMENTAL MODELLING

In Chapter 5, the kinetic desulphurisation model proposed by Chiang et al was adapted accordingly, resulting in a one-dimensional steady state model describing the momentum, heat and mass transfer in an ascending gas-liquid-powder plume for the conditions relevant to the Saldanha Steel desulphurisation injection process. A separate model proposed by Seshadri et al was employed to account for the contribution of the topslag, as well as carry-over slag, to the overall desulphurisation rate. The governing differential equations were

manipulated into ten stiff, coupled, first-order differential equations for the three phase velocities, the temperatures of the liquid, gas and particles associated with the liquid and associated with the bubbles, the sulphur concentration in the plume and the utilisation of the particles in the liquid and on the bubbles. A MATLAB program (Appendix B) was developed to perform the required desulphurisation calculations as well as in-depth sensitivity analysis on key parameters.

MODEL VALIDATION

It was revealed through experimental verification that 70 percent of the calcium carbide particles will remain trapped inside the carrier gas bubbles upon injection into the melt, thereby drastically decreasing the effectiveness of the desulphurisation procedure. Bearing this in mind and subject to a set of default industrial parameters, the proposed model was trained and its subsequent prediction ability tested through comparison with different sets of industrial values. It was found that the model demonstrated exceptional accuracy in forecasting final sulphur concentration values in liquid iron after a specified injection time.

Table 7.1 Comparison between experimental and model values

	Test	Experimental	Model	Accuracy
Final sulphur value	No.1	0.041	0.0407	99.2%
[wt %]	No.2	0.032	0.0331	96.6%

RESULTS AND DISCUSSION

One of the main advantages of the model lies in its ability to characterise the velocity, temperature and utilisation profiles of the three phases, thus creating a virtual "snapshot" of the conditions within the plume at a certain time. The following conclusions concerning these various parameters were reached:

❑ The time that each phase spends in the plume has a direct relation to the recirculation velocity value of the liquid iron in the ladle car. In turn, the recirculation velocity is a function of the terminal velocity of the carrier gas bubble in the melt.

❑ The particles that associate with the melt upon injection, will reach bulk liquid temperature basically at once, while the temperature of the particles trapped inside the bubble will increase along with the temperature of the carrier gas.

❑ As a result of the substantial disparities between the ensuing mass transfer coefficients, the particles in the melt will reach 65% utilisation, while the particles trapped inside the bubbles will only reach as little as 1% utilisation.

Apart from having the capacity to examine the sulphur concentration in the melt for the duration of an injection procedure, the model also has the ability to investigate the influence of manipulated and disturbance variables on the outcome of the final sulphur concentration. The following conclusions concerning these variables has come about as a result of comprehensive sensitivity analyses:

❑ If was shown that the reagent flowrate was the most influential variable. Owing to the high level of utilisation potential of the particles associated with the melt, even the slightest increase in calcium carbide flowrate (bearing in mind that the fraction of

particles inside the bubbles remain equal to 0.7), resulted in a sizeable decrease in the injection time required for the iron to reach the obligatory final sulphur concentration of 0.036 weight percent.

❑ Lowering the lance into the melt and thereby increasing the depth of reagent injection can also reduce the required injection time. Increased residence time inside the plume as well as topslag-metal interface renewal as a result of added stirring, are revealed as the two main causes for the reduction.

❑ Varying the carrier gas flowrate has comparatively little effect on the final outcome.

❑ If was found that a decrease in the initial mass of iron will result in a reduction in the required injection time.

❑ Another change inducing a decrease in the required injection time is a reduction of the diameter of the individual calcium carbide particles. While still keeping the overall mass flowrate constant, a decrease in particle diameter will entail an increase in the total surface area available for desulphurisation.

Table 6.5 have shown that the potential per annum savings at Saldanha Steel as a result of decreased injection times if an average of two ladles are being desulphurised each day. Throughout the injection procedure, the melt has a cooling rate of 4.3 °C for every minute of injection. It will be up to the ConArc furnace to reheat each new metal charge to a tapping temperature of 1640 °C – a procedure that costs money! Decreased injection time therefore leads to reduced production costs.

Although all the results contained in this section is of particular interest to the Saldanha Steel scenario, it also provides invaluable information and insights into the important variables and parameters playing a role in injection desulphurisation processes in general, along with the influence that changing conditions can have on the end result of such a

procedure. Saldanha Steel uses dedicated suppliers of reductant and iron ore, bith of high quality and low sulphur content. Not all refineries are as fortunate as Saldanha Steel though and have a far more serious and pressing sulphur inclusion problem and this report and its findings can serve as a tool for future investigations.

RECOMMENDATIONS

❑ The proposed desulphurisation program does not account for subtle changes in the sulphur partition ratio of the topslag as the injection process continues.

$$\text{Log}L_S \quad = \quad \text{Log}f_S + \text{Log}K_{eq} + \text{Log}C_S - \text{Log}a_{\underline{o}} \tag{7.1}$$

with K_{eq} representing the equilibrium constant of Equation 2.5. Through the use of relevant software packages e.g. FACTSAGE, the preceding equation could be included within the structure of the model.

❑ The cost estimation in this study was performed with the exclusive aim to provide a very rough first estimation of any expected savings from the proposed production changes. It is recommended that a more in-depth investigation into all possible financial implications should be undertaken in order to get an improved fiscal idea of any subsequent repercussions.

❑ It is recommended that possible interactions between important parameters be further explored.

8. REFERENCES

1. Aldrich, C. (2002). <u>The Exploratory Analysis of Metallurgical Process Data with Neural Networks and Related Methods</u>. Amsterdam, Elsevier Science B.V.

2. Analects, N. M., H. Lee and P.C. Hayes (1993). "Sulphur partition between CaO-SiO2-Ce2O3 and carbon saturated iron." <u>ISIJ International</u> **33**(5): p. 549 - 555.

3. Bodsworth, C. and H. B. Bell (1972). <u>Physical Chemistry of Iron and Steel Manufacture</u>, Longman.

4. Callister, W. D. (1994). <u>Materials Science and Engineering - An Introduction</u>, John Wiley & Sons.

5. Chiang, L. K. (1987). A Kinetic Study of Hot Metal Desulphurisation by Calcium Carbide Powder Injection, McMaster University: 326.

6. Chiang, L. K., G. A. Irons, W.K. Lu and I.A. Cameron (1991). "Kinetic Studies of Calcium Carbide Hot Metal Desulphurisation by Powder Injection." <u>ISS Transactions</u> **12**.

7. Constantinides, A. and N. Mostoufi (1999). <u>Numerical Methods for Chemical Engineers with MATLAB Applications</u>, Prentice Hall PTR.

8. Duffy, J. A., I. D. Ingram and I.D. Sommerville (1978). "Acid-base properties of molten oxides and metallurgical slags." <u>Journal of the Chemical Society</u> **74**: p. 1410 - 1419.

9. Engell, H. (1988). "Kinetic Model for the Influence of Carry-Over Slag in Ladle Metallurgy." <u>Steel Research</u> **59**(12): p. 527 - 531.

10. Farias, L. R. and G. A. Irons (1985a). "Plume Fluid Flow and Heat Transfer in Powder Wire Injection Processes." : 59 - 63.

11. Farias, L. R. and G. A. Irons (1985b). "A Unified Approach to Bubbling-Jetting Phenomena in Powder Injection into Iron and Steel." <u>Metallurgical Transactions B</u> **16B**: 211 - 225.

12. Farias, L. R. and G. A. Irons (1986). "A Multi-Phase Model for Plumes in Powder Injection Refining Processes." <u>Metallurgical Transactions B</u> **17B**: 77 - 85.

13. Fogler, H. S. (1992). External Diffusion Effects on Heterogeneous Reactions. <u>Elements of Chemical Reaction Engineering</u>. New Jersey, Prentice Hall International: 543 - 606.

14. Geldenhuis, K. and C. Pistorius (2000). <u>Short Course in Pyrometallurgy - Saldanha Steel</u>, Saldanha Steel, University of Pretoria.

15. Guthrie, R. I. L. and G. A. Irons (1978). "Bubble Formation at Nozzles in Pig Iron." <u>Metallurgical Transactions B</u> **9B**: 101 - 110.

16. Hayes, P. C. (1993). <u>Process Principles in Materials & Minerals Production</u>, Hayes Publishing Company.

17. Ilegbusi, O. J., M. Iguchi and W. Wahnsiedler (2000). _Mathematical and Physical Modelling of Materials Processing Operations_, Chapman & Hall.

18. Incropera, F. P. and D. P. D. Witt (1990). _Fundamentals of Heat and Mass Transfer_, John Wiley & Sons.

19. Irons, G. A. (1999). "Metallurgical Aspects of Desulphurisation." _Transactions of IMA-Seminar_: 21 - 38.

20. Irons, G. A. and R. I. L. Guthrie (1978). "Bubble Formation at Nozzles in Pig Iron." _Metallurgical Transactions B_ **9B**: p. 101 - 110.

21. Irons, G. A. and R. I. L. Guthrie (1980). "Bubbling Behaviour in Molten Metals." _Canadian Metallurgical Quarterly_ **19**(4): p. 381 - 387.

22. Iwamasa, P. K. and R. J. Fruehan (1997). "Effect of FeO in the slag and silicon in the metal on the desulphurisation of hot metal." _Metallurgical and Materials Transactions_ **28B**: p. 47 - 57.

23. Kanjilal, P. P. (1995). _Adaptive prediction and predictive control_, Peregrinus.

24. Laas, H. (2002). Personal Communication, Saldanha Steel.

25. Lancaster, G. F. (1993). _Metallurgy of Welding_, Chapman & Hall.

26. Lin, Z. and R. I. L. Guthrie (1995). "A Model for Slag Foaming for the In-Bath Smelting Process." _Transactions of the ISS_(May): 67 - 73.

27. Meraikib, M. (1997). "Partition of Sulphur and Manganese between Blast Furnace Slag and Hot Metal." Iron and Steelmaking **24**(3): p. 230 - 238.

28. Morsi, Y. S., W. Yang, B.R. Clayton and N.B. Gray (1999). "Experimental Investigation of Swirl and Non-Swirl Gas Injections into Liquid Baths using Submerged Vertical Lances." Canadian Metallurgical Quarterly **39**(1): p. 87 - 98.

29. Nilsson, R., D. Sichen and S. Seetharaman (1996). "Estimation of sulphide capacities of multi-component silicate melts." Scandinavian Journal of Metallurgy **25**: p. 128 - 134.

30. Nzotta, M. M. (1997). "Experimental determination of sulphide capacities in the Al2O3-MgO-SiO2, Al2O3-MnO-SiO2, Al2O3-MgO-CaO slags in the temperature range 1773-1932K." Journal of Metallurgy **26**: p. 169 - 177.

31. Nzotta, M. M., D. Sichen and S. Seetharaman (1999). "A Study of the sulfide capacities of iron-oxide containing slags." Metallurgical and Materials Transactions B **30B**: p. 909 - 920.

32. Oryall, G. N. and J. K. Brimacombe (1976). "The Physical Behaviour of a Gas Jet Injected Horisontally into Liquid Metal." Metallurgical Transactions B **7B**: 391 - 403.

33. Parsons, R. (1978). Statistical Analysis - A decision making approach. New York, Harper & Row.

34. Pelton, A. D., G. Eriksson and A. Romero-Serrano (1993). "Calculation of Sulfide Capacities of Multi-component Slags." <u>Metallurgical Transactions B</u> **24B**: p. 817 - 825.

35. Polking, J. C. (1995). <u>Ordinary Differential Equations - Using MATLAB</u>, Prentice Hall.

36. Reddy, R. G. and M. Blander (1989). "Modeling of sulfide capacities of silicate melts." <u>Metallurgical Transactions B</u> **20B**: p. 137 - 140.

37. Reifferscheid, M. and W. Pluschkell (1994). "Development of a Numerical Model Simulating the Desulphurisation of Liquid Steel." <u>Steel Research</u> **65**(8): p. 309 - 313.

38. Richardson, F. D. (1974). <u>Physical Chemistry of Melts in Metallurgy</u>, Academic Press Incorporated.

39. Richardson, F. D. and C. J. B. Fincham (1952). "A Stoichiometric combustion method for determination of sulphur in slags." <u>Journal of the iron and Steel Institute</u> **172**: p. 53 - 55.

40. Richardson, F. D. and C. J. B. Fincham (1954). "Sulphur in silicate and aluminate slags, Journal of the Iron and Steel Institute." <u>Journal of the Iron and Steel Institute</u>: p. 4 - 16.

41. Rosenqvist, T. (1974). <u>Principles of Extractive Metallurgy</u>, McGraw Hill.

42. Sahai, Y. and R. I. L. Guthrie (1982). "Hydrodynamics of Gas Stirred Melts: Part I. Gas/Liquid Coupling." <u>Metallurgical Transactions B</u> **13B**(p. 193 - 202).

43. Salas, S. L. and E. Hille (1990). Calculus, John Wiley & Sons.

44. Sano, M. and K. Mori (1983). Circulating Flow Model in a Molten Metal Bath with special respect to Behaviour of Bubble Swarms and its Application to Gas Injection Processes. 3rd International Conference on Refining of Iron and Steel, Lulea, Sweden, Mefos.

45. Sano, Y., N. Yamaguchi and T. Adachi (1974). "Mass Transfer Coefficients for Suspended Particles in Agitated Vessels and Bubble Columns." Journal of Chemical Engineers of Japan **7**(4): 255 - 261.

46. Schürmann, E. and H. Delhey (1990). "Thermodynamics of Desulphurisation Reactions during the treatment of Hot Metal with Calcium and Calcium Compounds." Steel Research **61**(2): p. 64 - 71.

47. Serway, R. A. (1992). Physics for Scientists & Engineers, Saunders College Publishing.

48. Seshadri, V., C. A. da Silva, I.A. da Silva and P. van Krüger (1997). "A Kinetic Model Applied to the Molten Pig Iron Desulphurisation by Injection of Lime-based Powders." ISIJ International **37**(1): 21 - 30.

49. Sheng, Y. Y. and G. A. Irons (1992). "Measurements of the Internal Structure of Gas-Liquid Plumes." Metallurgical Transactions B **23B**: p. 779 - 788.

50. Sommerville, I. D. and D. J. Sosinsky (1986). "The Composition and Temperature Dependence of the Sulfide Capacity of Metallurgical Slags." Metallurgical Transactions B **Volume 17B**: p. 331 - 337.

51.Streeter, V. L. and E. B. Wylie (1979). <u>Fluid Mechanics</u>, McGraw-Hill Book Company.

52.Szekely, J. and N. J. Themelis (1971). Gas Bubbles in Liquid. <u>Rate Phenomena in Process Metallurgy</u>, Wiley-Interscience: 684 - 709.

53.Szekely, J. and N. J. Themelis (1971). Single Particle Reaction Systems. <u>Rate Phenomena in Process Metallurgy</u>, Wiley-Interscience: 601 - 638.

54.Talballa, M., P. K. Tojan and L.O. Brockway (1976). "Mechanism of Desulphurisation of Liquid Iron Carbon Alloy with Solid CaC2 and CaO." <u>AFS Transactions</u>: 775 - 786.

55.Turkdogan, E. T. (1980). <u>Physical chemistry of high temperature technology, New York</u>. New York, Academic Press.

56.Wagner, C. (1975). "The concept of the basicity of slags." <u>Metallurgical Transactions B</u> **6B**: p. 405 - 409.

57.Younger, M. S. (1979). <u>A Handbook for Linear Regression</u>, Duxbury Press.

58.Zill, D. G. and M. R. Cullen (1992). <u>Advanced Engineering Mathematics</u>. Boston, PWS-Kent Publishing Company.

9. APPENDIX A – MODEL PARAMETERS

The following parameters represent the desulphurisation situation at Saldanha Steel and was utilised as the default values in the proposed desulphurisation model as seen in Appendix B.

PARAMETER	ABB.	VALUE	UNIT
Desulphurisation reagent characteristics			
Specific heat capacity of the calcium carbide	Cppow	2,000	J/kg·K
Drag coefficient of reagent particles in liquid iron	CDp	0.44	
Reagent particle diameter	dp	7.5×10^{-6}	m
Molar density of calcium carbide	Cp	34,321	mol/m^3
Density of the calcium carbide particles	ρ_P	2,200	kg/m^3
Emissivity of the calcium carbide particles	ε_p	0.5	
Carrier gas characteristics			
Specific heat capacity of the nitrogen gas	Cpgas	$(2\times10^{-4}\cdot\text{Temp}) + 1000$	kJ/kg·K
Drag coefficient of nitrogen spherical-cap bubbles	CDg	2.66	
Temperature of the nitrogen gas at the point of injection	TempN$_2$	298	Kelvin
Pressure of the nitrogen gas at the point of injection	PN$_2$	300,000	Pa
Thermal conductivity of the nitrogen gas	Kg	$(5\times10^{-5}\cdot\text{Temp}) + 0.0123$	W/m·K
Viscosity of the nitrogen gas	μ_g	$(2\times10^{-8}\cdot\text{Temp}) + 2\times10^{-2}$	Pa·s
Engineering gas constant - Nitrogen	Reng	296	m^2/s^2·K
Liquid iron characteristics			
Specific heat capacity of the liquid iron	Cpliq	654	J/kg·K
Density of liquid iron	ρ_l	7,000	kg/m^3
Emissivity of the liquid iron	ε_i	0.9	
Thermal conductivity of the liquid iron	Kl	32.1	W/m·K
Viscosity of the liquid iron	μ_l	6×10^{-3}	Pa·s
Bulk temperature of the liquid iron	Temp	1700	Kelvin
Sulphur characteristics			
Sulphur diffusivity in liquid iron	D$_S$	5×10^{-9}	m^2/s
Sulphur concentration at the particle reaction	C$_{ips}$	1.102×10^{-7}	mol/m^3

interface			
Atomic weight of the sulphur	Msul	32	g/mol
Constant values			
Stefan Boltzman constant	σ	5.67×10^{-8}	$W/m^2 \cdot K^4$
Universal gas constant	R	8.314	$J/mol \cdot K$
Atmospheric pressure	P_{atm}	101,300	Pa
Universal gravitational acceleration	g	9.81	m/s^2
Lance and ladle car characteristics			
Diameter of the ladle car	Dladle	3.5	m
Diameter of the injection orifice	Dorifice	0.013	m
Number of orifices in the injection lance	NumOrifice	2	

10. APPENDIX B – SOURCE CODE OF SIMULATION MODEL

PLUME

```matlab
%***** MAIN STRUCTURE OF THE PROGRAM *****

global MFRP Z Apl METWT Temp PN2 TempN2 Reng MFRG g Patm
Rhol db Cb METVOL

%***** INPUT VARIABLES *****

disp('INITIAL VARIABLES')
disp('
');
  METWT = input('\ Initial mass of iron [kg]   =   ');
  WTS = input('\ Initial sulphur content [wt%]   =   ');
  Temp = input('\ Initial temperature of the bath [Kelvin]
=   ');

disp('
');
disp('LANCING CONDITIONS and VARIABLES')
disp('
');
  MFRP = input('\ Total mass flowrate of the CaC2 particles
[kg/s]   =   ');
  QR = input('\ Total volumetric flowrate of the N2 through
the injection lance [m3/s]   =   ');
  Z   =   input('\  Depth  of  the  ladle  [m]      =
');
```

```matlab
    PN21 = input('\ Initial pressure of the N2 in the lance
before entering the ladle [bar]   =   ');
    NumOrifice  =  input('\  Amount  of  orifices  in  the
injection lance  =   ');


    %METWT = 95000;
    %WTS = 0.077;
    %Temp = 1700;


     %MFRP = 0.5;
     %QR = 0.014;
     %Z = 2.2;
    %PN2 = 300000;
     %NumOrifice = 2;


%***** PARAMETER FITTING *****


Dpl = 1.7; % Diameter of the break-through area of the
plume [m]


%***** PARAMETERS AS SEEN IN APPENDIX A *****


PN2 = PN21*100000; % Pressure of the nitrogen gas at the
point of injection [Pa]
TempN2 = 298; % Temperature of the nitrogen gas at the
point of injection [K]
Dladle = 3.5; % Diameter of the ladle car [m]
Dorifice = 0.013; % Diameter of the injection orifice [m]
Reng = 296; % Engineering gas constant - Nitrogen [m2/s2*K]
Patm = 101300; % Atmospheric pressure [Pa]
Rhol = 7000; % Density of liquid iron [kg/m3]
MSul = 32; %[g/mol] % Atomic weight of sulphur [g/mol]
g = 9.81; % Universal gravitational acceleration  [m/s2]
```

```matlab
%***** OTHER PARAMETERS *****

Apl = 3.142*(Dpl^2)/4; % Area of the ladle car [m2]
f = 0.7; % Particle parameter position


%***** CONDITIONS AT THE LANCE *****

DensN2Lance = PN2/(TempN2*Reng);
MFRG = QR*DensN2Lance;


%***** RECIRCULATION VELOCITY OF THE LIQUID IRON *****

QRM = MFRG/((Patm+(Rhol*g*Z))/(Reng*300));
Ul    =    (1.17*(QRM*g*Z*(Apl^2))^0.339)/(3.142*((Dladle^2)-
(Dpl^2))/4);


%***** SPHERICAL-CAP BUBBLE SIZE *****

db                                                             =
(6*(0.083*((QRM/NumOrifice)^0.867)*(Dorifice^0.435))/3.142)
^(1/3);


%***** INITIAL CONDITIONS *****

Ug = Ul + sqrt(0.5*g*db);
Up = Ul;


%***** AUXILIARY VARIABLES *****

PlumeVol = Apl*Z;
METVOL = METWT/Rhol;
TSPAN = [0 Z];
```

```matlab
MolSul = 1000*(((WTS/100)*METWT)/MSul);
Cb = MolSul/METVOL;


%***** LOOP *****

TotalInjTime = input('\ Injection Time (in seconds)    = ');
NumIters = 1;
i = 1;


Cbhistory = zeros(1,NumIters);
UtilHistory = zeros(1,NumIters);


while (i <= NumIters),

%***** SOLVE EQUATIONS *****

  Y0 = [Ug Ul Up 300 300 Temp Temp Cb 0 0];
  [T,Y] = ode15s('PlumeII',TSPAN,Y0);

  if NumIters == 1
    V = Y(end,3);
    U = Y(1,3);
    Slope = (V-U)/Z;
    ResTimePlume = (1/Slope)*log(V/U)
    NumIters = ceil(TotalInjTime/ResTimePlume);
  end;

  newCb = Y(end,8);
  CplUit = Cb - newCb;
  MolUit = CplUit*PlumeVol;
  MolSul = MolSul - MolUit;
  WTS = MolSul*MSul/METWT/10;
```

```matlab
    Cb = MolSul/METVOL;


    Jpl = Y(end,10);
    Jpg = Y(end,9);
    Util = (Jpl*(1-ef))+(Jpg*ef);



%***** DISPLAY STATUS *****


    disp([num2str(Cb)]);
    Cbhistory(i) = Cb;
    disp([num2str(Util)]);
    UtilHistory(i) = Util;


    i = i + 1;

end;


%figure(1); clf;
%plot(T,Y(:,[4 5 6 7]),'-*');
%title('Final temperature distributions');
%ylabel('Temperature');
%xlabel('Distance');
%grid on;


%figure(2); clf;
%plot(T,Y(:,[9 10]),'-*');
%title('Utilisation of particles on the bubbles and in the
liquid');
%ylabel('Utilisation');
%xlabel('Distance');
%grid on;
```

```matlab
%figure(3); clf;

%plot(T,Y(:,[1 2 3]),'-*');

%title('Final velocity distributions');

%ylabel('Velocity');

%xlabel('Distance');

%grid on;


%figure(4); clf;

%plot(T,Y(:,[8]),'-*');

%title('Final sulphur distributions');

%ylabel('Sulphur concentration [mol/m3]');

%xlabel('Distance');

%grid on;


%figure(1); clf;

%plot(T,Y(:,[6 7]),'-*');

%title('Liquid temperature distributions');

%ylabel('Temperature');

%xlabel('Distance');

%axis([0 2 1699.8 1700]);

%grid on;


%figure(4); clf;

%plot(T,Y(:,[1 2 3 9 10]),'-*');

%title('Final velocity and utilisation distributions');

%xlabel('Distance');

%grid on;


%figure(5); clf;

%plot(Cbhistory);

%title('Sulphur concentration vs. time');

%xlabel('Iteration');

%grid on;
```

```matlab
%figure(6); clf;
%plot(UtilHistory);
%title('CaC2 utilisation in liquid vs. time');
%xlabel('Iteration');
%grid on;


function Model = Eerste(T,Y)


global MFRP QR Apl METWT Temp Reng PN2 TempN2 MFRG g Patm
Rhol db Cb METVOL f


f = 0.7;


%***** PARAMETERS AS SEEN IN APPENDIX A *****


dp = 0.000075; %CaC2 particle diameter [m]


CDg = 2.66; % Drag coefficient of reagent particles in
liquid iron
Cppow = 2000; % Specific heat capacity of the calcium
carbide [J/kg.K]
Cpliq = 654; % Specific heat capacity of liquid iron at
1500°C [J/kg.K]
Cpgas = (0.0002*Temp+0.9539)*1000; % Specific heat capacity
of N2-gas [J/kg.K]
Cp = 34321; % Molar density of the CaC2 [mol/m3]
Kl = 32.1; % Thermal conductivity of liquid iron [W/m.K]
Kg = 5E-05*Temp + 0.0123; % Thermal conductivity of
nitrogen gas [W/m.K]
Ds = 5e-9; % Sulphur diffusivity [m2/s] from Atomic
Transport in Liquid Metals, Shimoji & Itami [m2/s]
```

```matlab
Sig = 5.67e-8; % Sigma for radiation of heat/Stefan
Boltzman constant [W/m2×K4]
Eml = 0.9; % Emissivity of liquid iron
Emp = 0.5; % Emissivity of CaC2 particle
Rhop = 2200; %Density of the CaC2 particle [kg/m3]
Visl = 0.006; %Viscosity of liquid iron [Pa.s]
Visg = 2E-08*Temp + 2E-05; %Viscosity of N2-gas [Pa.s]
R = 8.314; % Universal gas constant[J/mol*K]
Patm = 101300; % Atmospheric pressure [Pa]
Cips = 1.102e-7; % Sulphur concentration at the particle
reaction interface [mol/m3]


%***** OTHER PARAMETERS *****


Ap = 4*pi*((dp/2)^2); % Area of the particle [m2]
Ab = 4*pi*((db/2)^2); % Area of the bubble [m2]


%***** INITIAL CONDITIONS *****


Thg = MFRG/(Rhog(T)*Y(1)*Apl);
X1 = MFRP/(Rhop*Apl*Y(1));
X2 = MFRP/(Rhop*Apl*Y(2));
Thp = (X1*f)+(X2*(1-f));
Thl = 1-Thg-Thp;



if Y(3) >= Y(2)
   Y(3) = Y(2)-0.0001;
end


Upl = Y(2)-Y(3);
Ugl = Y(1)-Y(3);
```

```matlab
%***** DRAG COEFFICIENT OF REAGENT PARTICLE *****


Re0 = dp*Upl*Rhol/Visl;
if Re0 < 2
    CDp = 24/Re0;
else
    CDp = 18.5/(Re0^0.6);
end


%***** FLUID MECHANICS EQUATIONS *****


Rhom = Thg*Rhog(T)+f*Thp*Rhop;


FBgp = Thg*(Rhol-Rhom)*g*Apl;
FBp = (1-f)*(Rhol-Rhop)*Thp*g*Apl;
FDgpl = 0.75*Rhol*CDg*((Y(1)-Y(3))^2)*Thg*Apl/db;
FDpl = 0.75*Rhol*CDp*((Y(2)-Y(3))^2)*(1-f)*Thp*Apl/dp;


F41 = FBgp-FDgpl;
F51 = FBp-FDpl;
F61 = FDgpl+FDpl;


F1 = F41/(2*Rhom*Y(1)*Apl);
F2 = F51/(2*(1-f)*Thp*Rhop*Y(2)*Apl);
F3 = F61/(2*Thl*Rhol*Y(3)*Apl);


%***** HEAT TRANSFER EQUATIONS *****



WW = f*Thp*db/(Thg*dp*Eml);
Pr0 = Cpliq*Visl/Kl;
hp = (Kl/dp).*(2+0.6*(Re0.^0.5)*(Pr0.^0.33));
```

```matlab
hb = (4*Rhog(T)*Cpgas*Kg*Ugl/(pi*db))^0.5;


Ur = Rhop*g*(dp^2)/(18*Visg);
Re2 = Rhog(T)*Ur*dp/Visg;
Pr2 = Cpgas*Visg/Kg;
hgp = (Kg/dp)*(2+0.6*(Re2^0.5)*(Pr2^0.33));
%hgp = 1;


G1 = (6*f*Thp*Sig/dp)/(WW+(1/Emp)-1);
G2 = 6*hp*(1-f)*Thp/dp;
G3 = 6*hb*Thg/db;
G4 = 6*hgp*f*Thp/dp;


T1 = ((Y(7)^4)-(Y(5)^4));
T2 = (Y(7)-Y(6));
T3 = (Y(7)-Y(4));
T4 = (Y(4)-Y(5));


Temp1 = G1*T1;
Temp2 = G2*T2;
Temp3 = G3*T3;
Temp4 = G4*T4;


F4 = (1/(Thl*Rhol*Cpliq))*((-G1*T1)-(G2*T2)-(G3*T3));
F5 = (1/(Thp*Rhop*(1-f)*Cppow*Y(2)))*(G2*T2);
F6 = (1/(f*Thp*Rhop*Cppow*Y(1)))*(G1*T1+G4*T4);
F7 = (1/(Thg*Rhog(T)*Cpgas*Y(1)))*(G3*T3-G4*T4);

%***** MASS TRANSFER EQUATIONS *****


EE = Ugl*g;
Re1 = EE*(dp^4)/((Visl/Rhol)^3);
Sc1 = Visl/(Rhol*Ds);
```

```matlab
Sh = (2+(0.4*(Re1^0.25)*(Sc1^0.333)));

kp = (Ds/dp)*(2+(0.4*(Re1^0.25)*(Sc1^0.333)));

kb = 0.951*(g^0.25)*(db^0.25)*(Ds^0.5);


J1 = 6*Thp*kp*(1-f)/dp;
J2 = 6*Thg*kb/db;


F8 = (1/(Thl*Apl))*(-J1*(Y(8)-Cips)-J2*(Y(8)-Cips));
F9 = (1/(Thp*(1-f)*Cp*Apl))*J1*(Y(8)-Cips);
F10 = (1/(Thp*f*Cp*Apl))*J2*(Y(8)-Cips);


%***** MATRIX CALCULATIONS *****


a = Y(8)*Y(2)*Y(1)*Y(3);
b = Cb*Y(2)*Y(1)*Y(3);
c = Y(1)*(Y(3)^2)*Y(2);
d = Temp*(Y(1)^3)*Y(3)*(Y(2)^2);
e = Y(7)*(Y(1)^3)*Y(3)*(Y(2)^2);
f = (Y(1)^3)*(Y(3)^2)*(Y(2)^3);


Jtotaal = (Y(10)*(1-f)) + (Y(9)*f);


Model = [F1;...
      F2;...
      F3;...
      F7;...
      F6;...
      F5;...
    ((F4/Y(3))+(F3*(d-e)/f));...
     ((F3*(a-b)/c)+(F8/Y(3)));...
      ((F10/Y(1))+(F1*Y(9)/Y(1)));...
      ((F9/Y(2))+(F2*Y(10)/Y(2)))];
```

TOPSLAG

```matlab
%***** MAIN STRUCTURE OF THE TOPSLAG PROGRAM *****

global MTWT CbBegin MCarry MolCarry Les MassFRP Kef Af
Rholiq MolMassSul

%****** INPUT VARIABLES *****

disp('INITIAL VARIABLES')
disp('
');
   %METWT = 95000;
   %WTS = 0.077;
    %Temp = 1700;
    METWT = input('\ Initial mass of iron [kg]   =   ');
   WTS = input('\ Initial sulphur content in liquid iron
[wt%]   =   ');
   Temp = input('\ Initial temperature of the bath [Kelvin]
=   ');

disp('
');
disp('LANCING CONDITIONS and VARIABLES')
disp('
');
   %MFRP = 0.50;
   %QR = 0.014;
   MFRP = input('\ Total mass flowrate of the CaC2 particles
[kg/s]   =   ');
   QR = input('\ Total volumetric flowrate of the N2 through
the injection lance [m3/s]   =   ');
```

```matlab
disp('
');
disp('CARRY-OVER SLAG FROM BLAST FURNACE')
disp('
');
   Les = 40;
    %MolCarry = 1.24;
    %MCarry = 1000;
   MolCarry = input('Initial sulphur concentration in carry-
over slag [wt%]   =   ');
   MCarry = input('Amount of carry-over slag [kg]   =   ');


%***** OTHER PARAMETERS *****

MSul = 32;
Ds = 5e-9;
Beeta = 500; % A constant value assigned to Beta - See
Equation 4.45 in Chapter 4.
Rhol = 7000;
Af = 5; % Topslag/metal reaction interface [m2]


%***** EQUATIONS *****

QReg = Qaksent*Temp1/273;
Kef = Beeta*((Des*QReg/Af)^0.5);


CbBegin = 10*PercentSul*Rholiq/MolMassSul


%***** SOLVE EQUATIONS *****

TSPAN = [0 InjTime]
Y0 = [CbBegin];
```

```matlab
[T,Y] = ode45('TopslagToets', TSPAN, Y0)
%plot (T,Y,'-*')


function Slak = TopslagToets(T,Y)


global MTWT CbBegin MCarry MolCarry Les MassFRP Kef Af
Rholiq MolMassSul


%***** TOPSLAG PROGRAM *****


A          =          ((MTWT*MolMassSul/(Rholiq*10))*(CbBegin-
Y))+(MCarry*MolCarry);
B = Les*(MCarry +(MassFRP*T));
C = (MolMassSul*Y/10)-(Rholiq*(A/B));
D = (Rholiq*10*Kef*Af/(MolMassSul*MTWT))*C;


Slak = -D;
```

11. APPENDIX C – MODEL VALIDATION

Default parameters

The data contained in Table C.1, has been filtered from an original data set containing 1495 rows of data (See Section 3.3). This was done to identifying data falling into a specific range of values.

Table 11.1 Default model parameters: Filtered industrial data

LID PRODUCTION DATA

START	Tap Mass	Start Sulphur	End Sulphur	CaC2 used	Inj.Time	
Time	Tons	%	%	kg	Mintes	MFRP
26-Sep-00	93200	0.075	0.041	240	6	0.67
17-Nov-00	95600	0.073	0.035	229	7	0.55
29-Nov-00	94400	0.075	0.033	236	8	0.49
5-Dec-00	94500	0.068	0.018	241	8	0.48
17-Dec-00	96800	0.079	0.039	230	7	0.55
17-Dec-00	96600	0.075	0.033	231	6	0.53
31-Dec-00	94200	0.076	0.045	201	7	0.40
4-Jan-01	94800	0.076	0.038	223	7	0.53
11-Jan-01	96000	0.079	0.045	251	10	0.44
13-Jan-01	92600	0.070	0.025	257	8	0.49
15-Mar-01	93000	0.082	0.033	287	9	0.53
18-Mar-01	94600	0.076	0.027	265	9	0.48
2-Apr-01	96000	0.076	0.036	330	10	0.55
28-May-01	94200	0.069	0.033	234	8	0.51
29-Jul-01	96800	0.085	0.041	231	9	0.43
7-Aug-01	94600	0.077	0.029	256	9	0.49
10-Aug-01	96400	0.081	0.040	195	6	0.54
10-Aug-01	96800	0.080	0.043	204	8	0.43
13-Aug-01	93800	0.083	0.036	241	7	0.57
20-Sep-01	95800	0.076	0.040	210	8	0.46
	95035	**0.077**	**0.036**	**240**	**7.9**	**0.51**
Standard deviation	1336	0.004	0.007	31	1.2	0.06
95% Confidence	± 506	± 0.0017	± 0.0026	± 12	± 0.46	± 0.023

These values were used in training the desulphurisation model and are summarised in Table 5.1.

Table 5.1 Default parameters

PARAMETER	PARAMETER VALUE
Initial sulphur value in the iron	0.077 wt%
Mass of iron in ladle	95086 kg
Injection depth	2.2 m (below the surface)
Carrier gas flowrate	0.014 m³/s (840 litre/min)
Calcium carbide flowrate	0.51 kg/s
Reagent injection time	7.9 minutes

CONDITIONS A

The data contained in Table C.2, has also been filtered from the same original data set containing 1495 rows of data in order to represent data that fall into a different range of values.

Table11.2 Conditions A: Filtered industrial data

LID PRODUCTION DATA

START Time	Tap Mass Tons	Start Sulphur %	End Sulphur %	CaC2 used kg	InjTime Minutes	MFRP
23-Sep-00	89400	0.014	0.014	56	3	0.31
25-Sep-00	96600	0.158	0.038	353	20	0.29
8-Oct-00	95200	0.049	0.049	53	3	0.29
13-Mar-01	92200	0.026	0.026	62	4	0.26
1-Apr-01	100200	0.063	0.047	101	5	0.34
4-Apr-01	92800	0.045	0.031	102	5	0.34
12-Jun-01	97200	0.079	0.020	354	20	0.30
12-Jun-01	99000	0.041	0.041	50	3	0.28
2-Sep-01	90200	0.132	0.094	292	16	0.30
10-Sep-01	95200	0.053	0.043	73	5	0.24
11-Oct-01	93800	0.058	0.037	108	7	0.26
15-Oct-01	95200	0.064	0.037	122	6	0.34
18-Oct-01	94800	0.089	0.046	204	12	0.28
21-Oct-01	98800	0.057	0.046	108	6	0.30
26-Oct-01	93800	0.068	0.044	130	8	0.27
Average values	**94960**	**0.067**	**0.041**	**145**	**8.2**	**0.3**

These average values were employed in testing the validity of the proposed model and are summarised in Table 5.3.

Table 5.3 Industrial conditions A

Parameter	Parameter value
Initial sulphur value in the iron	0.067 wt%
Mass of iron in ladle	94960 kg
Injection depth	2.2 m (below the surface)
Calcium carbide flowrate	0.3 kg/s
Reagent injection time	8.2 minutes

CONDITIONS B

Table 11.3 Conditions B: Filtered industrial data

LID PRODUCTION DATA

START	Tap Mass	Start Sulphur	End Sulphur	CaC2 used	InjTime	
Time	Tons	%	%	kg	Minutes	MFRP
12-Oct-00	111000	0.0630	0.0377	198	6	0.55
16-Oct-00	120000	0.0083	0.0083	114	4	0.48
24-Oct-00	111200	0.0908	0.0463	250	9	0.46
6-Nov-00	117000	0.0553	0.0263	180	6	0.50
6-Nov-00	110000	0.0584	0.0240	243	8	0.51
6-Nov-00	113400	0.1235	0.0188	557	17	0.55
7-Nov-00	114600	0.0667	0.0413	162	6	0.45
7-Nov-00	116400	0.1023	0.0553	249	8	0.52
7-Nov-00	111200	0.0871	0.0380	248	8	0.52
12-Nov-00	113000	0.0528	0.0158	256	8	0.53
17-Nov-00	118000	0.0468	0.0318	165	6	0.46
23-Nov-00	111600	0.0759	0.0493	165	6	0.46
29-Nov-00	110000	0.0475	0.0245	249	8	0.52
30-Nov-00	110800	0.0508	0.0224	204	7	0.49
4-Dec-00	109800	0.0372	0.0198	182	6	0.51
23-Dec-00	112000	0.0473	0.0200	256	8	0.53
23-Dec-00	111400	0.0488	0.0185	297	9	0.55
4-Jan-01	111400	0.0357	0.0275	177	6	0.49
4-Jan-01	110800	0.0778	0.0336	263	8	0.55
8-Jan-01	120400	0.0576	0.0268	322	10	0.54
8-Jan-01	111600	0.0701	0.0913	203	7	0.48
8-Jan-01	115200	0.0625	0.0305	264	8	0.55
11-Jan-01	110000	0.0617	0.0130	351	11	0.53
18-Jan-01	119400	0.0613	0.0211	352	11	0.53
21-Jan-01	117800	0.0640	0.0471	252	8	0.53
11-Feb-01	112800	0.0621	0.0163	427	14	0.51
19-Feb-01	110800	0.0608	0.0371	206	7	0.49
24-Mar-01	113000	0.0793	0.0162	453	16	0.47
31-Mar-01	117000	0.0774	0.0398	304	10	0.51
9-Apr-01	109800	0.0570	0.0254	203	7	0.48
20-Aug-01	111000	0.0756	0.0478	212	7	0.50
21-Oct-01	111200	0.0753	0.0500	263	9	0.49
Average Values	**113133**	**0.063**	**0.032**	**255**	**8**	**0.51**

Table 5.5 Industrial Conditions B

Parameter	Parameter value
Initial sulphur value in the iron	0.063 wt%
Mass of iron in ladle	113133 kg
Injection depth	2.62 (below the surface)
Calcium carbide flowrate	0.51kg/s
Reagent injection time	8 minutes

STOICHIOMETRIC UTILISATION OF CALCIUM CARBIDE PARTICLES AFTER DESULPHURISATION

At Saldanha Steel the desulphurising agent is calcium carbide with desulphurisation taking place in accordance to the following equation (Irons, 1999).

$$CaC_2 + S_{(\%inFe)} \Leftrightarrow CaS + 2C \tag{1.1}$$

Based on the default industrial values as seen in Table 5.1, the amount of sulphur removed during the injection process, is calculated as follows

$$S_{removed} = \left[\frac{\left(S_{Begin} - S_{End} \right)}{METWT \cdot M_S} \cdot 100 \right] [kmol]$$

$$S_{removed} = \left[\frac{\left(0.077 - 0.036 \right)}{95086 \cdot 32} \cdot 100 \right] [kmol]$$

$$S_{removed} = 1.22 \ kmol$$

Assuming a stoichiometric reaction based on Equation 1.1, 1.22 kmol calcium carbide would have had to react with the removed sulphur ($S_{removed}$).

$$CaC_{2 - required} = S_{removed} \times M_{CaC_2} [kg]$$

$$CaC_{2 - required} = 1.22 \times 64.1 [kg]$$

$$CaC_{2 - required} = 78 kg$$

However, according to Table 5.1, the **actual** average amount of calcium carbide utilised during the desulphurisation procedure was **240 kg**, pointing towards a genuine reagent utilisation of 32.5%.

Table 11.4 Particle utilisation

	Theoretical [kg]	Actual [kg]	Utilisation [%]
CaC_2 required for reaction	78	240	32.5

UTILISATION OF CALCIUM CARBIDE PARTICLES – TOPSLAG CONTRIBUTION

The individual contributions of the topslag and the plume towards desulphurisation was analysed and the results can be seen in Figure C.1.
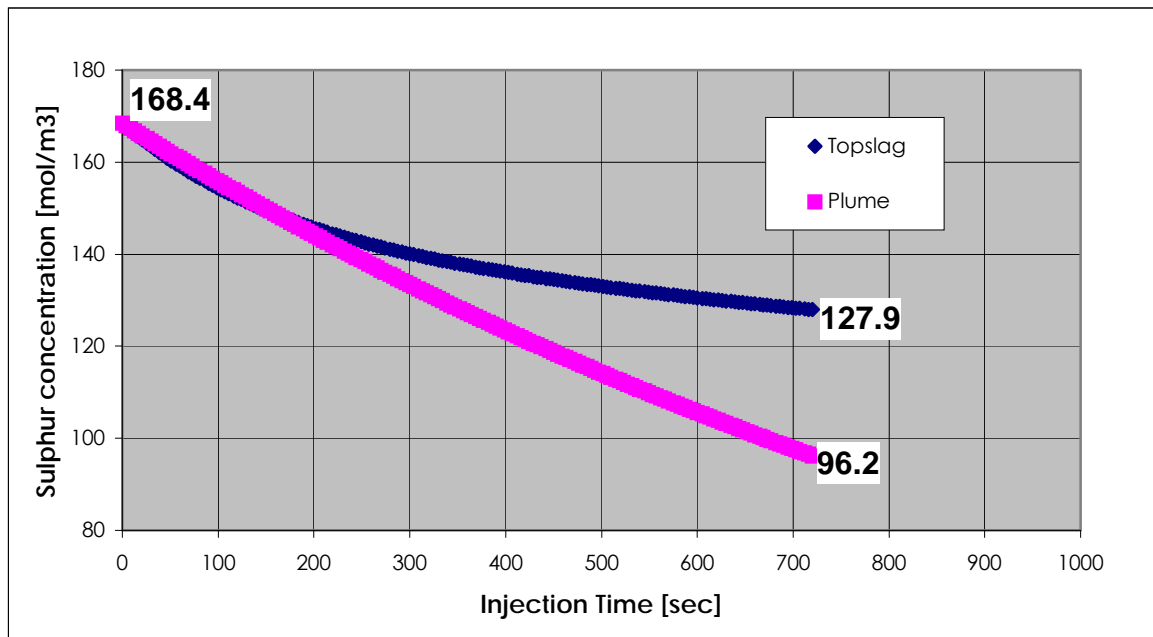
Figure 11.1 Individual contribution of topslag and plume towards the desulphurisation process

When considered individually, the plume and the topslag would reduce the sulphur concentration within the iron from 168.4 mol/m^3 to 96.2 mol/m^3 and from 168.4 mol/m^3 to 127.9 mol/m^3 respectively.

$$\text{Topslag contribution} = \left[\frac{(168.4-127.9)_{Topslag}}{(168.4-96.2)_{Plume}+(168.4-127.9)_{Topslag}}\right]\cdot 100$$

This results in a topslag contribution of **36 %** towards the total utilisation of the calcium carbide particles.

In Section 5.2 it is shown that when the calcium carbide particles reach the topslag, it has only utilised 24.5 % ot it's full desulphurisation potential. When it is considered that the once the particles are taken up in the topslag, it delivers another 36 % utilisation of that expected in the plume, the overall utilisation of amounts to 33.3 %.

Overall utilisation   =   (24.5) × (1.36 – as a result of the topslag)

Overall utilisation   =   33.3 %

12. APPENDIX D – "OPERATORS INSTINCT" ADDITIONS

The operators at Saldanha Steel relies on their knowledge of the system when adding calcium carbide to melt, with the intension of providing the ConArc with iron that has a sulphur content of 0.036 weight percent or lower.

Table 12.1 Operators instinct: Calcium carbide addition and corresponding injection times

Initial sulphur content [weight % S]	CaC$_2$ addition [kg]	Injection time at flowrate of 0.5 kg/s
> 0.1 wt% S	add 380 to 300 kg	12.7 – 10 minutes of lancing
> 0.08 wt% S	add 300 to 250 kg	10 – 8.3 minutes of lancing
> 0.065 wt% S	add 250 to 180 kg	8.3 – 6 minutes of lancing
> 0.045 wt% S	add 180 to 150 kg	6 – 5 minutes of lancing

Table E.1 assumes that the sulphur concentrations reflected in Table 3.1 will coincide with the minimum required injection times, while the "Removed sulphur content" values reveals the amount of sulphur being removed in order to reach the obligatory value of 0.036 weight percent.

Table 12.1 Operators instinct: Minimum calcium carbide addition and corresponding injection times

Removed sulphur content [weight % S]	CaC$_2$ addition [kg]	Injection time at flowrate of 0.5 kg/s [minutes]	Injection time at flowrate of 0.5 kg/s [seconds]
0.064	300	10	600
0.044	250	8.3	500
0.029	180	6	360
0.009	150	5	300

The values in the left and right columns in Table E.1 were graphically compared with model values (See Figure 6.12) and are depicted in Figure E.2.
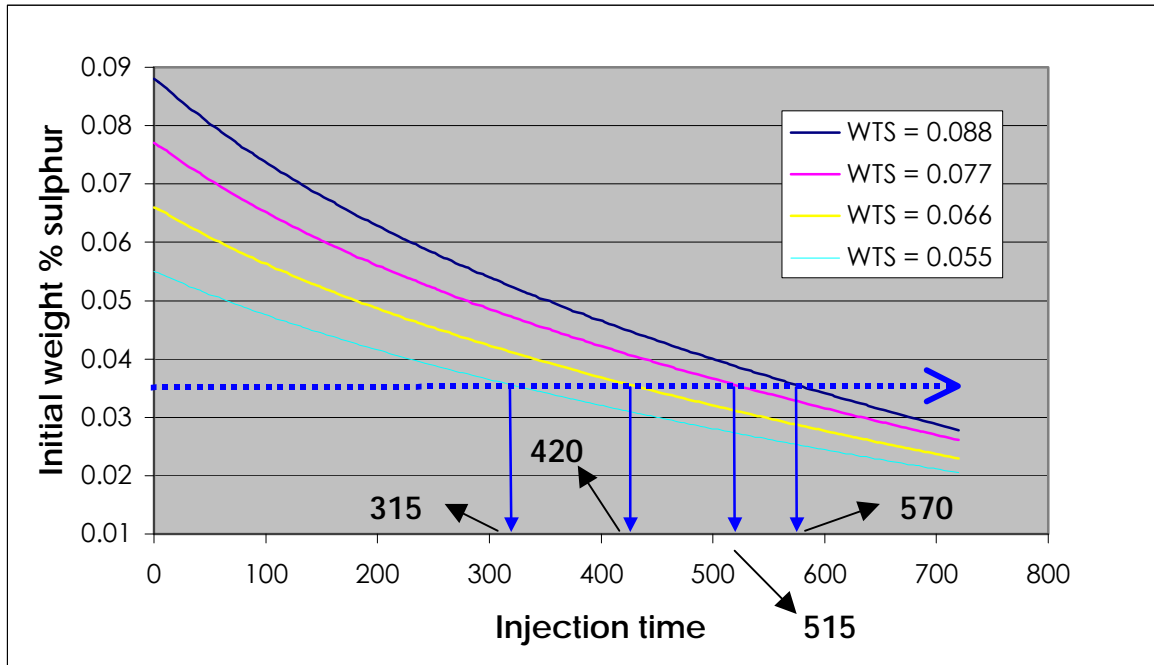

Figure 6.12 Variation in desulphurisation injection time as a function of the initial concentration of sulphur
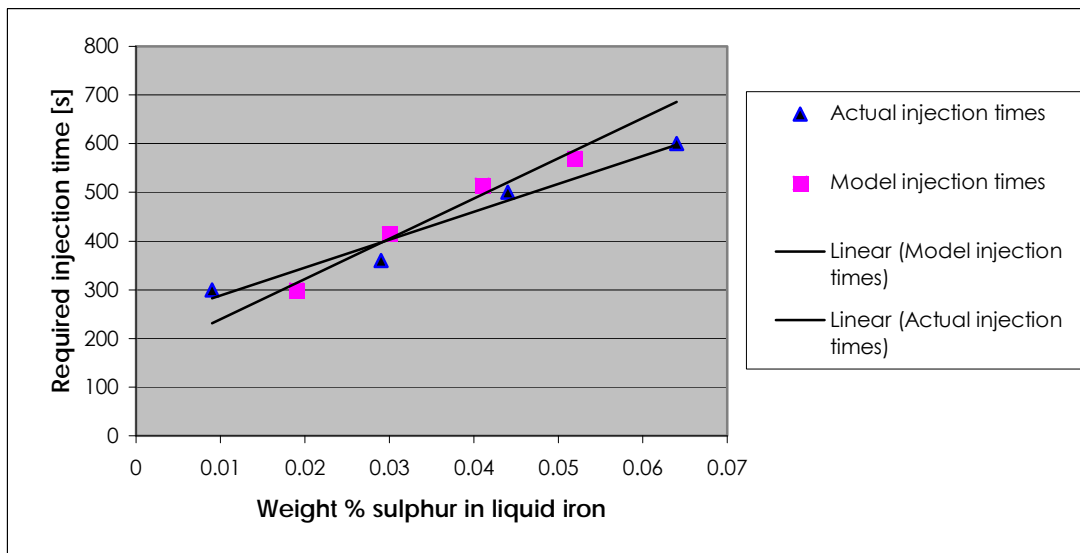

Figure 6.13 Comparison between model and experimental values between injection times as a function of various initial sulphur concentrations in the liquid iron

13. APPENDIX E – INJECTION TEMPERATURE LOSS

The loss of temperature experienced by the liquid iron as a result of the injection process, was experimentally determined.   Temperature measurements were taken every 90 seconds during a six minutes of injection. The experiments were performed at the LID unit at Saldanha Steel with the kind assistance of the personnel on the plant.

Table 13.1   Recorded temperature loss of the liquid iron as a result of the desulphurisation process

LID PRODUCTION DATA

Injection time [min]	Temperature [°C]					
	16-Feb-02	16-Feb-02	17-Feb-02	21-Feb-02	16-Mar-02	17-Mar-02
0	1457	1459	1442	none	none	1297
1.5	1449	1449	1438	1454	1431	1295
3	1444	1444	1428	1447	1425	1287
4.5	1439	1430	1423	1441	1415	none
6	1430	1428	1418	1438	none	none
	6	6	6	4.5	3	3
InjTime	360	360	360	270	180	180
delta T	27	31	24	16	16	10
	4.5	5.2	4.0	3.6	5.3	3.3
Average liquid iron temperature loss		**4.3**		**[°C/min of injection]**		

14. APPENDIX F – SALDANHA STEEL PROCESS DESCRIPTION

COREX

The melter-gasifier (COREX) is tapped at a desired temperature of approximately 1500°C. Hot liquid iron flows down a refractory runner, which comprises of ceramic bricks fitted to a tiltable trough. As the liquid iron proceeds to flow down the runner towards the ladle, the temperature of the molten iron drops by roughly 50 to 100°C. (The runner is kept warm while not tapping to prevent freezing). The iron flows into the tilter, which feeds one of two preheated iron ladles standing underneath the tapping floor. The ladles are preheated by means of any one of four burners that is situated next to the COREX, north and south sides. The burner flames are designed for long flame practice to ensure heating of all ladle sides especially the floor. The refractories are heated to 1100-1200°C. The iron enters the ladles at approximately 1450°C. Upon contact with the pre-heated bricks; the temperature of the liquid iron will drop to 1350-1400°C inside the ladle. These tapped ladles will now line up to wait for their turn at the LID unit.

A maximum of seven ladles can stand in line at this particular unit. The aim though is to get this number to as low as possible seeing the temperature of the molten iron in the ladles decreases while exposed to the elements. A protective slag layer on top of the molten iron does reduce unnecessary oxidation and keeps cooling rate down to 16°C for every hour it's not used. The personnel at Saldanha Steel is currently managing to keep the amount of ladles waiting in line at the LID down to just three. With the CONARC treating roughly one ladle per hour, the temperature in the third ladle will drop by 48°C in three hours. Just before charging the CONARC the temperature of this ladle will therefore

be roughly 1300-1350°C (When ladles are hot and used often, the iron temperature might be as high as 1375-1400°C.)

LIQUID IRON DESULPHURISATION (LID)

Straight after tapping at the COREX, a sample is taken and sent to the lab for analyses (takes between two to 10 minutes with flash analyses). A temperature measurement of the molten iron is also taken while still in the trough on its way to the ladle. This particular will then proceed to wait in line at the Liquid Iron Desulphurisation (LID) section, ready to be desulphurised if required.   Seeing that the Saldanha Steel process is almost completely integrated, the turnaround time for this ladle will strongly depend on the preceding and subsequent processes.

Two to ten minutes after taking the first iron sample, the lab analyses will reach the COREX personnel, identifying the composition of the tapped molten metal.   These results will automatically be relayed to the LID operator on call. The following values will register:

Temperature of the melt in the through at the COREX
Weight percent content of S, C, Si, Mn, P and some other minor elements

If the LID area is clear the ladle will officially be "announced" and the time registered.   The operator proceeds by manually positioning a platform (car) above the new ladle from the control room. The platform allows for the operator to safely take temperature measurements and sample from directly above the ladle.

At this point the operator will get up, put on regulatory safety equipment and enter the furnace area, climb on top of the platform and continue with the sampling procedures:

Two large rods are provided for sampling. The operator will attach a R18 (once-off) sampling probe on one of the rods and a R9 (once-off) temperature probe to the other rob and then physically stick them into the molten metal. While the temperature value will immediately be registered, the iron sample must be quenched and immediately delivered to the laboratory for analysis.

After a few minutes, the subsequent analyses will automatically register at the LID substation – containing the weight percent contents of the S, C, Mn, P and Si in the molten iron. It is however a custom for the current LID operators to phone the lab and verbally acquire the wt% S in the ladle before it is even entered into the computer system.

According the Saldanha Steel regulations all COREX batches containing more that 0.03 weight % sulphur upon entering the LID section, must be desulphurised. Based on the aforementioned lab analyses the LID operator will then decide whether or not the current ladle situated underneath the platform will be desulphurised.

At this point formal protocol is partially abandoned for more informal procedures[1]. Since desulphurisation also takes place in the arc furnace itself (unlike a BOF), there is no great urgency to adhere to any set of stringent criteria at the LID unit. Bearing this in mind, the formal value of 0.03 weight percent sulphur before it is necessary to desulphurise has increased to a general value of 0.04 weight percent sulphur. Desulphurisation is performed by injecting very fine calcium carbide

---

[1] All relevant information was required in October 2000 and operating procedures could have since been revised.

particles through a lance that blows the reagent into the molten metal at a point 0.5m from the bottom of the ladle. Nitrogen is used as the transport gas. The decision of how much calcium carbide should be used and the treatment time necessary, use to be determined by a specific model prepared for this particular purpose. At the present moment the model has also been abandoned for an "operators' instinct" approach, relying on experience and gut feeling to perform the desulphurisation. The calcium carbide reagent is kept in a large silo but fed to the LID unit from another, much smaller holding vessel. This smaller vessel is charged from the bigger one almost immediately after desulphurisation. This ensures that the reagent is always ready for use. This particular smaller vessel can hold a maximum of 800 kg of CaC_2.

The operators use the following values as rule-of-thumb when desulphurising:

> 0.1 wt% S = add 380 to 300 kg CaC_2 (7.6 – 6 minutes of lancing)

> 0.08 wt% S   = add 300 to 250 kg CaC_2 (6 – 5 minutes of lancing)

> 0.065 wt% S   = add 250 to 180 kg CaC_2 (5 – 3.6 minutes of lancing)

> 0.045 wt% S   = add 180 to 150 kg CaC_2 (3.6 – 3 minutes of lancing)

After desulphurisation, the operator repeats the sampling procedure mentioned above. The temperature is recorded automatically and the laboratory does another elemental analysis.

CONARC

It is the general practice at Saldanha Steel to not charge a ladle into the CONARC if the liquid iron's temperature is less than 80-100°C above liquidus temperature, determined from LID analysis. During charging of

the CONARC the molten iron temperature will drop by another 50°C – 100°C. It was found that the liquidus temperature of the average ladle containing molten iron is about 1105°C, thus fixing the minimum temperature of ladle charging at 1250°C. This is done for very practical reasons:

Preventing skull formation in launder cars
Preventing freezing of iron in launder car
Ensure molten bath is available for top lance ignition

Blowing phase

The main objective of the blowing phase is the removal of carbon and silicon, as well as the melting of the Direct Reduced Iron (DRI) produced at the MIDREX plant.
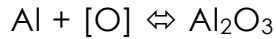
Charging

The steel in the furnace is tapped at an aim temperature of 1640 °C. After tapping, 30 tons of hot heel will remain in the furnace, which includes 3 – 5 tons of slag. The main reasons for this is to prevent the loading of fresh iron onto the refractory bricks of the furnace, thus preventing excessive and premature refractory erosion. The steel, along with the remaining slag will be highly oxidized. The steel and the slag will contain dissolved oxygen and wustite respectively – with wustite being by far the biggest problem. Immediately adding the new batch of carbon saturated steel to this decidedly oxidized mixture will trigger highly exothermic reactions
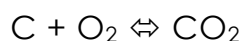
$C + O_2 \Leftrightarrow CO_2$ (Btu = 14096)

Pure Al nipples are therefore added to deoxidise the bath, thereby converting al the dissolved oxygen and wustite to Al_2O_3 and Fe respectively

$Al + FeO \Leftrightarrow Al_2O_3 + Fe$

$Al + [O] \Leftrightarrow Al_2O_3$
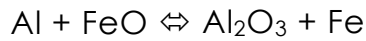
Charging the CONARC takes an average of 5 minutes, but can go on for up to 8-9 minutes due to large ladles and sculled ladle spouts. While the furnace is being prepared for the next heat it will decrease in temperature at a cooling rate of 2°C per minute. After tapping, the slide gate for the taphole is cleaned and filled with refractory sand. The furnace is levelled, refractories inspected and iron loaded if required. After charging anything between 70 and 115 tons of molten iron into the furnace, the blowing process will commence. Ninety nine point five percent (99.5%) pure oxygen is fed through a top lance straight into the molten mass at a speed of 1.98 Mach and a flow rate of about 160 Nm^3 / min, which remains constant throughout the blowing process (this value can be changed, if furnace conditions allows). At these early stages the bath is dominated by a few important reactions:

$C + \frac{1}{2}O_2 \Leftrightarrow CO$ (Btu = 3952 per lb C)

$C + O_2 \Leftrightarrow CO_2$ (Btu = 14096 per lb C)

$CO + \frac{1}{2}O_2 \Leftrightarrow CO_2$ (Btu = 4350 per lb CO)

$Si + O_2 \Leftrightarrow SiO_2$ (Btu = 13190 per lb Si)

Carbon Oxidation

Upon coming into contact with the oxygen, the carbon in the liquid iron reacts exothermically with the oxygen in the bath and produces CO gas. A further 10% of the CO gas will again react with oxygen to form CO_2.

This reaction realises 3.5 times more energy than the previous one but plays a less significant role due to the small percentage of conversion. (Post Combustion technology is being used in some plants)

Silicon Oxidation

Along with all other trace elements like for example Mn and Mg, Si is also oxidised and transported to the slag. The importance of this particular reaction is found in the large amount of heat it generates per kilogram of Si initially found in the molten iron. In essence it is the most important heat source during the blowing phase and will ensure that the process is autogenous, implying that no external heat source is required.

Flux Addition

At this stage computerised flux addition will be performed and controlled by the Level 2 control system through its communication with the various PLC units. Based on LID analysis done on the iron and tap analysis performed on the steel, Level 2 calculates the amount of SiO_2 in the bath. It will now automatically release enough lime (CaO) from its PLC-controlled holding tank to establish a B2-basicity value (CaO/SiO_2)[2] of 2.4-2.6. Within the confounds of Level 2 it possesses a digital copy of a graph depicting Basicity (B2) vs. %MgO solubility. Level 2 will determine the basicity of the bath, calculate the corresponding amount of MgO soluble in the blend and then by design, add enough of the MgO (40%)/CaO (60%) mixture to, not only satisfy but exceed that mark by approximately 1 - 2%. In this way the surplus of MgO will ensure that the refractory brick lining containing mostly MgO, will be protected and not oxidised into the molten bath, thus causing its unnecessary erosion and subsequent failure.

---

[2] All Saldanha Steel's basicity calculations are based on the B_2 standard.

Bath temperature

Internal thermodynamic calculations, utilizing amongst other variables the total amount of oxygen already fed to the bath, will determine the carbon quantity that has been oxidised. Following that, pre-programmed thermodynamic and empirical equations will determine the equivalent amount of elements that has been removed from the steel, the quantities of oxides formed in the slag, the corresponding amount of internal heat already generated and the temperature of the bath. If it is found that $T_{bath} < 1575$ °C, the corresponding oxygen quantity (translating into blowing time) still required to reach the desired temperature will be calculated and conveyed to the blowing unit. This entire control process will repeat itself every ten seconds until the bath has reached a minimum temperature of 1575 °C. If it is found that $T \geq 1575$ °C, the point of DRI (Direct Reduced Iron) addition is reached.

DRI addition

No DRI is ever added to the molten bath at the beginning stages of the oxygen blow. To prevent possible coalition of DRI particles due to a stagnant bath, all additions are made after the bath has been properly stirred. DRI will be released into the furnace with the intention to stabilize the temperature of the bath at 1575 °C. Once more Level 2 will rely on pre-programmed layers of data sets and equations to calculate the exact amount of DRI necessary to counter-act the corresponding rise in temperature due to the exothermic reactions. With the addition of DRI, fresh SiO_2, C, Mn, S, P_2O_5 and FeO will enter the bath, requiring extensive re-working of the control loop by again starting with the initial basicity calculations. The control system will keep on updating the blowing control unit every ten seconds with the newly calculated amount of

oxygen (blowing time) still required, while simultaneously relaying to the DRI control unit the exact quantity needed to sustain a temperature of 1575 °C in the bath. If at any time it is found that C ≤ 0.2 weight % of molten steel, the blowing stage will be finished and oxygen, flux and DRI addition will be terminated. (The blowing phase will thus react to a Celox measurement taken in the bath by an operator on the tap floor)

Arcing Phase

The main objective of the arcing phase is to ensure that the furnace load reaches 200 tons of refined steel.

Electrodes

Upon reaching the end of the blowing phase, three electrodes are positioned above the surface of the bath. These graphite electrodes are composed of a mixture of finely divided, calcined petroleum coke mixed with about 30% coal tar pitch as a binder, plus proprietary additives unique to each manufacturer. Also moved in position is the door lance for carbon and oxygen injection. This is required for foamy slag production and decarburisation. The extra carbon helps to promote a foamy slag through gas formation and bubble release and involves the following reactions

$C + \frac{1}{2}O_2 \Leftrightarrow CO$ $\qquad\qquad$ (BTU = 3952 per lb C)
$C + O_2 \Leftrightarrow CO_2$ $\qquad\qquad$ (BTU = 14096 per lb C)
$CO + \frac{1}{2}O_2 \Leftrightarrow CO_2$ $\qquad\qquad$ (BTU = 4350 per lb CO)

The injection of 99.5% pure oxygen into the bath serves the dual purpose of further decarburising the slag from C ≤ 0.2% to C ≤ 0.04% and to

promote a foamy slag. Foamy slag and bubble formation in the arc phase is of great monetary concern. Electrodes covered and protected by foamy and gaseous slag while striking, will operate at an efficiency rate of as high as 85-90%, whereas uncovered electrodes will only reach levels of as high as 40-50% due to radiation losses to the refractory lining and water cooled panels of the furnace.

Internal loop

Throughout the arc phase up to the time just before tapping, the internal control loop will ensure that the temperature remains constant between 1575-1590 °C. As in the blowing phase, the inevitable rise in temperature due to the introduction of electrical energy through the electrodes and the introduction of chemical energy through the varies exothermic reactions will be countered by the control system by feeding just the right amount of DRI into the bath. Both of the CONARC furnaces has a maximum steel capacity of 200 tons. Due to the 4 – 5% carbon content of the COREX iron and the 92% metallisation of the MIDREX DRI, the furnace will be fed with 220 tons of material – thereby ensure at least 200 tons of ConArc load of which, 170t will be tapped as refined steel to provide the Ladle Heating Furnace (LHF). Near the end of the arcing phase, the amount of carbon in the steel would have dropped to the regulatory level of 0.04 weight %. The total wustite content in the slag will be approximately 20 wt% and rising fast. The presence of increasing levels of FeO will cause the slag to become less viscous and without the presence of carbon in the steel to promote bubble formation, the level of the foam will drop considerably and leave the electrodes exposed. At this point the oxygen, carbon and DRI addition will cease only if enough DRI has been added to allow a 170t tap mass to the LHF. The arc will keep striking until the temperature of the bath is 1640 °C before tapping commences.

That concludes the process description from Corex to Conarc.